

Predicting Infections in Preterm Infants with Thermal Imaging Technology

Erik Wirianto



Predicting Infections in Preterm Infants with Thermal Imaging Technology

by

Erik Wirianto

to obtain the degree of Master of Science
at the Delft University of Technology,
to be defended on Thursday, February 25th, 2021 at 09.00.

| | | |
|-------------------|---|----------------------|
| Student number: | 4773284 | |
| Project duration: | December 9th, 2019 – February 25th , 2021 | |
| Thesis committee: | Prof. dr. P. J. French, | TU Delft, supervisor |
| | ir. K. Rassels, | TU Delft, supervisor |
| | Prof. dr. A. J. P. Theuwissen, | TU Delft |
| | Prof. dr. F. C. T. van der Helm, | TU Delft |

This thesis is confidential.

An electronic version of this thesis is available at <http://repository.tudelft.nl/>.

Abstract

Neonatal sepsis is a dangerous non-specific disease in babies, especially neonate/newborns. It is one of the leading causes of neonate mortality rate, because of the difficulty to diagnose, leading to late or false treatment. Previous research has found the promising feature of artificial intelligence or machine learning in solving the problem. After analysing hours of the electronic health record data available, they are able to diagnose sepsis condition on neonates. However, the accuracy and time needed before diagnosis are still concerning considering the risk of mistreated or late diagnosed sepsis cases. In this research, machine learning and thermal imaging technology is used to explore the possibility of predicting sepsis. 57 thermal videos from 26 babies are processed to track the highest skin temperature visible to the thermal camera. The temperature data then is utilized to train and test several machine learning models for predicting sepsis cases. Support Vector Machine (SVM) was found to be the best sepsis predictor using time-series variation of the temperature data as the feature. The model needs 10-30 minutes of thermal recording, 19 minutes in average, to predict sepsis and achieved 82% accuracy. Simulation also shows the high possibility in increasing the accuracy when more data/thermal videos are available to train the model. High accuracy model with fast reacting sepsis prediction could help doctors precisely treat septic neonates in timely manner, decreasing the mortality rate for sepsis cases.

Acknowledgement

This thesis is the result of a hard and arduous work, but also tremendous help from many people around me. Without them, I definitely would not be able to finish this thesis.

I want to thank my parents, brother, and my girlfriend who always supported me and believed in me no matter what. I cannot express my gratitude enough for them.

I also want to give my thanks to Paddy French and Kianoush Rassels, as my supervisors and mentors, for giving me support, guidance, and advice that greatly help me finish this thesis.

I am also thankful for Laura Van der Meer, Marjan Wagenveld-Meijer, and all doctors, nurses, and staffs at Reinier De Graaf and Haga Ziekenhuis. I hope this thesis could help them in anyway possible.

I want to give my gratitude to Jason, Adi, Fabian, and all members and past members of the remote sensing group, who have been helping me and working alongside with me. I hope I could also be a help in their work.

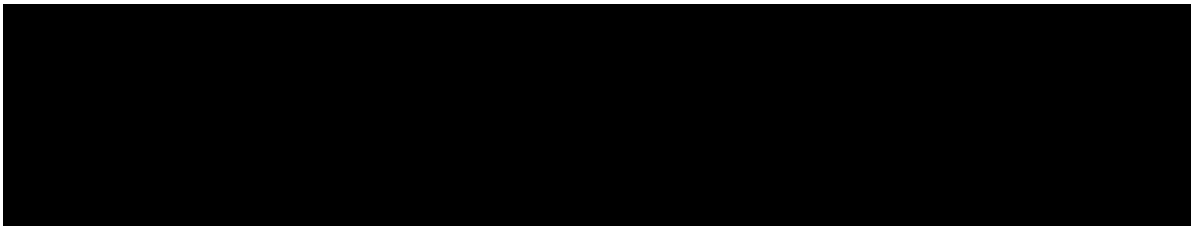
I express my thanks to all members and staffs of the bioelectronics group and EWI department, and anyone who contributed to this thesis work.

Lastly, I hope this thesis could be beneficial for readers and any future research in relating topic.

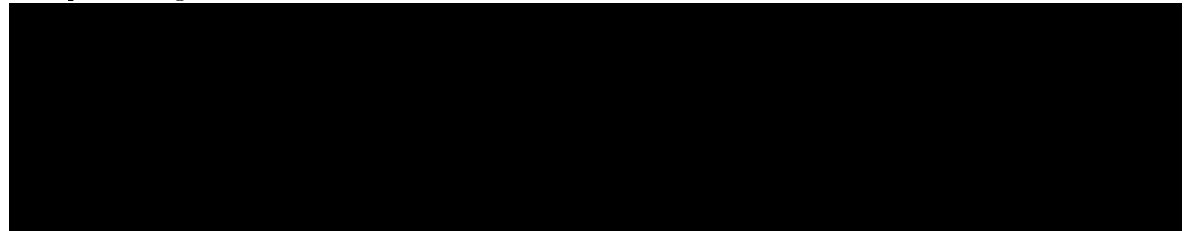
Erik Wirianto
Delft, February 2021

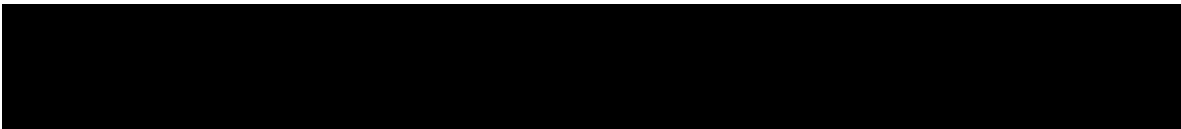
Contents

| | | |
|-------|--|----|
| 1 | Introduction | 1 |
| 1.1 | Premature Baby | 1 |
| 1.1.1 | Neonatal Skin | 1 |
| 1.1.2 | Thermoregulation and Temperature Measurement | 2 |
| 1.1.3 | Incubator Care for Neonates | 2 |
| 1.1.4 | Neonatal Infection (Sepsis) | 3 |
| 1.2 | Research Goal. | 3 |
| 2 | Technical Background and Research | 4 |
| 2.1 | Thermal Imaging | 4 |
| 2.1.1 | Thermal Radiation | 4 |
| 2.1.2 | Thermal Measurement Model | 5 |
| 2.1.3 | Total Measurement Error | 6 |
| 2.2 | Optical Flow Algorithm | 8 |
| 2.2.1 | Gunnar Farneback Optical Flow Algorithm | 8 |
| 2.2.2 | Pyramid Scaling in Optical Flow | 9 |
| 2.3 | Feature Point Detection and Matching | 11 |
| 2.3.1 | Image Feature Detectors and Descriptors | 11 |
| 2.3.2 | Feature Matching | 14 |
| 2.4 | TCP/IP Communication | 14 |
| 2.5 | Infection (Sepsis) | 16 |
| 2.5.1 | Sepsis Risk and Clinical Symptoms. | 17 |
| 2.5.2 | Core-peripheral Temperature Difference. | 17 |
| 2.6 | Machine Learning for Sepsis Prediction. | 17 |
| 2.6.1 | Logistic Regression. | 17 |
| 2.6.2 | Naive Bayes | 18 |
| 2.6.3 | Support Vector Machine | 19 |
| 2.6.4 | K-Nearest Neighbour | 19 |
| 2.6.5 | Decision Tree and Random Forest | 20 |
| 2.6.6 | Adaboost. | 21 |
| 2.6.7 | Gradient Boosting | 22 |
| 2.6.8 | Feature Selection. | 22 |
| 3 | Experiments and Results | 24 |

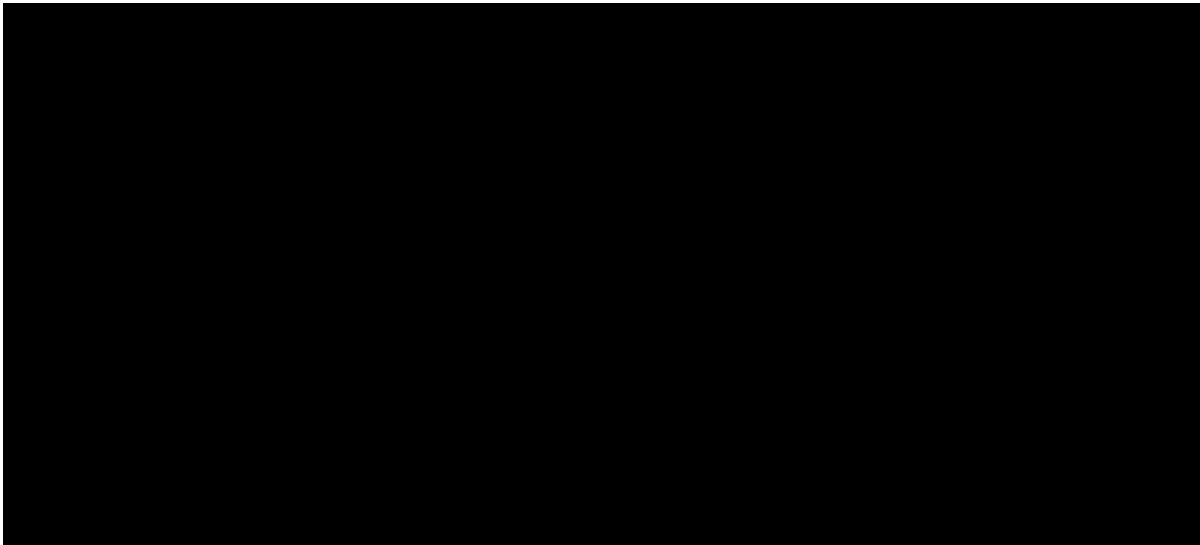


| | | |
|---|-----------------------------|----|
| 4 | Pre-processing Filter Chain | 33 |
|---|-----------------------------|----|

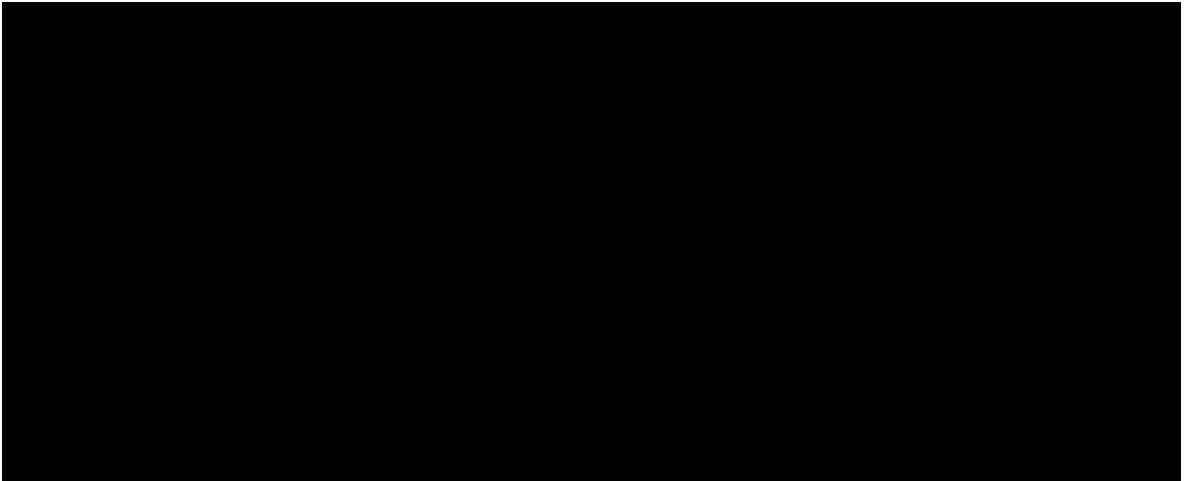




| | | |
|---|-----------------------|----|
| 5 | System Implementation | 47 |
|---|-----------------------|----|



| | | |
|---|-------------------------------------|----|
| 6 | Supplementary System Implementation | 67 |
|---|-------------------------------------|----|

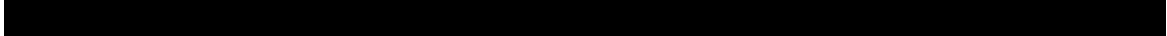


| | | |
|-----|---------------------------------|----|
| 7 | Conclusion | 81 |
| 7.1 | Conclusion | 81 |
| 7.2 | Future Recommendation | 81 |

| | | |
|--|--------------|----|
| | Bibliography | 84 |
|--|--------------|----|



| | | |
|----|--|----|
| .2 | Appendix: FLIR SC305 Datasheet | 94 |
|----|--|----|



Introduction

1.1. Premature Baby

Preterm or premature baby is a baby born at fewer than 37th weeks' gestational age (GA), or more than 3 weeks before the estimated due date. Every year, around 5%-18% babies, or estimated 15 million babies, born in premature condition across 184 countries [1]. Preterm baby can be divided into more sub-categories: moderately to late preterm (32-37 weeks of GA), very preterm (28-32 weeks of GA), and extremely preterm (under 28 weeks of GA). Preterm babies are more susceptible to diseases and harms because of their not fully developed organs and immune system. Hence, preterm infants usually are taken care inside an incubator, to be able to control the suitable environment for the babies. Unfortunately, almost half of deaths in babies under 5 years old happen in neonatal period (less than 4 weeks old) and premature birth complication is the leading cause of them [2].

1.1.1. Neonatal Skin

Skin is the outer most organ of human body. It functions as protection against UV radiation and pathogens, body temperature regulator and sensory preceptor. These functions are not fully developed yet for body skin of the neonates, even less so in preterm ones. After birth, normally, the skin starts to develop those functions and reaches maturity in the first year. For premature babies, this development starts after two to three weeks after birth [3].

The skin consists of two layers: the epidermis, and dermis. The epidermis is a superficial layer, which acts as a first line of defence against pathogens from outside of the body. The outer layer of epidermis, called corneum stratum, is formed at 21 weeks of gestation. Both the epidermis and the corneum stratum have lower thickness in preterm neonates than those of adults [4], which means it requires careful treatment to the skin. The base layer which generates epidermis, can be easily damaged and consequently leads to scar formation after healing [5].

In most neonatal care, skin sensors are used to monitor vital signs of the baby and the usage of those sensors may damage the fragile and sensitive skin of preterm neonates and increase the risk of infection [6, 7]. The removal of skin sensor also increases transepidermal water loss (TEWL) at the sensor location, which is correlated with damaged skin barrier function [8]. In an effort to control TEWL, restore skin elasticity, and skin homeostatis sustenance, emollients can be applied to the skin [9]. There are some controversy surrounding emollients, as some claim it increases the risk of infection [10], while others have found a reduction of nosomical infections when sunflower oil was topically applied, without side effects [11]. Another concern due to the thin corneum stratum is that the skin is highly permeable to topically applied agents, which if absorbed, can cause toxic systemic effects and lead to illness or even death [12]. Similarly, repeatedly applying disinfectant such as isopropyl alcohol to neonate skin can induce systemic intoxication and can cause severe haemorrhagic skin necrosis [13].

1.1.2. Thermoregulation and Temperature Measurement

Humans are homeotherm, which means they try to preserve their body temperature regardless of the environmental condition. Normal core temperature of human body is around 37 °C. Few degrees higher or lower of the core temperature is an indicator for abnormal condition in the body [14]. In neonates, their core temperature needs to be in very specific range, 36.5–37.5 °C and a thermoneutral environment (TNE) to prevent the neonate from thermal stress. The TNE temperature, however, depends greatly on weight, age of gestation, and age of life of the baby, and also whether the neonate is clothed or not. For example, for a very preterm neonate, the TNE temperature is kept at 34–35 °C when the baby is naked, and 28–30 °C while clothed [15].

Adults produce heat in response to cold temperature by several methods, peripheral vascular constriction, inhibition of sweating, voluntary muscle movements, involuntary muscle movements, and nonshivering thermogenesis. Neonates also adapt in cold environment by increased metabolic rate [16], however, the heat production is different compared to adults. Neonates primarily produce heat using nonshivering thermogenesis [16]. The heat produced by a neonate is highly dependent on the body weight [17].

Monitoring and managing temperature of new-born infants are basic requirements in neonatal nursing care. Similar to adult, temperature of a neonate can show a lot about the condition of the baby (e.g. adverse condition) [18–20], hence an accurate thermal measurement would really benefit the baby. Current common thermal measurements for neonate are placed in rectum, axilla, ear, and forehead, with rectal and axillary thermal measurement frequently regarded as the golden standard [21–23]. However, these golden standard temperature measurements are not ideal for the baby as they could cause some degree of distress to the baby when the measurements are taken. Other disadvantages such as perforation of the rectum, infection/hygienic concern, and irritation also cause some concerns for rectal thermometer [24, 25]. For axillary thermometer, babies have to be in a certain position or handled in such a way in order to get accurate measurement. These measurements are also done once in a period of time to minimize discomfort to the baby. For continuous temperature measurement, a skin temperature sensor is used. However, as discussed before, skin sensor has its downside, such as damaging the skin and increasing infection risk.

1.1.3. Incubator Care for Neonates



Figure 1.1: Dräger Caleo® incubator

Due to underdeveloped mechanisms to control their body temperature, it is crucial that neonates do not lose excessive heat, or get too warm. In order to guard them against hypothermia or hyperthermia, they are often placed in an incubator. An incubator is a transparent box with controlled environment inside and in

which a neonate is taken care of. Different incubators have different features, for example, incubator Dräger Caleo has an air control mode, baby temperature control mode, powered vertical height adjustment as main features, and humidity control, and oxygen level control as optional features. These features allow baby to be taken care in optimal environment.

The environment is generally controlled by fan to circulate the air inside the incubator, servocontrol to control the heater, water dispenser for humidifying the incubator, and oxygen valve. Heat exchange between the environment and the neonate happens by convection of the air to the skin of the baby. Air temperature colder than the skin of the neonate would result in convective heat loss due to the velocity of the air flow. Higher velocity would mean higher heat transfer from the skin to the environment. Modern incubators should thus not have an air flow velocity higher than 6 to 8 cubic decimetre per second (cds). However, this low air flow also does reduce the ability to warm hypothermic neonates as quickly as possible [26]. Despite the advantage of being able to monitor and regulate the environment around the baby, incubator has some disadvantages: it is expensive, both in purchase and in use, and creates barrier between mother and her new-born to bond and breastfeed [27]. Moreover, heat is not distributed equally inside the incubator, creating hot and cold spots. In one study, the cold spots in the incubator are found to have elevated levels of staphylococci bacteria, which is the main cause for late-onset sepsis in preterm neonates [28].

1.1.4. Neonatal Infection (Sepsis)

Looking at the premature birth complication more closely, major causes of the complication are varied in different areas of the world, but most researches agreed that neonatal infection/sepsis is one of the leading causes [29–31]. Neonatal sepsis is a generalized systemic/whole body infection occurring in new-born infants. In this report, more specific infections, such as meningitis and pneumonia, are included in the sepsis definition. Infection is caused by invasion of virus, bacteria or other microorganism. It causes reaction from the body immune system to fight the foreign organism, which usually involving inflammation [32]. Neonatal sepsis can be acquired through several ways [33]:

- In utero transplacentally (through ruptured membranes)
- Intrapartum (in the birth canal during delivery)
- Postpartum (external source after birth)

neonatal sepsis usually divided into 2 categories, early onset neonatal sepsis (EONS) and late onset neonatal sepsis (LONS). EONS occurs If the neonate shows sepsis symptoms within 3 days of birth. Usually, neonate with EONS acquires the infection from organisms intrapartum. Meanwhile, LONS is when the sepsis symptoms occur more than 3 days after the birth, and the pathogens come from the environment or postpartum.

1.2. Research Goal

- Predicting infection (sepsis) in preterm infants using contactless monitoring system (infrared camera)

2

Technical Background and Research

2.1. Thermal Imaging

Thermal imaging is an imaging technique detecting infrared radiation, usually in the long-infrared range (9-14 μm), and producing image of the radiation. Human body emits significant radiations of wavelength in range 4 to 30 μm , with peak at 9 μm [34], which is suitable for the thermal imaging. Thermal imaging has been used in the medical scene more than 50 years, first used to find breast cancer in women. Compared to X-ray, computed tomography (CT), and mammography, thermal imaging is not harmful as it does not emit any radiation. It is a real time non-contact measurement method, like a normal camera. From the image of the radiation, the difference of temperature between one object and the other can be seen, and also determine the temperature of the object, even though the accuracy of the measurement depends on a lot of variables. In case of thermal imaging on preterm infants, incubator environment is also affecting the measurement [35]. The hood of the incubator is generally made out of polymethyl methacrylate (PMMA) (also known as acrylic or plexiglass) or polycarbonate. Unfortunately, these materials are very poor for infrared wave transmission, so thermal imaging cannot look through these materials [36].

2.1.1. Thermal Radiation

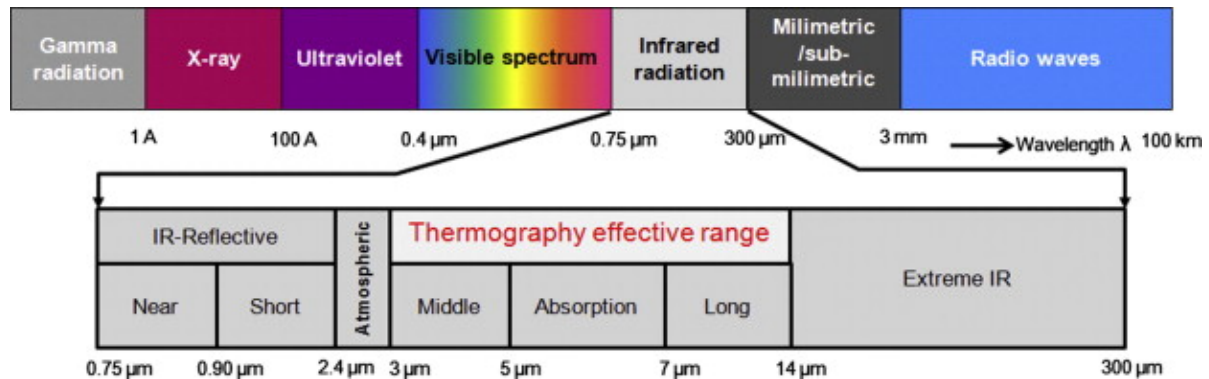


Figure 2.1: Infrared region within electromagnetic spectrum. [35]

The infrared (IR) band of the electromagnetic spectrum has been shown in detail in figure 2.1. IR can be divided into five sub-bands: near, short, middle, long, and extreme. In the atmosphere, particles in the air, such as H₂O, CO₂, and many others absorb certain wavelengths of the radiation, reducing the transmission. As seen in the figure 2.2, from 3 to 5 μm and from 7 to 14 μm the transmission is almost 100%, which is why long infrared range is preferable for thermal imaging.

According to Planck's Law, every object with temperature above absolute zero radiates electromagnetic radiation, includes radiation in infrared wavelength. The radiation increases with increasing temperature as described in Stefan-Boltzmann law, total radiant energy emitted by a surface of a black body is equal to Stefan-

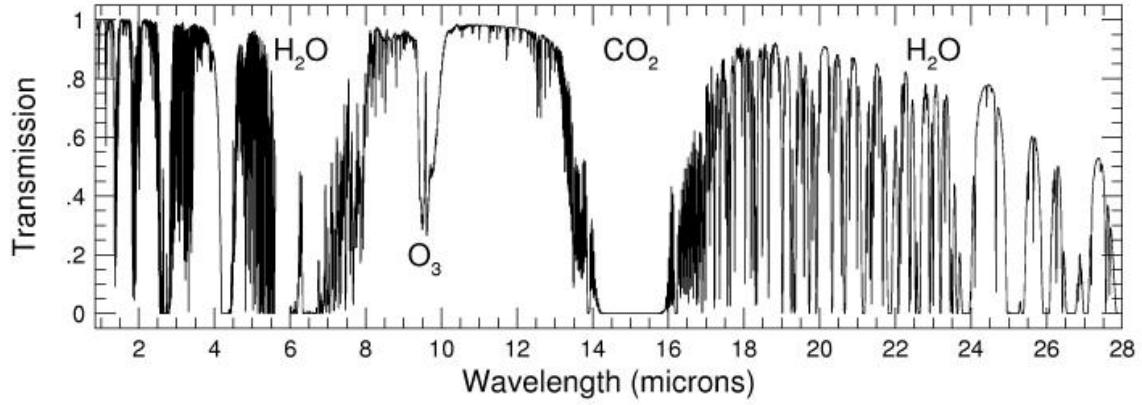


Figure 2.2: Infrared transmission in the atmosphere for wavelength 1-28 μm . [37]

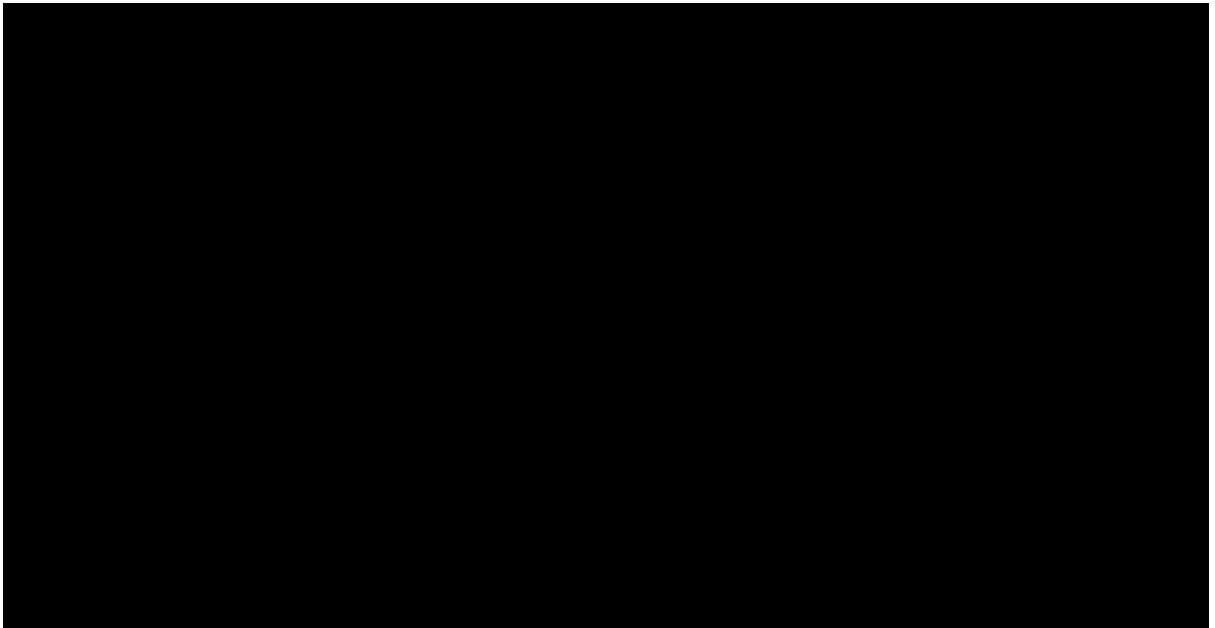
Boltzmann constant, $\sigma = 5.670373 \times 10^{-8} [\text{W m}^{-2} \text{K}^{-4}]$, multiplied with fourth order of the object temperature in Kelvin [38].

$$E_b = \sigma T^4 \quad (2.1)$$

A black body is defined as a surface that absorbs incoming radiation and reflecting none, which means that all the radiation emitted is originated from the black body itself. However, no real-world object is a black body. Real object surface emits radiation less than a black body does. The percentage of black body emissive power is called emissivity, ϵ . Human skin has emissivity of 0.97-0.98 in wavelength range of $1\mu\text{m} < \sigma \leq 14\mu\text{m}$ [39, 40], which means that around 2-3 percent of the radiation from human body is a reflection from objects around the human body.

The radiant energy emitted from object then can be measured by infrared camera. This infrared camera captures the infrared wave coming from the object and then using the formula from the manufacturer, calculating the temperature of the object from the received infrared radiance. The calculation also compensates for environment variables, such as humidity, distance, atmospheric temperature, etc, that would have effects on the object radiance.

2.1.2. Thermal Measurement Model



A generalized model of thermal measurement of neonate inside an incubator is shown in the figure 2.3. There are 6 sources of radiation detected by the camera, (1) infrared window, (2) atmosphere outside the incubator, (3) atmosphere inside the incubator, (4) the actual neonate that is being measured, (5) reflection of ambient object inside incubator, and (6) reflection of ambient object outside incubator. The infrared window can be an infrared transparent foil. If the measurement setup does not use window (open hole), sources number 1 and 6 can be disregarded.

From the model, an equation [35] can be written as:

$$\text{[Redacted Equation (2.2)]} \quad (2.2)$$

where variable T , ϵ , δ , and R are temperature, emissivity, transmittance, and reflectance respectively, with description *detector* means the infrared camera, *obj* means object measured, *amb1* and *amb2* mean ambient object inside and outside the incubator, *atm1* and *atm2* mean atmosphere inside and outside incubator, and *w* means infrared window.

If there is no infrared window, the total radiation received by the camera can be segmented as radiation from actual object measured, reflective radiation from other objects around the object measured, and radiation of the atmosphere between object and infrared camera. The equation then, can be modified from equation 2.2 to:

$$\text{[Redacted Equation (2.3)]} \quad (2.3)$$

Object Measured Radiation

The radiation coming from the object measured is the specific desired radiation to determine the temperature of the object, in this case the neonate. However, the radiation will go through the atmosphere and infrared window (if there is any), which will attenuate the radiation. If not compensated, the infrared camera will underestimate the temperature of the object. The compensation is shown in the formula as dividing the object temperature with transmittance of atmosphere and infrared window. Lower transmittance can be caused by the window or particles in the atmosphere.

Reflective Radiation

In the infrared wavelength, neonate is not a black body, which means the neonate is reflecting some radiation from objects around it. This reflectivity depends on the emissivity of the object, in this case emissivity of neonate is 0.97-0.98 [39, 40]. High emissivity means that almost all radiation is coming from the actual object, hence more accurate approximation of the temperature. Even so, 2-3% of the radiation is still coming from the temperature of objects around the neonate. This yields small measurement error and needs to be compensated. The compensation in the formula is in the T_{amb1} part of the equation.

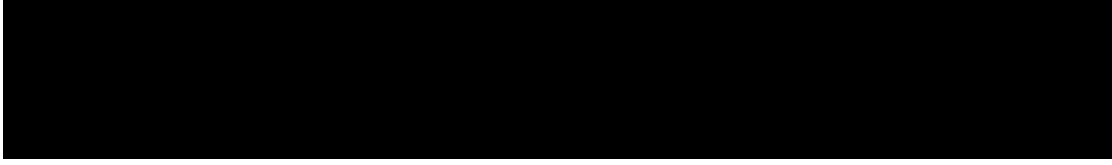
Atmospheric Radiation

Particles in the atmosphere can attenuate infrared radiation in air transmittance, however, these particles also radiate heat because of their temperature, causing additional incoming radiation to the camera. Hence, in the equation, the atmospheric temperature contribute to the total radiation.

2.1.3. Total Measurement Error

Temperature measurement of infrared camera would have error measurement which can be caused by error of method, calibration error, and electronic path error. In real condition, error of method is coming from incorrect evaluation of object emissivity, ambient temperature, atmospheric temperature, relative atmospheric humidity, distance from camera to object, and atmospheric transmission and radiance [41]. There is also contribution of detector noise in the camera.

Based on the general model from figure 2.3, error simulation from Infrared Thermography : Errors and Uncertainties (Minkina & Dudzik, 2009), and experiment, the total measurement error budget for a thermal imaging measurement on neonate inside an incubator can be summarized in equation:


(2.4)

where T_{error} is the total temperature error of the measurement, T_{obj} is the actual temperature of the object, ϵ is emissivity of the object, $T_{ambient}$ is the temperature of objects around the measured object, $T_{atmosphere}$ is the atmospheric temperature, d is distance of object from camera, ω is relative humidity of the environment, T_n is thermal noise from camera, T_l is thermal lens forming error, and T_c is the calibration and electronic path error.

From the error budget equation, it is clear that from the 5 environmental variables (emissivity, ambient and atmosphere temperature, distance, and humidity), most contribution is coming from the emissivity and ambient temperature. However, as the emissivity of human body is known, emissivity setting error would be minimal, leaving ambient temperature as the major error contributor.

2.2. Optical Flow Algorithm

Optical flow is the movement of objects or other feature points like edges, surfaces, etc. in a video source caused by relative motion between the observer and the observed region [43]. This can be observed as change of pixel colour or brightness. This means that optical flow is the apparent motion of individual pixels on the image frame. This can be used to get a rough estimate of physical motion on the observer's plane of view. However, most methods that compute optical flow assume that the colour intensity of a pixel is invariant under the displacement from one video frame to the next. This means that optical flow can be expressed in

$$I(x, y, t) = I(x + dx, y + dy, t + dt) \quad (2.5)$$

where $I(x,y,t)$ is the pixel intensity of a point (x,y) on a frame at a given time (t) . Assuming that there is only small intensity change in the pixels between two consecutive frames, equation 2.5 can be approximated using Taylor series as

$$I(x + dx, y + dy, t + dt) = I(x, y, t) + \frac{\partial I}{\partial x} dx + \frac{\partial I}{\partial y} dy + \frac{\partial I}{\partial t} dt + \sum_{n=2}^{\infty} \frac{1}{n!} \left[\left(\frac{\partial}{\partial x} dx + \frac{\partial}{\partial y} dy + \frac{\partial}{\partial t} dt \right)^n I \right] \quad (2.6)$$

Then, truncating the higher order terms results in:

$$\frac{\partial I}{\partial x} dx + \frac{\partial I}{\partial y} dy + \frac{\partial I}{\partial t} dt = 0 \quad (2.7)$$

Dividing equation 2.7 w.r.t. dt can be approximated by:

$$\Rightarrow \frac{\partial I}{\partial x} u + \frac{\partial I}{\partial y} v + \frac{\partial I}{\partial t} = 0 \quad (2.8)$$

where $u = \frac{dx}{dt}$ and $v = \frac{dy}{dt}$, giving us the relative speed of the pixel intensity along each axis. $\frac{\partial I}{\partial x}$, $\frac{\partial I}{\partial y}$ and $\frac{\partial I}{\partial t}$ are the frame's gradients along their respective axes. This gives a good approximation of movement and/or direction of an object from an observer's point of view without using object detection. But u and v are unknown variables and they are part of only one equation making the solution incomplete. However, there are methods to address this issue. There are two different types of optical flow algorithms based on computational intensity; sparse and dense optical flow. Sparse optical flow calculates the flow vectors of special features like edges or user selected feature points on a frame. It will be tracking the pixel intensity of the selected points on the frame. It is not always accurate but fast and easy to compute. Implementations of sparse optical flow include the Lucas–Kanade method, the Horn–Schunck method, the Buxton–Buxton method etc. Dense optical flow gives the flow vectors of the entire frame i.e. all pixels are given a flow vector. Despite of having higher accuracy, it is slow and computationally expensive. One example of dense optical flow is the Gunnar Farneback algorithm.

2.2.1. Gunnar Farneback Optical Flow Algorithm

Gunnar Farneback Algorithm is a dense optical flow algorithm that uses polynomial expansion to approximate the neighbourhood of each pixel [42]. It estimates the motion, or displacement, field from only two frames and tries to compensate for the background motion. A local signal model can be expressed in a local coordinate system as,

$$f_1(x) = x^T A_1 x + b_1^T x + c_1 \quad (2.9)$$

where A_1 is a symmetric matrix, b_1 a vector and c_1 a scalar. They are the global approximation coefficients of an image. Let us construct a new signal f_2 by a global displacement by d :

$$f_2(x) = f_1(x - d) = (x - d)^T A_1 (x - d) + b_1^T (x - d) + c_1 \quad (2.10)$$

$$= x^T A_1 x + (b_1 - 2A_1 d)^T x + (d^T A_1 d - b_1^T d) + c_1 \quad (2.11)$$

$$= x^T A_2 x + b_2^T x + c_2 \quad (2.12)$$

$$\Rightarrow A_2 = A_1 \quad b_2 = (b_1 - 2A_1 d) \quad c_2 = (d^T A_1 d - b_1^T d) + c_1 \quad (2.13)$$

Looking at equation 2.13, it is possible to solve for d ; given A_1 is non-singular

$$2A_1 d = (b_2 - b_1) \quad \Rightarrow \quad d = \frac{1}{2} A_1^{-1} (b_2 - b_1) \quad (2.14)$$

Ideally from equation 2.13 $A_1 = A_2$ but in real applications, the average of the two is used for a good approximation. Instead of taking the global coefficients, $A_1(x)$, $b_1(x)$ & $c_1(x)$ would be the local approximation coefficients. This gives the following equations,

$$A(x) = \frac{A_1(x) + A_2(x)}{2} \quad (2.15)$$

$$\Delta b(x) = (b_2(x) - b_1(x)) \quad (2.16)$$

This can be expressed as,

$$A(x)d(x) = \Delta b(x) \quad (2.17)$$

where $d(x)$ indicates that the global displacement d in equation 2.10 is replaced by displacement field varying spatially. This is done assuming that the local polynomials in the two frames are equal except for a certain displacement. The spatial variation in the polynomial expansions will introduce errors in the constraints in equation 2.17. However, for small displacements the error is not problematic, but larger displacements increase the problem. This can be solved when a priori knowledge about the displacement field is known i.e. comparing the first signal polynomial at x to the second signal polynomial at $x + \hat{d}(x)$, where $\hat{d}(x)$ is the a priori displacement field. Then the relative displacement can be estimated between the real value and the rounded a priori estimate, giving the following equations,

$$\hat{x} = x + \hat{d}(x) \quad (2.18)$$

$$A(x) = \frac{A_1(x) + A_2(\hat{x})}{2} \quad (2.19)$$

$$\Delta b(x) = (b_2(\hat{x}) - b_1(x)) + A(x)\hat{d}(x) \quad (2.20)$$

2.2.2. Pyramid Scaling in Optical Flow

In order to filter out the small amplitude noise, optical flow also performs scaling down the image or frame in lower resolutions to only respond to the major changes as shown in fig2.4 [43]. The process of scaling an image to lower resolutions while parallelly considering the original resolution is called pyramid scaling. A scaling factor (≤ 1) decides the fraction by which the image resolution is reduced i.e. for 0.5 scaling factor, resolution of the image halves at every level or layer. The number of layers decide on the level to which the scaling will be performed.

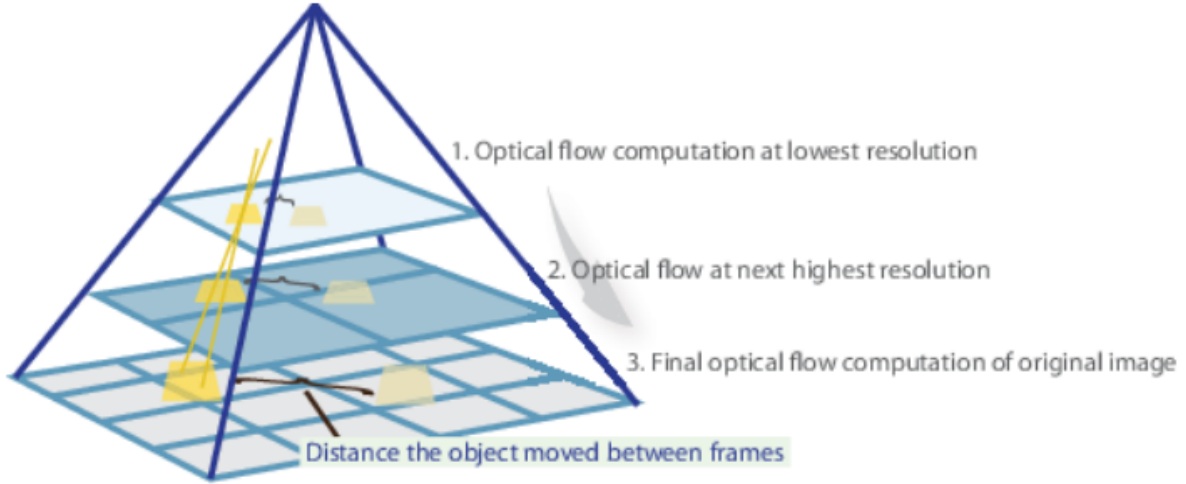


Figure 2.4: Pyramid Scaling for Optical Flow [44]

In pyramid scaling, the image is being represented by image pyramid, with the lowest pyramid level is the original image [43]. The image in higher pyramid levels can be defined as:

$$\begin{aligned}
 I^L(x, y) = & \frac{1}{4} I^{L-1}(2x, 2y) + \\
 & \frac{1}{8} (I^{L-1}(2x-1, 2y) + I^{L-1}(2x+1, 2y) + I^{L-1}(2x, 2y-1) + I^{L-1}(2x, 2y+1)) + \\
 & \frac{1}{16} (I^{L-1}(2x-1, 2y-1) + I^{L-1}(2x+1, 2y+1) + I^{L-1}(2x-1, 2y+1) + I^{L-1}(2x+1, 2y-1))
 \end{aligned} \quad (2.21)$$

Where I is the image and L is the pyramid level.

Practical maximum L values are 2, 3, or 4. For an image of 640x480, the fourth pyramid image will have size of 40x30, and it does not have any benefit to go beyond level 4.

Then, highest pyramid level is processed with optical flow to create initial guess flow vector g^L , which consists of x and y component (g_x^L and g_y^L). The flow vector is used to calculate pixel displacement vector d^L , which also consists of x and y component (d_x^L and d_y^L), that minimizes the matching error function between 2 consecutive image ϵ^L :

$$\epsilon^L(d_x^L, d_y^L) = \sum_{x=u_x^L-\omega_x}^{u_x^L+\omega_x} \sum_{y=u_y^L-\omega_y}^{u_y^L+\omega_y} (I^L(x, y) - I^L(x + g_x^L + d_x^L, y + g_y^L + d_y^L))^2 \quad (2.22)$$

Where $u = u_x, u_y$ is a point in the image I and ω_x and ω_y is the neighborhood integration window size.

Moving down one level at a time, the new initial guess of the flow vector can be expressed as:

$$g^{L-1} = 2(g^L + d^L) \quad (2.23)$$

Then, the pixel displacement vector d^{L-1} can also be calculated, until L reaches 0, which is the original image. With this technique, calculation of d^L can be kept as a very small number while computing high overall pixel displacement, means less number crunching.

2.3. Feature Point Detection and Matching

2.3.1. Image Feature Detectors and Descriptors

In order to compare similarities or correspondences between multiple images, it is required to isolate a set of distinct features between these images in order to be able to classify and compare them. Feature point detection is a low-level image processing operation which means that it is usually the first operation on an image that examines every pixel to see if there is a feature present; like edges and corners or smooth regions with similar features called blobs and ridges. There are two types of image features can be extracted from an image, as mentioned in [45];

- **Global Features:** These try to describe an image as a whole and can classify the property of all the pixels in the image; like colour histogram, texture etc into one multi-dimensional feature vector. This can be used to find images of similar nature. However, these cannot distinguish between background and foreground.
- **Local Features :** The image is represented based on its local structures or interest regions and some of its salient features. This includes a set of local feature descriptors/vectors that are affine and scale invariant. They are better suited for finding other occurrences of the similar objects or region of pixels in the images.

These relevant features points or keypoints are then converted into an affine, orientation and scale invariant feature vector representation for the image data around the detected features; providing **feature descriptors**. These descriptors are later used to match the similarities between different images. The purpose of local invariant features is to provide a representation that can efficiently match then with another image despite there being shifting, scale or orientation changes. In order to detect feature points invariant of scale, affine or orientation changes for the interest regions between images, there are methods that use a continuous filter kernel to check for distribution or gradient or looking for a maximally stable region around the detected feature points; as mentioned in [46]. Area around each keypoint that is considered for the descriptor is usually taken in a circular or elliptical pattern.

In order to make sure that the feature point detectors and descriptors work efficiently, the following properties [45] need to be satisfied;

- **Robustness:** to be able to detect the same feature points irrespective of shifting, rotation or noises.
- **Repeatability:** to be able to detect the same features of the same interest region repeatedly under different viewing conditions.
- **Accuracy:** to accurately localize the same image features in different images; especially for image matching tasks.
- **Generality:** to be able to detect features that can be used in different applications.
- **Efficiency:** to be able to detect features in images fast enough to support real-time applications.
- **Quantity:** to be able to detect all or most of the features in the image.

Some of the examples of commonly used image feature descriptor algorithms are;

1. Scale Invariant Feature Transform (SIFT): This algorithm consists of four steps [46];
 - (a) Estimate a scale space extrema using the Difference of Gaussian (DoG).
 - (b) Keypoints are localized and refined by removing the low contrast points.
 - (c) Orientation is estimated based on local image gradient.
 - (d) Generate descriptors for each feature point of image based on image gradient and the estimated orientation.

It is useful for cases like image rotation, affine transformations, intensity or perspective change.

2. Gradient Location-Orientation Histogram (GLOH): It is very similar to the SIFT descriptor, but uses log-polar coordinates for keypoints instead and then tries to reduce the size of the descriptor [47].

3. **Speeded-Up Robust Features Descriptor (SURF)**: it is an alternative to SIFT [46]; but much faster and more robust. The steps for this algorithm are;
 - (a) Instead of DOG averaging, squares are used for localizing keypoints since it is less complex and much faster.
 - (b) Uses a scale invariant blob detector around the detect a stable neighbourhood of pixels around the keypoints.
 - (c) Wavelet response for each of the keypoints' regions is taken in both horizontal and vertical directions and their responses are used for the feature point descriptors.

This also allows the detector to be parallely run on different image scales, making it capable of much faster performance.
4. **Binary Robust Independent Elementary Features (BRISK)**: This algorithm performs simple binary comparison test and uses hamming distance for comparison tests [45]. This means that the algorithm compares the pixel intensity around the detected feature points which gives sufficient information and provides with binary feature descriptors, which is faster and more efficient. The descriptors are then matched based on the hamming distance between them. This algorithm relies on a relatively small number of tests to represent an interest region as a binary string and also tends to yield higher recognition rates, provided there are no large in-plane rotations.
5. **Features from Accelerated Segment Test (FAST)**: It uses corner detection method to extract the feature points and is very suitable for real-time applications because of its higher speed [45]. The steps for this algorithm are;

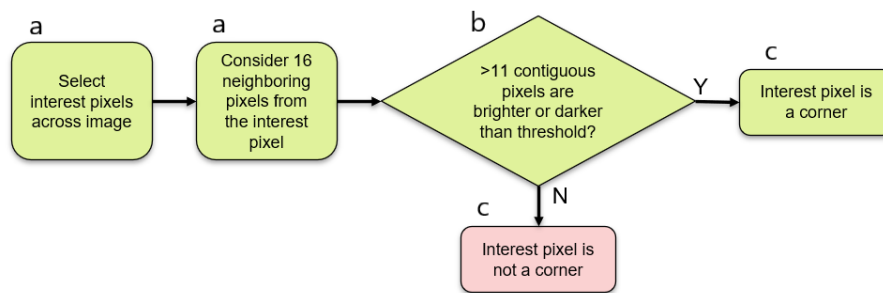


Figure 2.5: FAST algorithm flowchart

- (a) Select interest points across the image and take 16 pixels surrounding each of these points under consideration; pixels that would lie on the path of a circle with radius of 3 pixels drawn from each feature point.
- (b) In the 16-point set for each interest point, check if there are a set of continuous pixels that are either brighter or darker than the pixel intensity of the feature points by a set threshold value.
- (c) Only if the condition is satisfied, the interest point is taken as a corner. This process is iterated over all interest points or for all pixels in the image.

The performance of this algorithm depends on the threshold value and the limit for minimum number of continuous pixels that need to be considered for the corner test; usually around 12. This process however has some disadvantages;

- The algorithm does not work well if the limit for minimum continuous pixels is less than 12 because there will be too many insignificant pixel included as interest points.
- The order of testing the 16 neighbouring pixels also determines the speed of the algorithm.
- It does not have any orientation component or detects scaling.

6. Oriented FAST and Rotated BRIEF (ORB): It is a fusion of the FAST key point detector and BRIEF descriptor; both these algorithms contribute to ORB's computational speed and efficiency; as mentioned in [48]. The steps for this algorithm are;

- (a) Initially to determine the key points, it uses the FAST algorithm. Since FAST does not have any orientation or scaling features, ORB creates a scaled image pyramid; similar to the one in fig.2.4, where it contains the down sampled versions of the same image and the FAST algorithm is run on every level. This makes the detected key points scale invariant.
- (b) Orientation is assigned based on the levels of pixel intensity change around the key points. In ORB it is done by using intensity centroid where it is assumed that a corner's intensity is offset from its centre, and the vector between the two points may be used to impute an orientation. For this, the moments of order $(p + q)$ of a patch m_{pq} is calculated; which is defined as,

$$m_{pq} = \sum_{x,y} x^p y^q I(x, y) \quad (2.24)$$

where (x,y) is the pixel coordinates and $I(x,y)$ is the respective pixel intensity. With these moments, the intensity centroid is calculated as;

$$C = \left(\frac{m_{10}}{m_{00}}, \frac{m_{01}}{m_{00}} \right) \quad (2.25)$$

This can be used to construct the vector from the centre of the keypoint to the intensity centroid; giving the orientation of the patch as,

$$\theta = \text{atan2}(m_{01}, m_{10}) \quad (2.26)$$

This can be used to rotate the patch and compute the descriptor with rotation invariance.

- (c) BRIEF takes all keypoints found in the previous step and converts it into a binary feature vector of around 128–512 bits string so that together they can represent an object. Then, the image is smoothed by using a Gaussian filter to remove any high frequency noises. After the image is smoothed, a patch \mathbf{p} is taken and a binary test τ is performed; which is defined as,

$$\tau(p; x, y) = \begin{cases} 1 & : p(x) < p(y) \\ 0 & : p(x) \geq p(y) \end{cases} \quad (2.27)$$

where $p(x)$ is the intensity of **point** \mathbf{x} in the patch \mathbf{p} ; both x and y are points inside the same patch. The feature point is defined as a vector of \mathbf{n} binary tests:

$$f_n(p) = \sum_{1 \leq i \leq n} 2^{(i-1)} \tau(p; x, y) \quad (2.28)$$

As the performance of BRIEF falls off sharply for in-plane rotation of more than a few degrees, ORB uses another method to steer BRIEF according to the orientation of the keypoints. For a feature point with \mathbf{n} tests and key point coordinate (x_i, y_i) , a $2 \times n$ matrix is defined as;

$$S = \begin{cases} x_1, x_2, \dots, x_n \\ y_1, y_2, \dots, y_n \end{cases} \quad (2.29)$$

With the patch orientation θ and its corresponding rotation matrix R_θ , the steered version of the \mathbf{S} matrix; namely S_θ is defined as;

$$S_\theta = R_\theta S \quad (2.30)$$

Now the steered BRIEF operator can be written as;

$$g_n(p, \theta) = f_n(p) \mid (x_i, y_i) \in S_\theta \quad (2.31)$$

Using equation 2.31, a lookup table of pre-computed BRIEF patterns is generated with an angle increment of $2\pi/30 = 12^\circ$. As long as there is consistency in the keypoint orientation angle θ , the respective S_θ can be used for computing its descriptor.

ORB algorithm specifies the rotated BRIEF algorithm with the following steps:

- i. Run the test equation 2.28 against all available patches.
- ii. Order the results of the tests by their hamming distance from a mean value of 0.5, resulting in the vector T.
- iii. A greedy search is performed on all the values in vector T:
 - A. Remove the first test from T into the result vector R.
 - B. Remove the next test from T and compare it against all tests in R. The test is discarded if its absolute correlation is greater than a previously set threshold value. If not, then the test add to R.
 - C. Repeat the process until there are 256 tests in R. If there are no more tests in T and there are fewer than 256 tests in R, raise the threshold value and repeat the process.

2.3.2. Feature Matching

Once the features and their descriptors have been created from multiple images, they need to be matched in order to look for similarities between the images. In order to achieve that, a **matcher** is used in combination with the feature point detector to use the information provided by the descriptors and match the interest regions from the query image to the others.

The feature matchers commonly used along with the feature descriptors are;

1. **Brute-Force (BF):** This algorithm compares each feature point from the first image to every other feature point on the other image by calculating distance between the feature points; as mentioned in [45]. As the feature points are multi-dimensional vectors describing the aspects of their respective images, the Euclidean distance calculated between them is calculated. However, if the descriptors are binary in nature like BRIEF, then the Hamming between them is calculated. After that, the points are sorted in ascending order based on distance. A match between two feature points is viable only when both points are the best matches for each other. This means that for any feature point p in the first image and feature point q in the second, p and q are a valid match with each other when q has the shortest distance with p of all points in the first image and p has the shortest distance with q of all points in the second image.
2. **Fast Library for Approximate Nearest Neighbours (FLANN):** This algorithm is optimized to be much faster than Brute-Force matcher; as mentioned in [49]. Instead of looking for the best match like the BF matcher, FLANN only finds a nearest neighbour. It builds a **k-d tree** of the feature points that will be used to search for an approximate neighbour. A **k-d tree** is a binary search tree, where each node of the tree is a k_{th} dimensional vector. This means that the matches provided by FLANN are fast but less accurate as compared to BF matcher.

BF matcher will provide accurate results but it will perform an exhaustive search comparing every feature point between the images, making it slow for large number of feature points. FLANN is much faster than BF but with a trade-off in accuracy. For data sets much larger than 1000 feature points, it would be more efficient to use FLANN as a matcher. Otherwise, BF matcher is a better approach.

2.4. TCP/IP Communication

Transmission Control Protocol/Internet Protocol (TCP/IP) is a reliable, heavy-weight and ordered communication protocol used to connect devices over an IP network, as mentioned in [50]; it consists of a large overhead/header of around 20-80 bytes; but most implementations have 40 bytes header. It is a connection-oriented protocol, which means that a connection needs to be established between the communicating devices i.e. the client and the server before transmitting data and should close after transmitting. In order to establish a connection, TCP/IP performs a three-way handshake [50]. The server is passive open; looking for connection requests from clients if not already established. When a connection is formed between a client to a server;

1. The client first sends a synchronize (SYN) bit set to the server requesting to start communication and what sequence number the client will use for its segments.

2. The server then responds to the client's request with SYN and the acknowledge (ACK) signal set, acknowledging the message from the client and informing its own sequence number it will be using to the client.
3. The client finally sends another ACK bit set to acknowledge the server's segment and then the data transfer process begins.

The TCP/IP model consists of four layers [50];

- **Application Layer** : It's responsible for implementing the communication part of the program. It includes node-to-node communication, synchronizing, user-interface specifications etc. Some of the protocols present in this layer are: Hypertext Transfer Protocol (HTTP), File Transfer Protocol (FTP), Secure Shell (SSH), etc.
- **Transport Layer** : It is responsible for the reliability of the link over the network and maintaining it through methods like flow control, correction of data, multiplexing, etc.
- **Internet Layer** : It is responsible for dealing with the packets and providing a functional method for transferring packets by connecting to independent networks for data transfer.
- **Network Access Layer** : It is responsible for determining how the data should be sent physically between devices over the same network. It is the lowest layer in the model.

The structure in fig.2.6 shows the format used for a TCP/IP message segment. It consists of around five or six 32 bits / 4 bytes long words of header, but the Options and Padding in the header can go upto 40 bytes depending on the connection parameters. As mentioned earlier, the commonly used size of the header is around 40 bytes; with Options and Padding around 20 bytes. The checksum in each header segment is used by the server to verify that the data is undamaged. If the data received is undamaged, the server sends a positive acknowledgment back to the client confirming a successful transfer. If the data is damaged, the server discards it and after a timeout period, the client will transmit the same data again until it receives the positive acknowledgment.

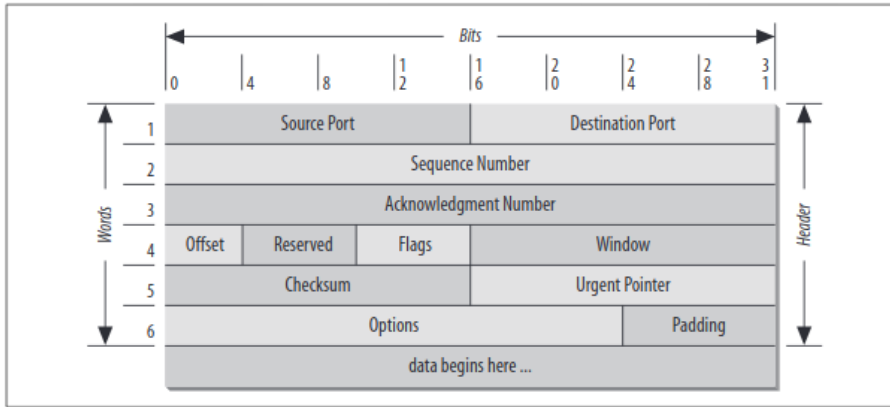


Figure 2.6: TCP/IP Segment Format[50]

With 40 bytes header, it is important to reduce overhead; it is the ratio between the header size to the message size. The maximum segment size (MSS) for a TCP/IP is the largest amount of data that the protocol can transport over the network; it is usually around 1460 bytes. Payload size larger than that is either discarded or segmented into multiple TCP segments. If the data payload is fragmented into multiple segments, then each segment gets its own header which adds extra 40 bytes for each segment.

$$\text{Overhead}(\%) = 100 * \text{INT}[(\text{Payload Size} / \text{MSS}) + 1] * (\text{Header Size}) / \text{Payload Size} \quad (2.32)$$

The overhead that constitutes the message packets after segmentation is mentioned in equation 2.32; which is only valid if the payload is not an integral multiple of the MSS. If the payload size is an integral multiple of the MSS, then it achieves the lowest possible overhead depending on the header size and the MSS.

$$\text{Lowest Overhead Possible}(\%) = 100 * \text{Header Size} / \text{MSS} \quad (2.33)$$

For a header size of 40 bytes and MSS of 1460 bytes, the lowest overhead that can be achieved is **2.7397%**. As seen in fig.2.7; for the formerly mentioned parameters, the overhead forms a saw-tooth shaped function where it dips to **2.7397%** when the package size is an integral multiple of MSS(1460 bytes). This is why it is preferable to have a payload size.

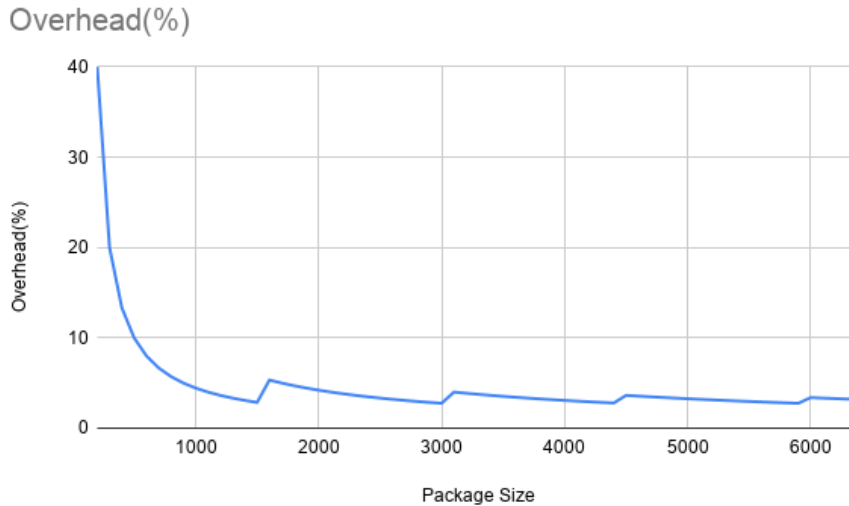


Figure 2.7: Overhead(%) for different message size

2.5. Infection (Sepsis)

Neonatal infection/sepsis proved to be a serious problem. In response to infection, the body releases anti-inflammatory substances that can damage healthy organs. It is especially dangerous to preterm infants, as their organs are not fully developed. Hence, it is important to treat sepsis as soon as the baby is diagnosed.

The first gateway to treat infection or sepsis in preterm infant is detecting and diagnosing it accurately. Once diagnosed, infection management with antibiotics can be administered to the baby. However, sepsis diagnosis is proven to be a difficult task. The clinical characteristics of neonatal sepsis are non-specific and difficult to differentiate to other conditions [51, 52].

The golden standard on diagnosing a sepsis is blood culture. Blood sample from the suspected baby is cultured to let the bacteria causing the sepsis grow. Then, the blood is tested to identify the bacteria, if there is any. However, this method takes time, 2-3 days after receiving blood sample, which is undesirable for timely treatment. Even more, there are still several problems regarding this diagnostic method and even the result may not be reliable. Antibiotic usage during pregnancy delivery, blood volume, and laboratory capabilities can affect the result of the diagnosis [52–54]. Based on interview with a neonatology doctor, blood culture produces only 10-20% positive result from all babies with suspected sepsis cases, even when the baby is diagnosed with sepsis by the doctor.

Other blood features, such as white blood cell count, proteins, and other bio-markers, are also studied for indication of sepsis. Unfortunately, most blood features are not sensitive enough to be in routine clinical use [55]. Doctor interview stated that those biomarkers are not definitive enough yet to be a standard diagnosing method. Moreover, it cannot be generalized that all hospitals to have access to laboratory tests, especially in developing countries [52].

Clinical symptoms are usually the first signs to be used to diagnose a disease, however, as discussed, neonatal sepsis has non-specific and varying symptoms. It means that the symptoms may indicate diseases other than sepsis, which would have to be treated differently. Even though the symptoms are not definitive, in the practice, combination of several symptoms on the baby can be concluded in sepsis diagnosis (most commonly

defined as clinical-sepsis, rather than proven-sepsis as in blood cultured proven), even before the result of blood culture test is out. This is also confirmed by a neonatology doctor, as she does not want to take any chance of missing a sepsis case. After being diagnosed, antibiotic treatment starts immediately.

2.5.1. Sepsis Risk and Clinical Symptoms

Since blood culture is taking a lot of time to give result and sepsis has non-specific symptoms, diagnosing a sepsis based on clinical symptoms alone usually depends on the experience of the doctor. To help the doctor, there is a guideline in the hospital where the research is done, to determine if a baby needs to be treated for sepsis. This guideline includes maternal risk, clinical symptoms, and decision flow of sepsis diagnosis. The guideline (in Dutch) and translation are included in the appendix .1.

The clinical symptoms mentioned in the guideline are similar to symptoms reported in researches, which are respiratory distress, lethargy, fever, hypothermia, poor feeding, apnea, tachypnea, grunting, tachycardia, bradycardia, etc [40, 55].

2.5.2. Core-peripheral Temperature Difference

Other than widely known symptoms of sepsis above, researchers are exploring other symptoms to hopefully discover specific symptom for sepsis. One promising symptom found is core-peripheral temperature difference (cpTD) of the baby. Core temperature of the baby is defined as rectal, axillary, or chest or back skin temperature of the baby. Peripheral temperature is defined as temperature of foot sole of the baby. Inside incubator, where the environment temperature is set to optimum, the difference between core and peripheral temperature of neonate should not be more than 2 °C. Several studies found and agree that cpTD of more than 2 °C for over 3-4 hours or more, even with adjustment to incubator temperature, is a strong indication of neonatal sepsis [56–61]. Result from the studies showed that cpTD has high sensitivity (65-80%) and specificity (82-86%) for neonatal sepsis. With such high sensitivity and specificity, this symptom could be introduced and added to the list of symptoms for sepsis detection, and may become primary screening symptom for neonatal sepsis.

2.6. Machine Learning for Sepsis Prediction

Machine learning (ML) is one of many applications of artificial intelligence that provides a statistical model that learns and improves from experience in the learning process without programmed explicitly. In the learning process, the model is being fed with training data set and adjust the model itself based on the pattern in the data. Once trained, the model would be able to receive new input data and give the output based on the experience of the learning process. ML models can be divided into three groups, supervised learning, unsupervised learning, and reinforcement learning. In supervised learning, each training data set has input data and known output. This is called labelled training data. Supervised learning is usually used for classification and regression problems. On the other hand, unsupervised learning would have only input data as the training data. The model is used to group similar input data or find structure from the input data. Lastly, reinforcement learning deals with known system environment and goal, without knowing the perfect solution. This specific learning is used to find the best sequential decision making in certain system state. In this research, supervised learning model is better suited, because a classifier model is needed. The model will be given input of vital signs from the neonate and it will classify whether the neonate is having sepsis or not.

Disease prediction or early detection using machine learning has been widely explored in the medical field [62]. However, almost all studies for sepsis prediction had adults as the research subject [63]. Many studies used different type of machine learning model, with the most common models are **Naive Bayes (NB)**, **Support Vector Machine (SVM)**, **Decision Tree (DT)** or **Random Forest (RF)**, and **Logistic Regression (LR)**.

2.6.1. Logistic Regression

Logistic regression is a statistical model that uses logistic function to model binary dependent variable. The dependent variable has two possible values, usually labelled as 1 and 0 or pass or fail. The logistic regression model itself only models the probability of output based on the input. To make it a classifier, a cutoff value is chosen and the point with probability greater than the cutoff value is classified as pass or 1 and the point below as fail or 0.

The logistic regression model can be written as:

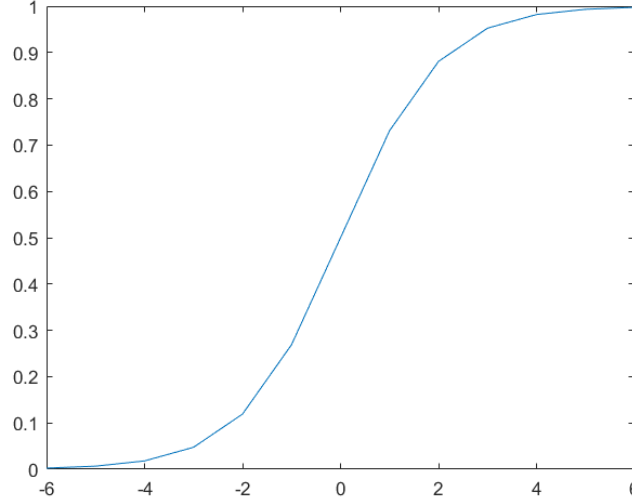


Figure 2.8: Standard logistic function: $y = \exp(x) / (1 + \exp(x))$

$$F(z) = \frac{1}{1 + e^{-z}} \quad (2.34)$$

where $z = \omega_0 + \omega_1 \cdot x_1 + \omega_2 \cdot x_2 + \dots + \omega_n \cdot x_n$.

$\omega_0, \dots, \omega_n$ are the regression coefficient of the model and will be calculated using Maximum Likelihood Estimation (MLE) and x_0, \dots, x_n are the features of input point of the dataset. $F(z)$ will calculate the probability of the binary outcome from the input point.

2.6.2. Naive Bayes

Naive Bayes classifier is a simple probabilistic classifier using Bayes' theorem with independence (naive) assumptions between the features. Bayes' theorem calculates the probability of an event occurring given the condition that other event has already occurred. It is usually written as:

$$P(A|B) = \frac{P(B|A)P(A)}{P(B)} \quad (2.35)$$

where A and B are the events mentioned. $P(A|B)$ means that the probability of event A occurs if event B has occurred. $P(A)$ and $P(B)$ are the probability of event A and B, respectively, occurs. Bayes' theorem can be applied to the machine learning data set as:

$$P(y|X) = \frac{P(X|y)P(y)}{P(X)} \quad (2.36)$$

where y is the class variable and X is the features of the dependent variable ($X = (x_1, x_2, \dots, x_n)$). Then, it can be expressed as [65]:

$$P(y|x_1, \dots, x_n) = \frac{P(y) \prod_{i=1}^n P(x_i|y)}{P(x_1|y)P(x_2|y)\dots P(x_n|y)} \quad (2.37)$$

Then, because the denominator remains constant for one input, it can be removed and rewritten as:

$$P(y|x_1, \dots, x_n) \propto P(y) \prod_{i=1}^n P(x_i|y) \quad (2.38)$$

Now, to make a classifier model, the probability of all possible values has to be found for class y given the set features of the input X . This can be expressed as:

$$y = \operatorname{argmax}_y P(y) \prod_{i=1}^n P(x_i|y) \quad (2.39)$$

Finally, the calculations left are the $P(y)$ and $P(x_i|y)$. If there are only two possible classes of y , the result of the calculation for both classes are compared. The input X then will be classified as the class with greater probability.

2.6.3. Support Vector Machine

SVM separates the patterns of two classes by constructing a hyperplane or set of hyperplanes in one or several dimensional space. The hyperplane can be written as $\tilde{w} \cdot \tilde{x}_i - b = y_i$, where \tilde{w} is the normal vector to the hyperplane, b is the bias, \tilde{x} is the point of each data set, and y is either 1 or -1, indicating the class to which the point belongs. If the two-class data set are linearly separable, there will be a hyperplane that passes between the two classes evenly. Given that there are no points on this hyperplane, a buffer zone can be created, as a translated version of the hyperplane itself. The width of this buffer zone is called the margin and can be calculated to as $\frac{2}{\|\tilde{w}\|_2}$. Whether a hyperplane correctly classifies a point can be written as:

$$\max(0, 1 - y_i(\tilde{w} \cdot \tilde{x}_i - b)), i = 1, \dots, n \quad (2.40)$$

If a point is correctly classified, the equation will equal 0, and a positive value otherwise. Then the goal of a good classifier is to minimize the equation:

$$\left[\frac{1}{n} \sum_{i=1}^n \max(0, 1 - y_i(\tilde{w} \cdot \tilde{x}_i - b)) \right] + \lambda \|\tilde{w}\|^2, \quad (2.41)$$

where λ determines the trade-off between increasing the size of margin and ensuring that the \tilde{x}_i is classified on the correct side of the margin.

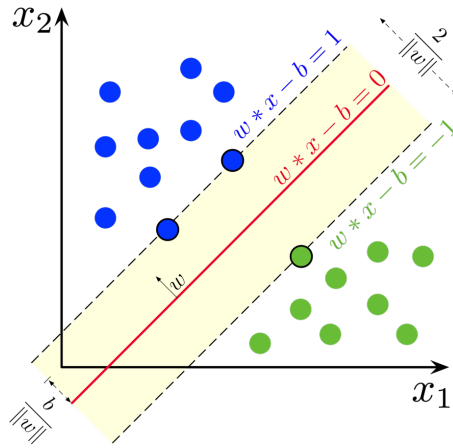


Figure 2.9: Maximum-margin hyperplane and margin for an SVM trained on two classes. [66]

2.6.4. K-Nearest Neighbour

KNN is a supervised learning algorithm and can be used for regression or classification problems. It is also categorized as lazy learning method, which means it does not calculate a predictive model from training data, instead, it tries to predict the result locally based on the whole available data set at the time the query is made. It relies on the value of the nearest neighbours and the distance from the data it wants to predict. Since distance to each neighbour is important, normalizing data set will improve the performance of this model type. Without normalization, features with different range would affect the prediction in different weight.

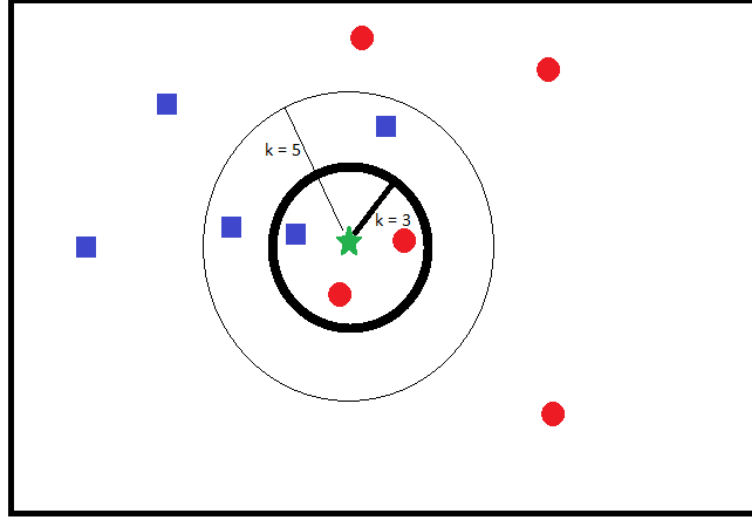


Figure 2.10: Example of KNN classification

To make a prediction, KNN model will use the entire data set and place every data in a multidimensional space. Each dimension represent each feature available from the data set. Then, k number of neighbours, which is defined by the user, from the test data in the space is retrieved. These neighbours will determine the label of the test data. It can use majority voting from the neighbours or another option also to include the distance of the neighbour as a factor ($1/\text{distance}$ factor to the label calculation).

To determine the nearest neighbor, many distance metrics can be used, e.g. Euclidean, Manhattan, Hamming, etc. Euclidean distance for example, measures distance of straight line between 2 points in Euclidean space, as follows:

$$d(x, y) = \sqrt{\sum_{i=1}^n (x_i - y_i)^2} \quad (2.42)$$

While Manhattan distance measures distance as sum of absolute differences of Cartesian coordinates, as follows:

$$d(x, y) = \sum_{i=1}^n (x_i - y_i) \quad (2.43)$$

These distance metrics will affect how the KNN algorithm choose the k -nearest neighbors, hence possibly producing different results.

2.6.5. Decision Tree and Random Forest

Decision tree learning is one of the predictive modelling machine learning algorithm using decision tree to make a conclusion of a problem from observations of the input variables. It can be used for classification or regression problems. Decision tree consists of nodes, branches, and leaves. Node is the test for the value of the attribute. Branch corresponds to the result of the node and connects to other node or leaf. Leaf is the terminal node where the outcome is predicted (label or distribution).

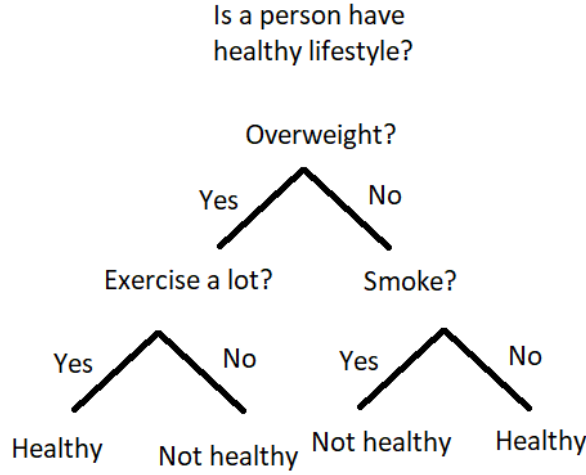


Figure 2.11: An example of decision tree

Decision trees are using recursive partitioning method or known as divide and conquer, as they split the data into subsets repeatedly until the algorithm determines that the subset data are homogenous or other stopping criteria has been met. To create a decision tree classifier, it starts by splitting the data at the tree root with feature that results in highest information gain (reduction in uncertainty towards the final result). Then, the data will be split again in an iterative process, until the samples in each leaf belong to a same class. However, this would likely cause overfitting if the depth of the tree is not limited.

Random forest is an ensemble learning method, means using multiple learning algorithm to get better predictive value, by constructing multiple decision trees and combining the output of each tree with average or majority voting. By using more trees, random forest can reduce the risk of overfitting from the decision tree model. This is because of two key point of random forest, random sampling of training data on each tree of the forest and random subsets of features considered in splitting the nodes. The idea is by training different trees train using different training data and each tree would have high risk of overfit to the respective training data, when combined, the forest will have lower risk of overfit.

2.6.6. Adaboost

Adaboost also uses ensemble method to solve classification and regression problem. Different from random forest, adaboost is a sequential learner, which means a new weak learner is created to learn and improve the accuracy of previous learners rather than generating weak models in parallel (parallel learner). A weak learner is added to the group of previous learners in order to reduce the error until the training data is perfectly fitted or maximum number of learners has achieved. Usually, adaboost uses short decision tree called stump as the weak learner.

Adaboost can also be written in form of:

$$F_T(x) = \sum_{t=1}^T f_t(x) \quad (2.44)$$

where $f_t(x)$ is the weak learner used to create the adaboost algorithm and x is the input to the algorithm.

In the iterative steps of adding new weak learners, adaboost will adjust the weight of each training data in the data set. It will decrease the weight of correctly classified data and increase the weight of wrongly classified data. It highlights the data which has not been correctly classified in the previous step, hence will force the next weak learner to focus more on the wrongly classified data. Once the wrongly classified data is minimal or the maximum number of iterations has been achieved, the iteration stops. Then, each weak learner in the group will be weighted based on the performance to the training set. The final model then will classify the test data with the majority voting calculated from all weak learners with their respective weight.

The adaboost algorithm building process to minimize classifying error $E_t(x)$ can be written in form of:

$$E_t(x) = E[F_{t-1}(x) + f_t(x)] \quad (2.45)$$

where $f_t(x)$ is the weak learner assessed to be added to the final classifier.

2.6.7. Gradient Boosting

Gradient boosting is similar to adaboost in which it is stage-wise additive model using weak learners to create a strong learner. The difference in both is how each model optimize the next addition of weak learner. While adaboost increases the weight of misclassified data for the optimization method, gradient boost tries to minimize loss function, which is a measure on how good the model is in fitting the training data. The loss function could be user specified; hence gradient boosting is more flexible than adaboost.

The building process of gradient boosting can be written in form of:

$$F_{t+1}(x) = F_t(x) + f_t(x) \quad (2.46)$$

or equivalently:

$$f_t(x) = F_{t+1}(x) - F_t(x) \quad (2.47)$$

where $F_t(x)$ is the current imperfect model, $f_t(x)$ is the weak learner considered to be added to the model, and $F_{t+1}(x)$ is the model after the weak learner is added. $f_t(x)$ will be fitted so that the residual $F_{t+1}(x) - F_t(x)$ is minimal. Each addition of weak learner will correct the error of the previous version of the model.

Another difference between the two is that in predicting the test data, all learners in the gradient boosting group have equal weight rather than adjusted weight based on each individual learner accuracy. This is because the loss function is calculated from the whole group rather than each and every weak learner. Another small different is that usually adaboost uses decision tree with only 1 split, while gradient boosting could use larger tree up to 8 splits, but still remains weak.

2.6.8. Feature Selection

Other than machine learning model, feature selection plays important part in determining the performance of the machine learning prediction. Feature selection is the process of selecting subset of important features for the model. Feature selection is used in order to simplify the model, shorten the training times, reduce the dimensional of the model, and generalize the model by reducing overfitting. This is because it is assumed that in the overall data, there may be redundant and irrelevant features which can be removed without sacrificing much information.

There are mainly three categories of feature selection method, wrapper, filter, and embedded;

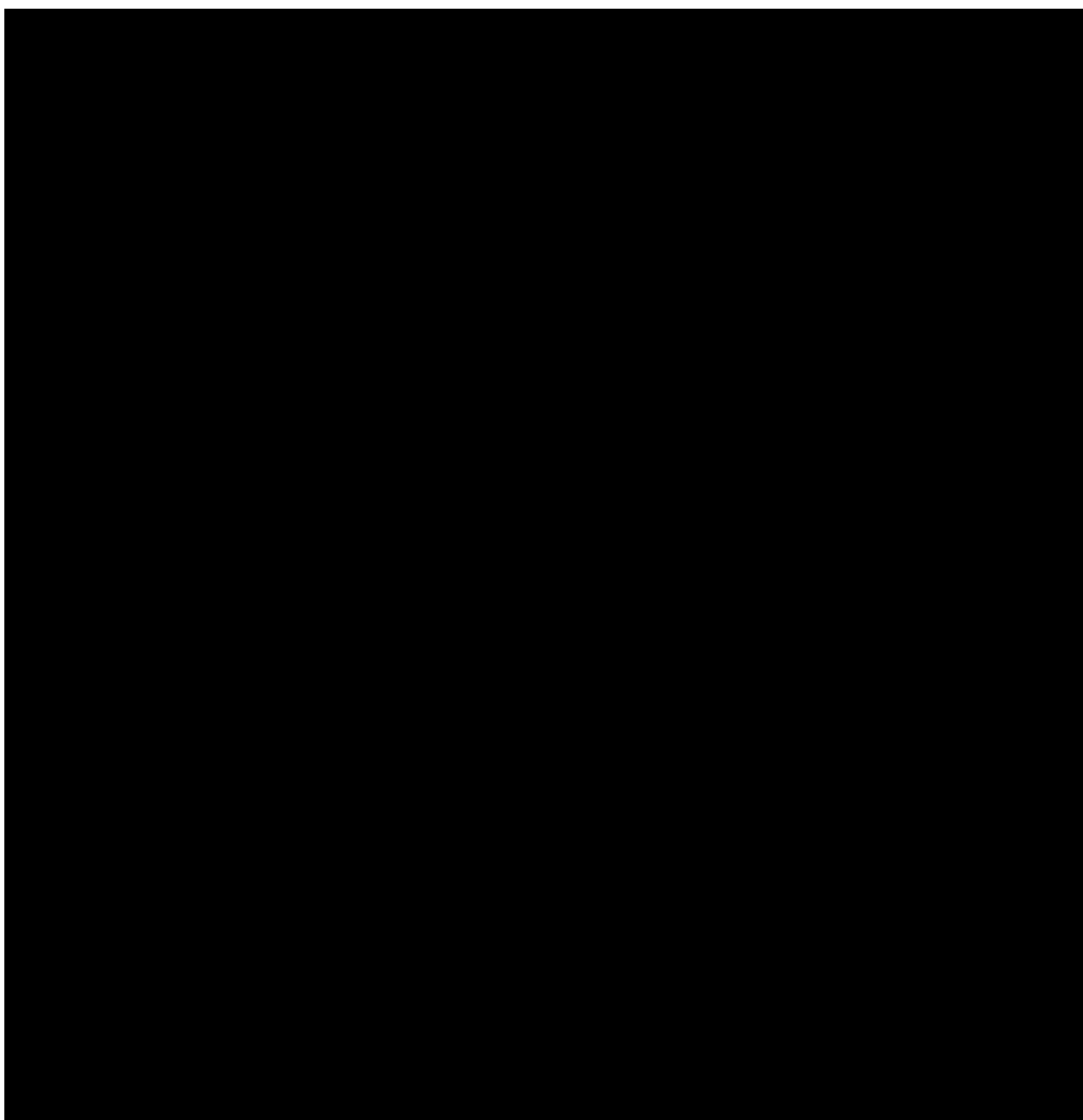
- **Wrapper** method use the model to score the feature subsets. Every feature subset is scored and then compared to find the most effective subset. This method is the most computationally expensive because of running the model on every combination of features. Examples of this method are forward selection, backward elimination, and genetic algorithm.
- **Filter** method use proxy measure to score the feature subsets. Common measures include Pearson correlation coefficient, mutual information, significance test, and many more. This method is less computationally expensive but usually result in lower prediction performance than wrapper method.
- **Embedded** method performs feature selection inside the model construction, by penalizing feature weight inside the model if the feature is calculated to be not important. The most common embedded methods are L1 (known as LASSO) and L2 (known as ridge regression) regularization. In term of computational complexity, embedded method usually comes between wrapper and filter method.

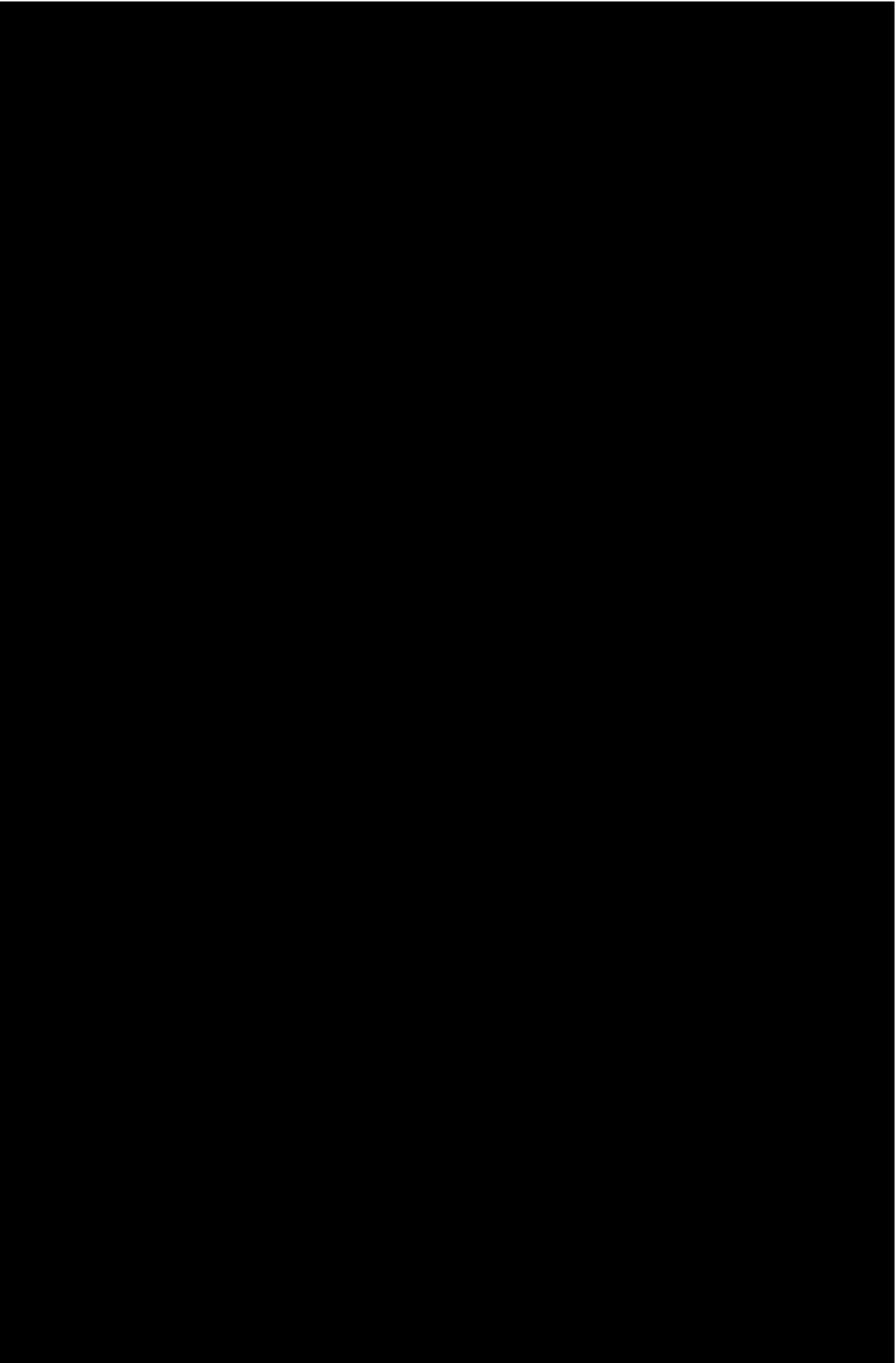
In the disease prediction studies using machine learning, researchers explored different sets of features for different diseases, such as electrocardiogram (ECG) wave record for heart disease and blood tests result for

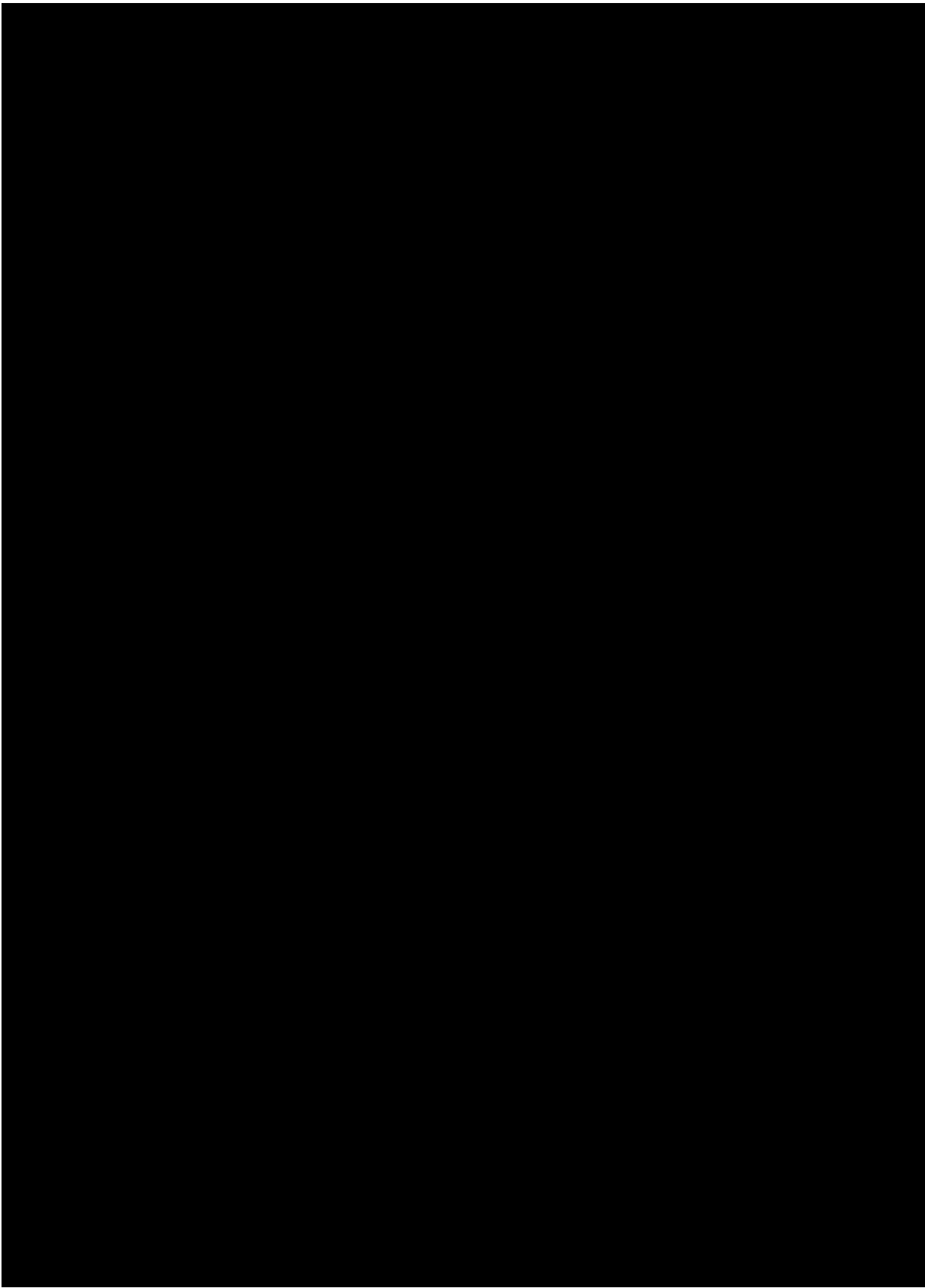
diabetes. For sepsis prediction, wide array of features was explored, including vital signs (heart rate, respiratory rate, temperature, etc), blood cell and protein count, demographic data, and observation from the doctor [63]. There are only few studies about neonatal sepsis prediction using machine learning and the features included in the studies comprise clinical assessment, comorbidities, laboratory tests, vital signs, need of support, ECG recording, and heart rate variabilities [64, 67, 68]. Broad spectrum of features was explored because of the fact that neonatal sepsis symptoms are non-specific. Thus, by expanding the search area, the algorithms were expected to find and select the best features representing neonatal sepsis and predict the sepsis accurately.

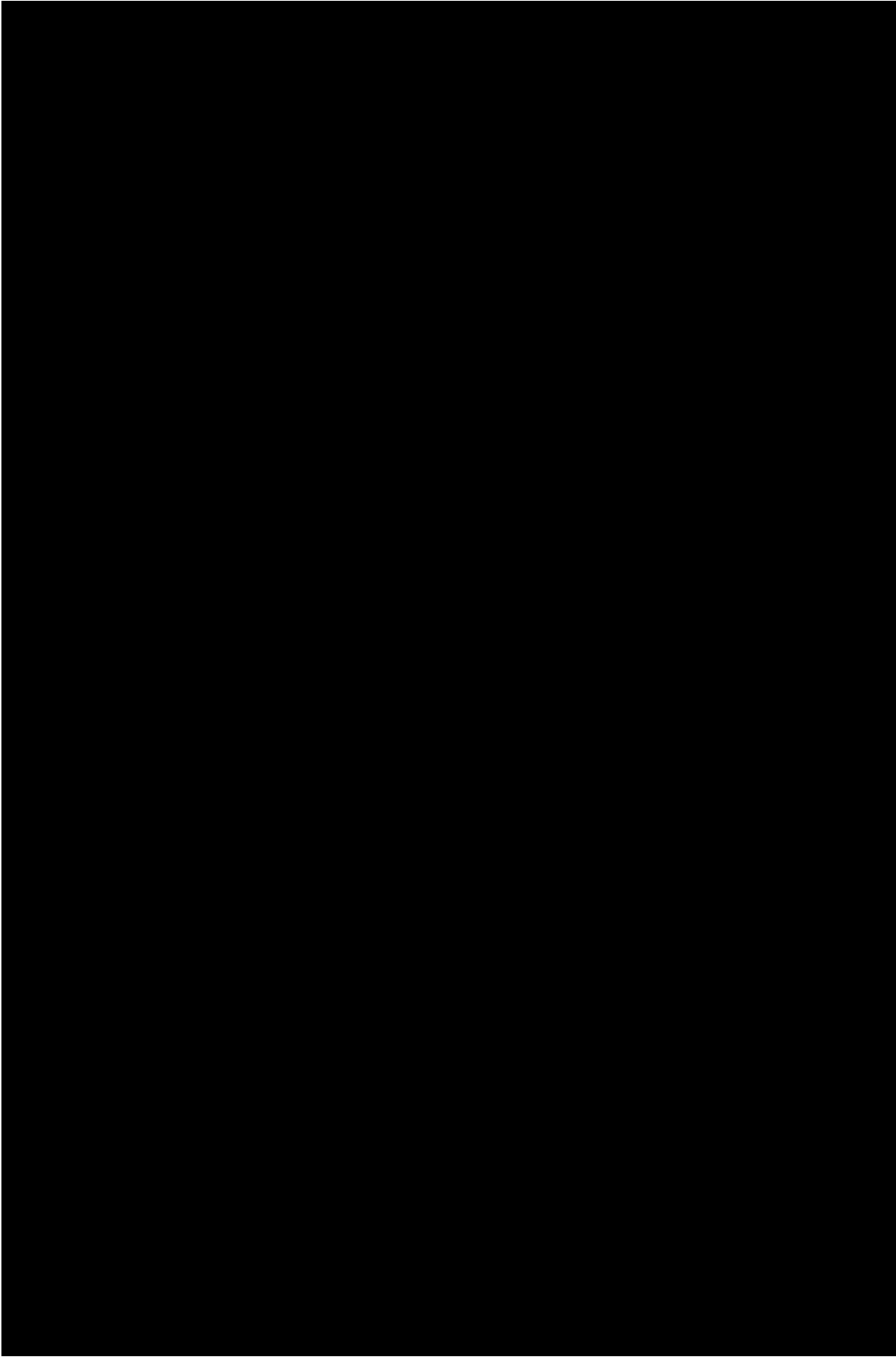
3

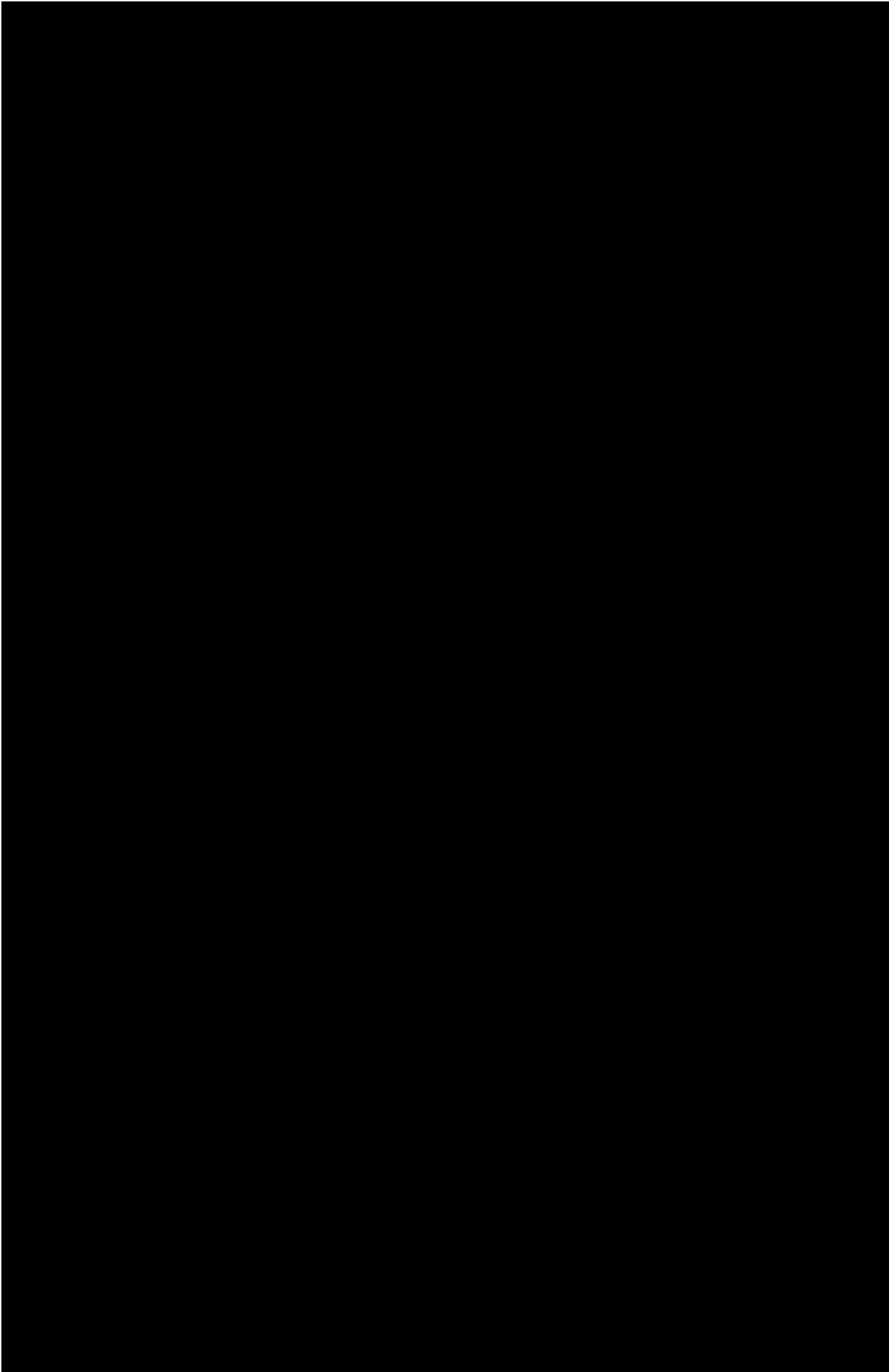
Experiments and Results

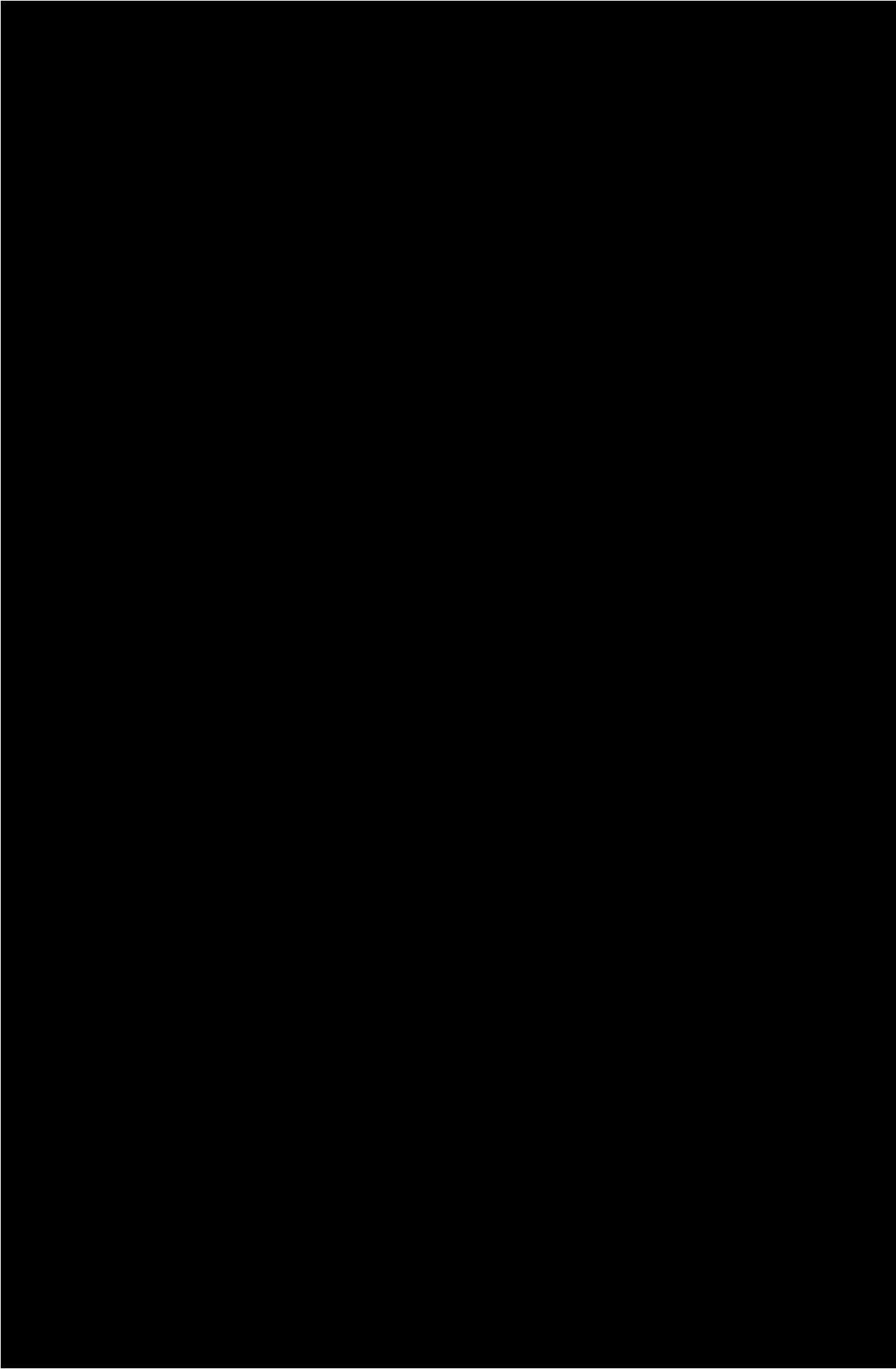


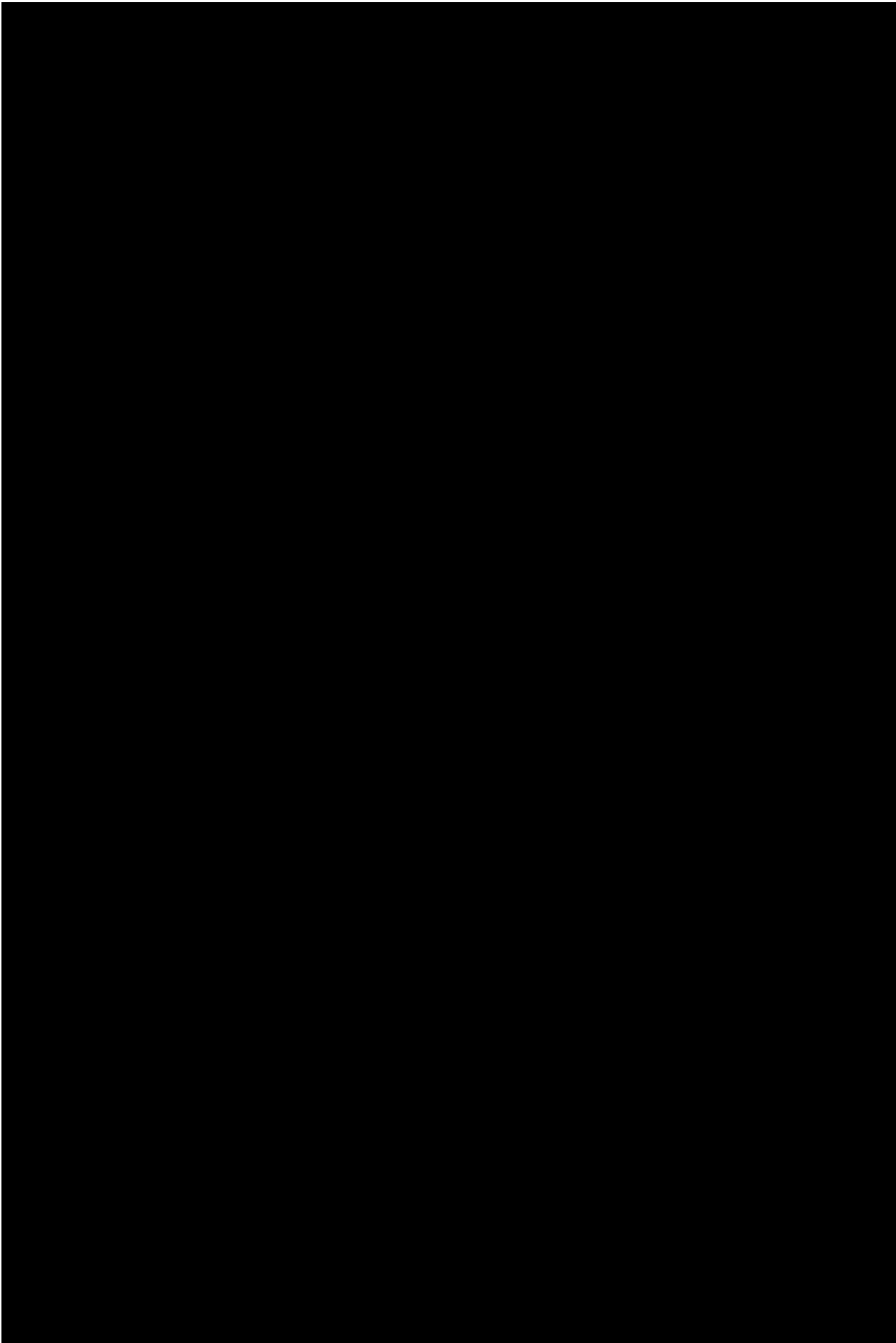


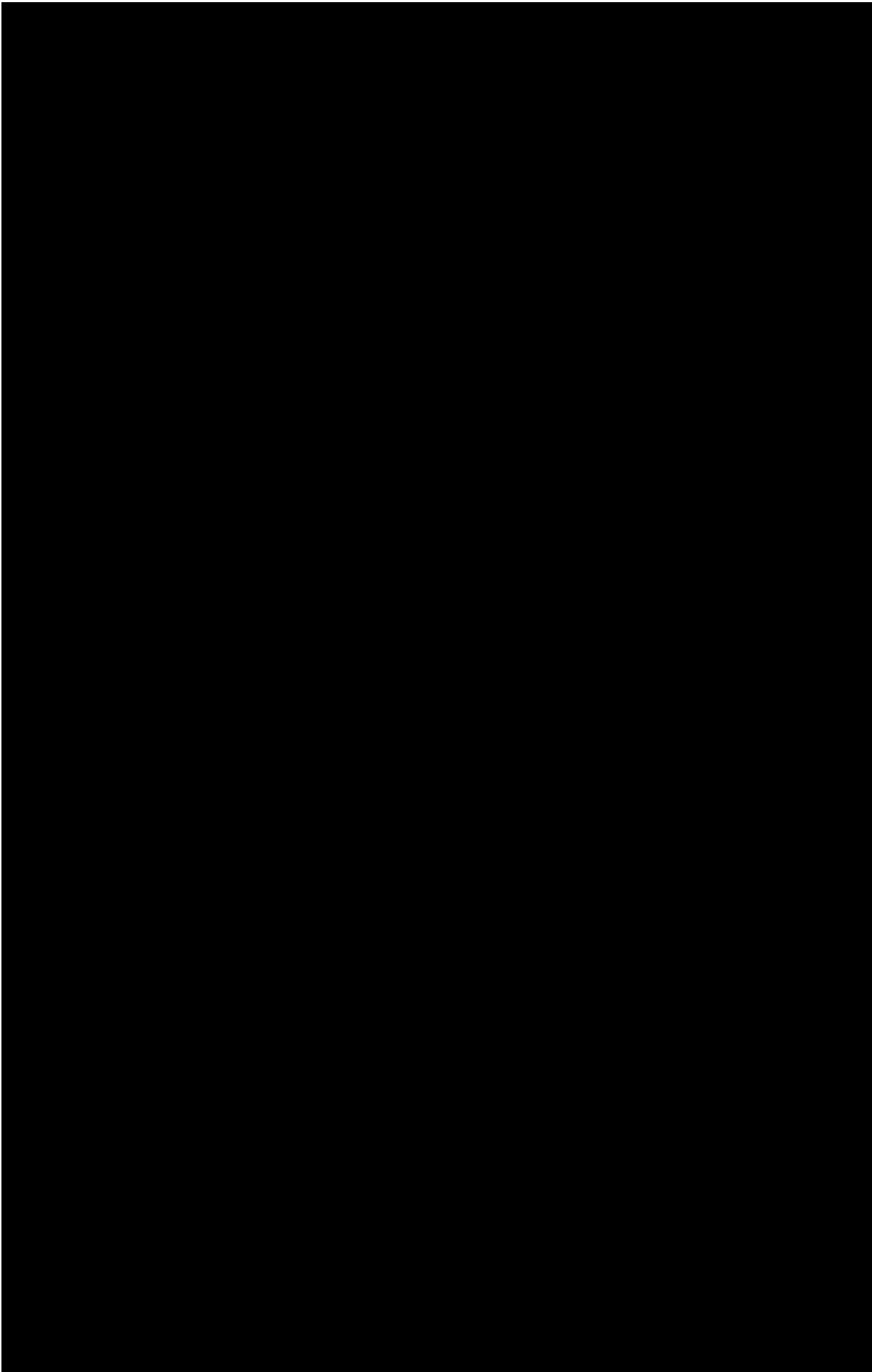


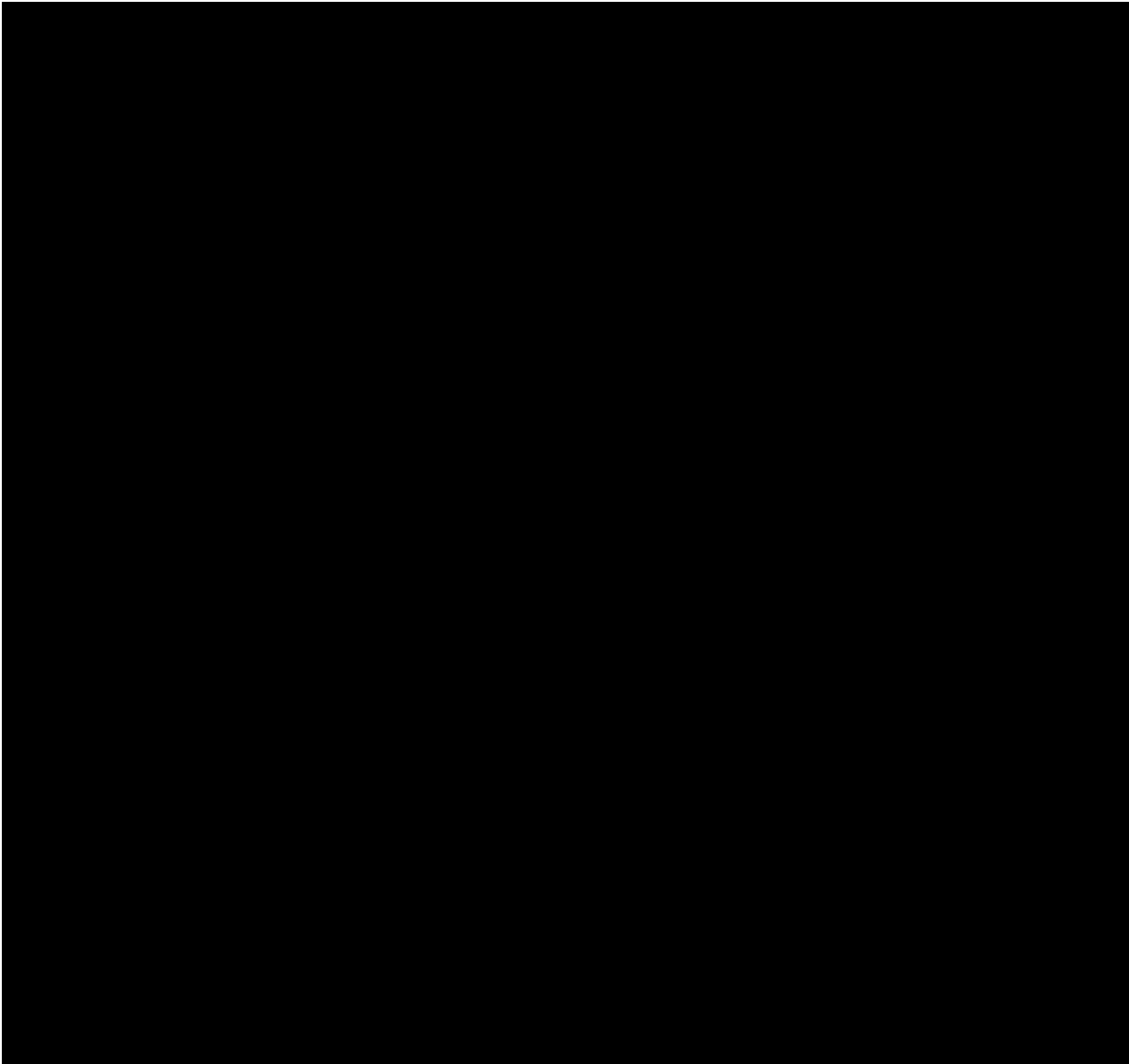








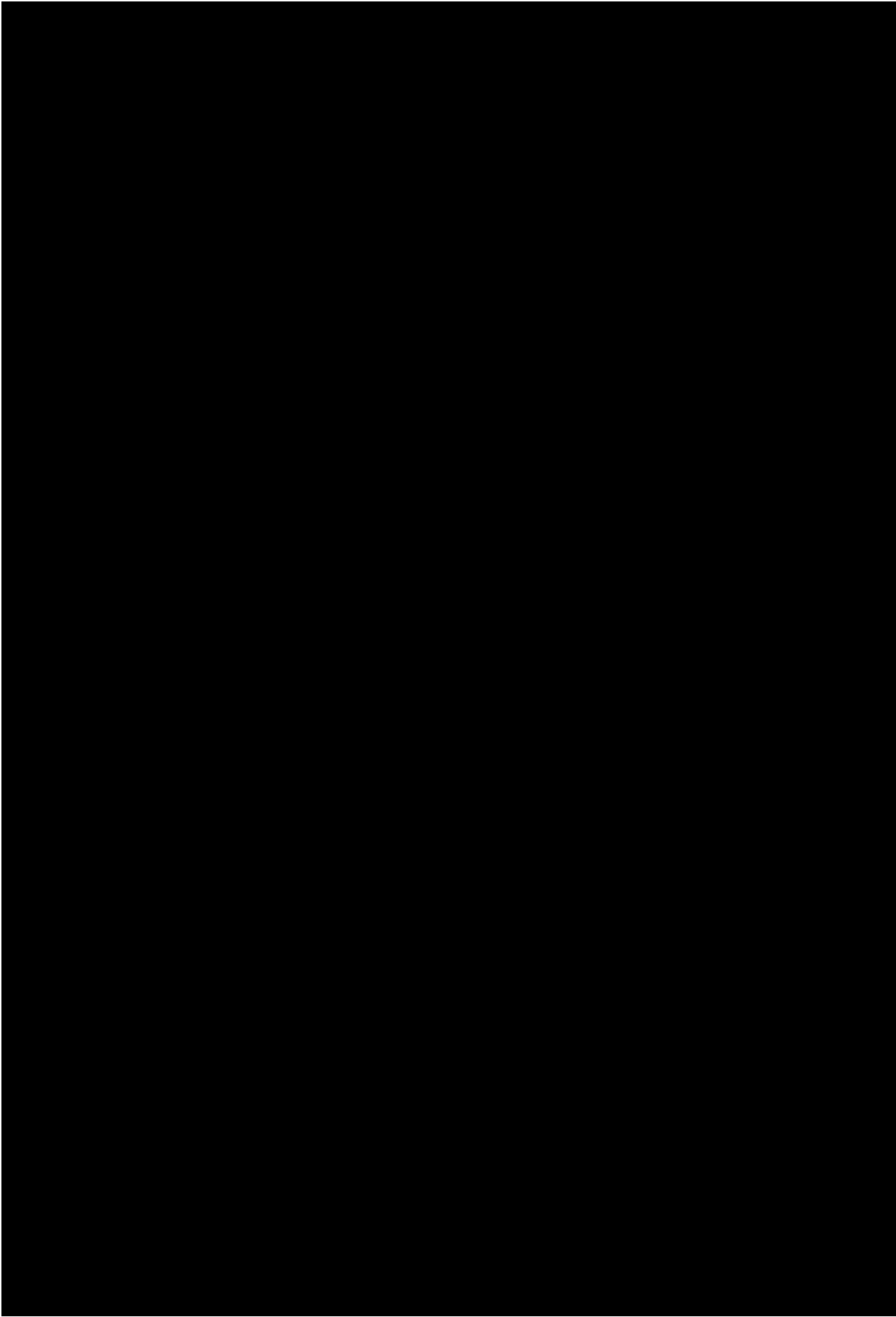


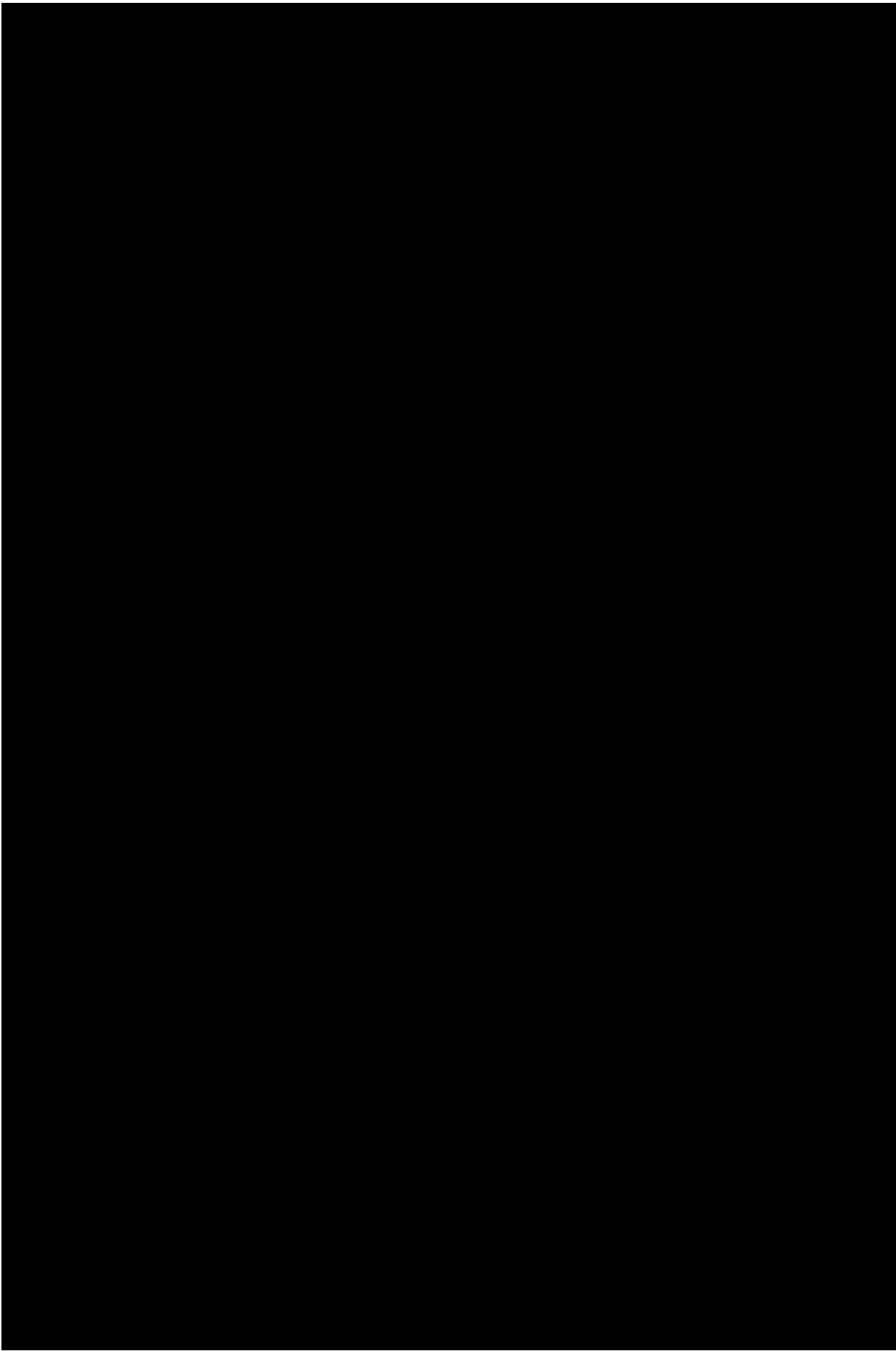


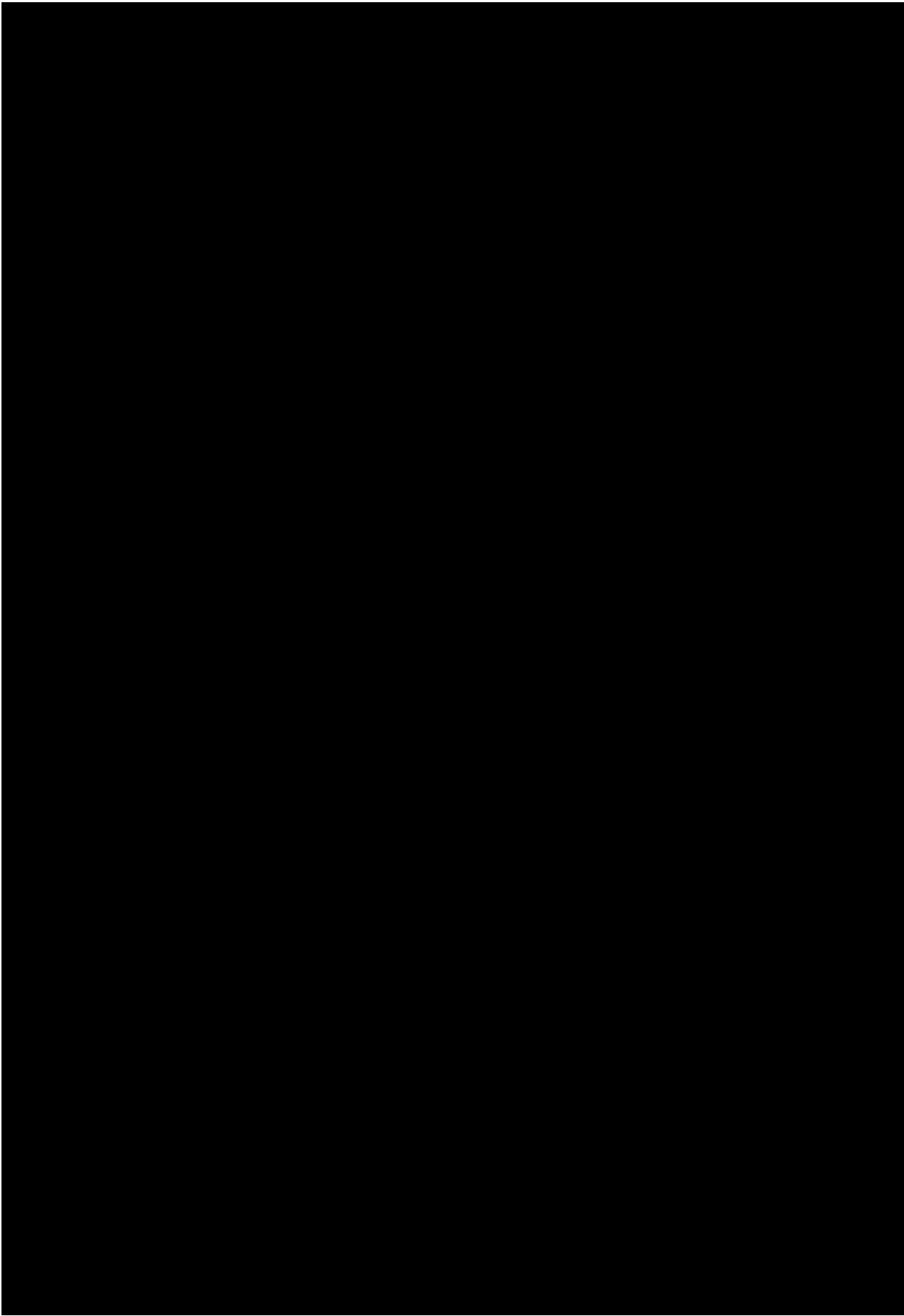
4

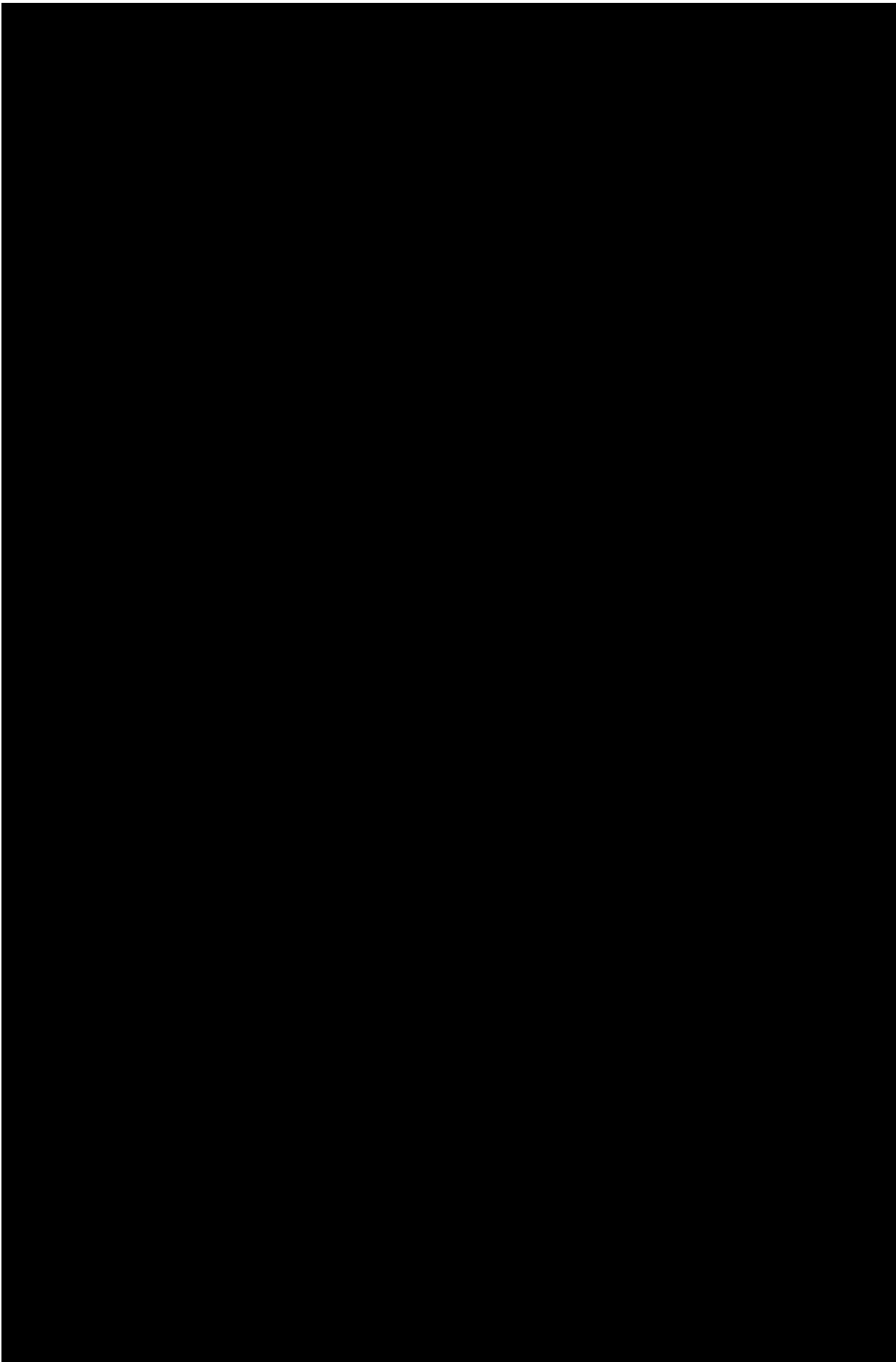
Pre-processing Filter Chain

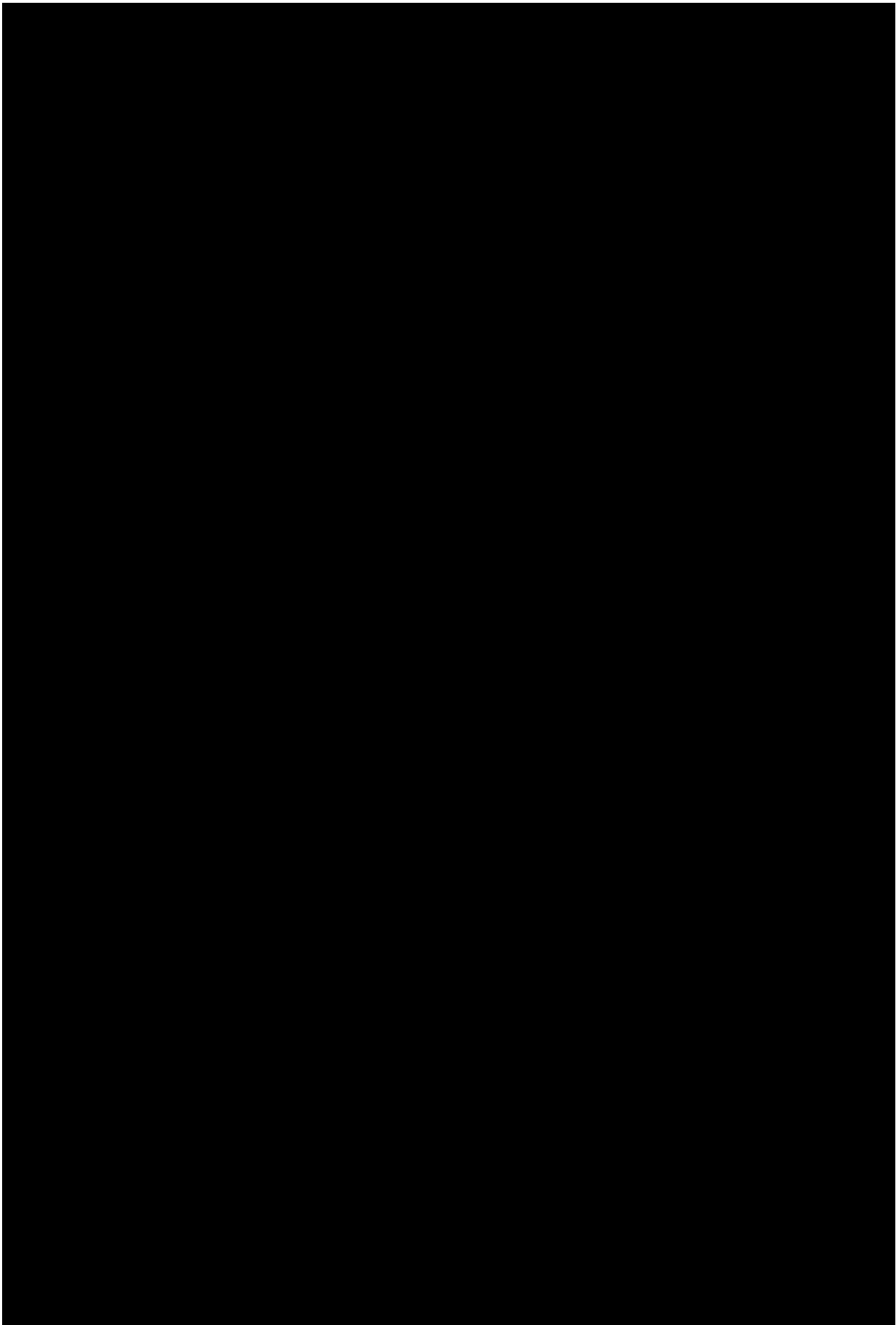


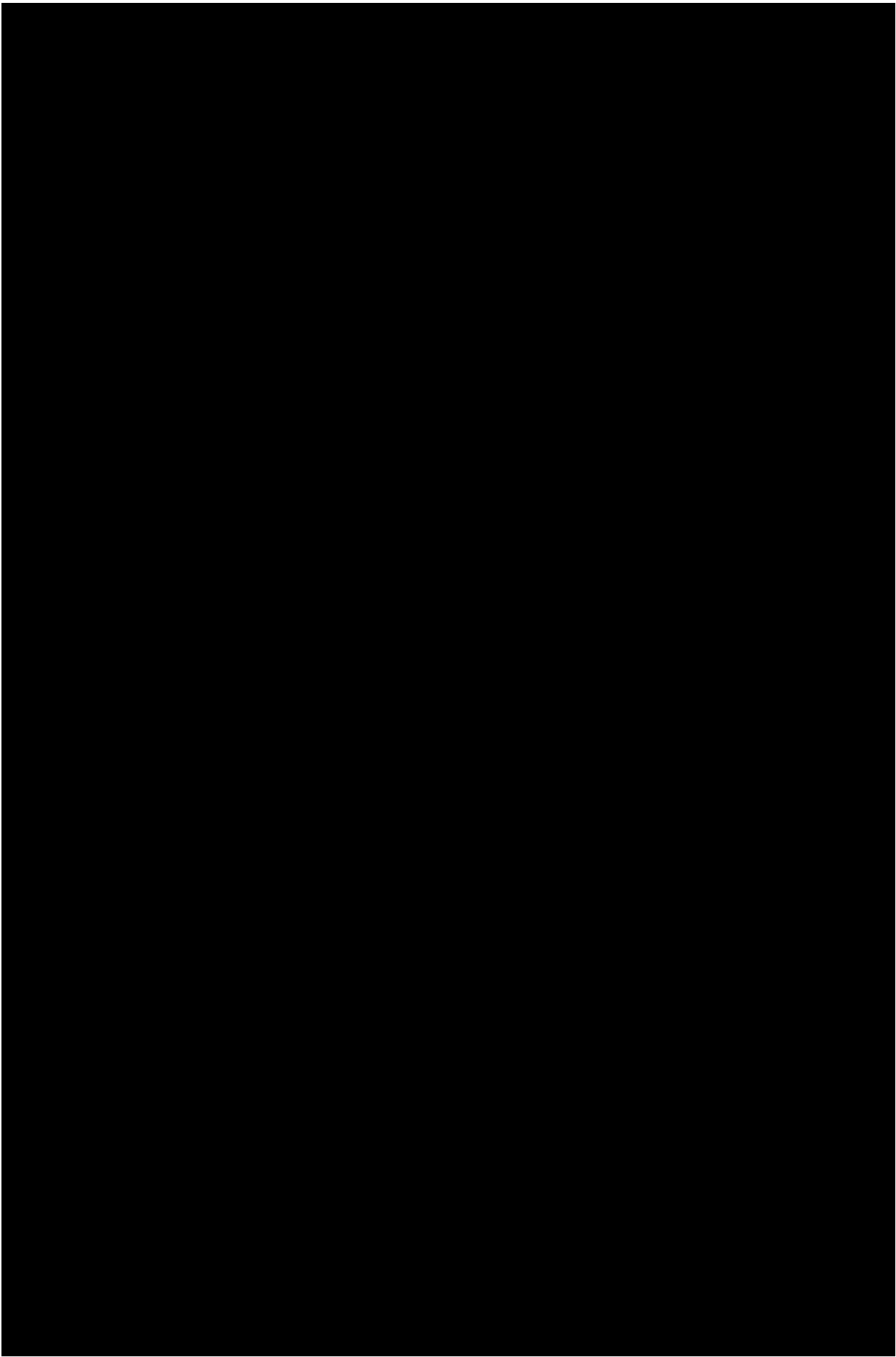


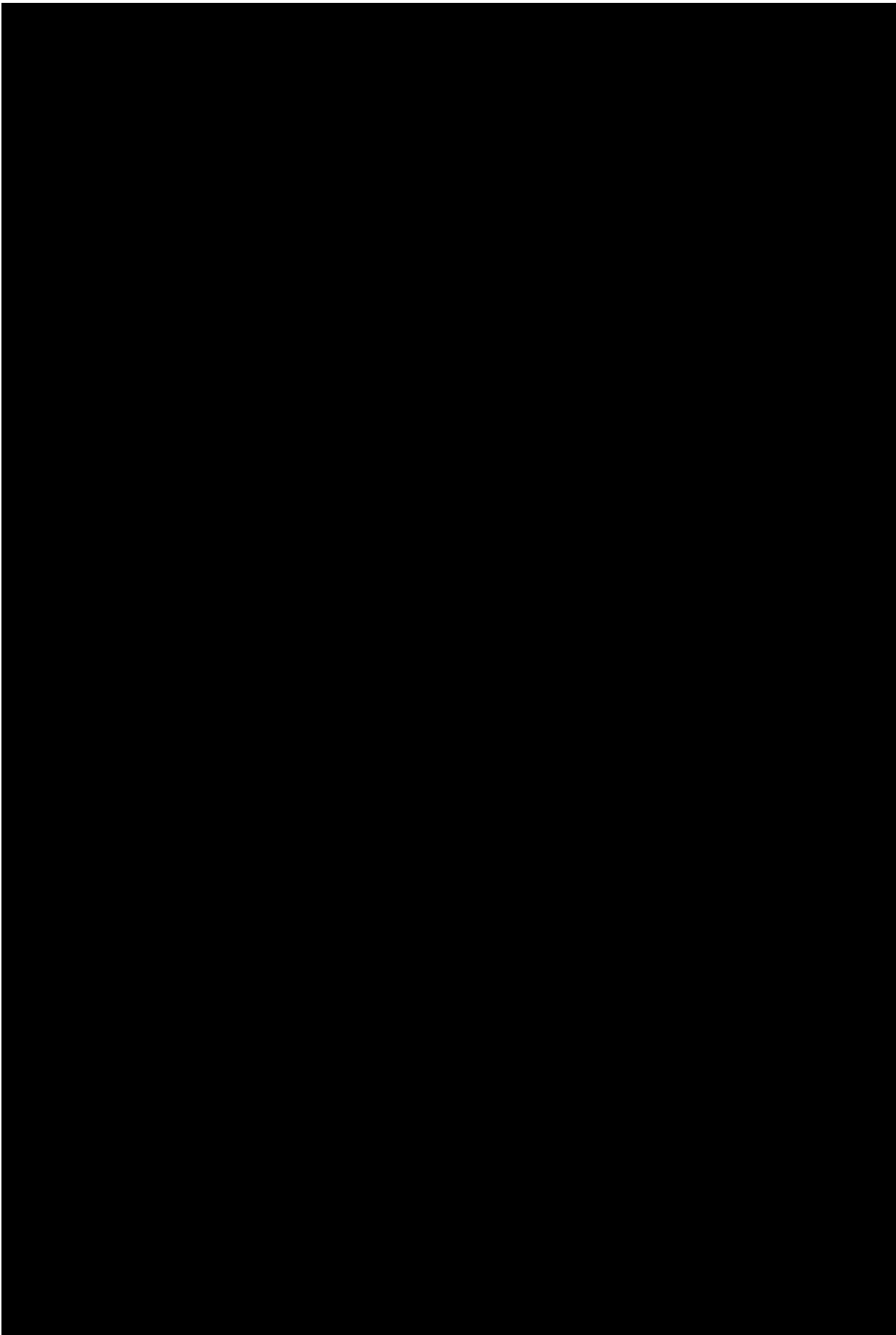


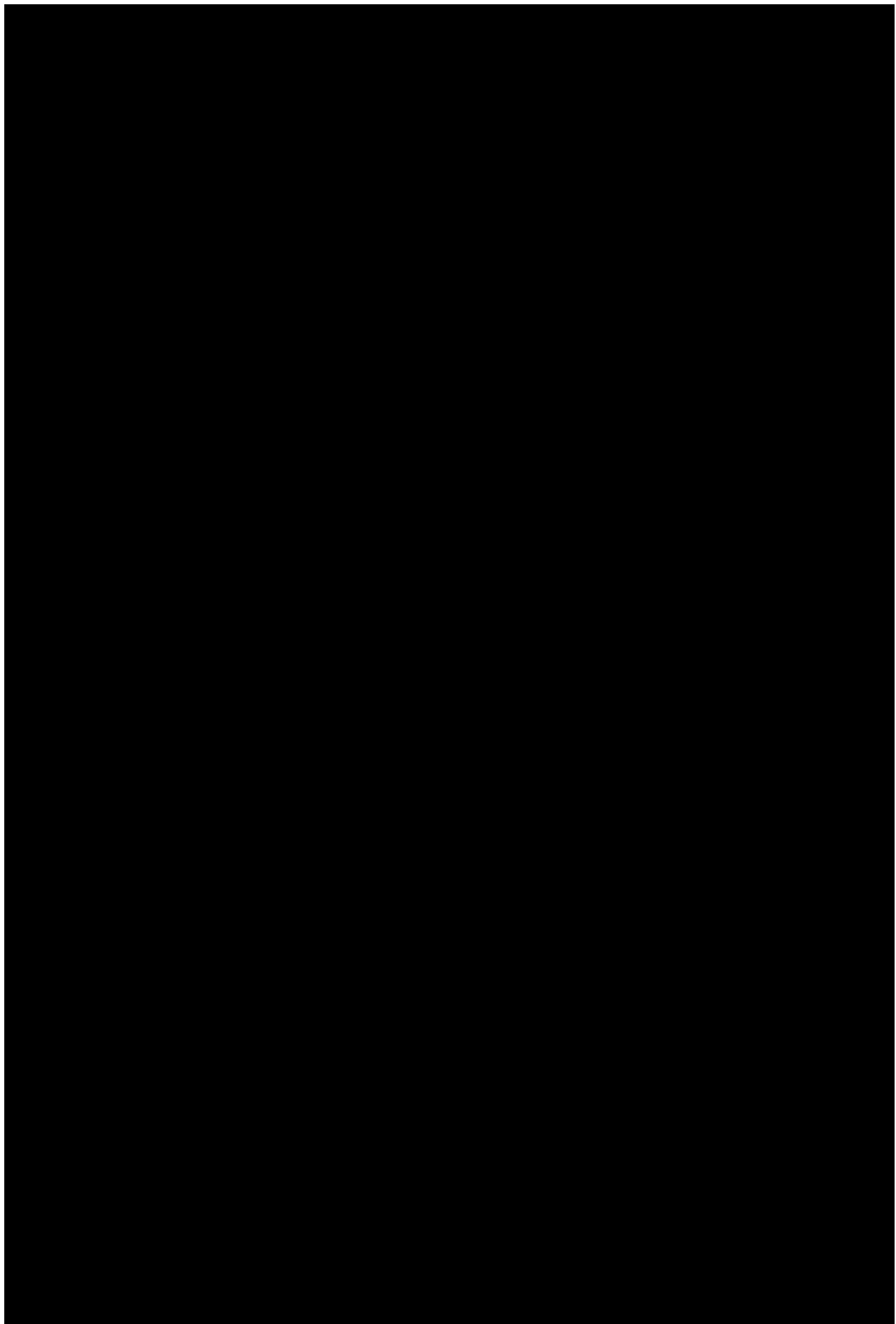


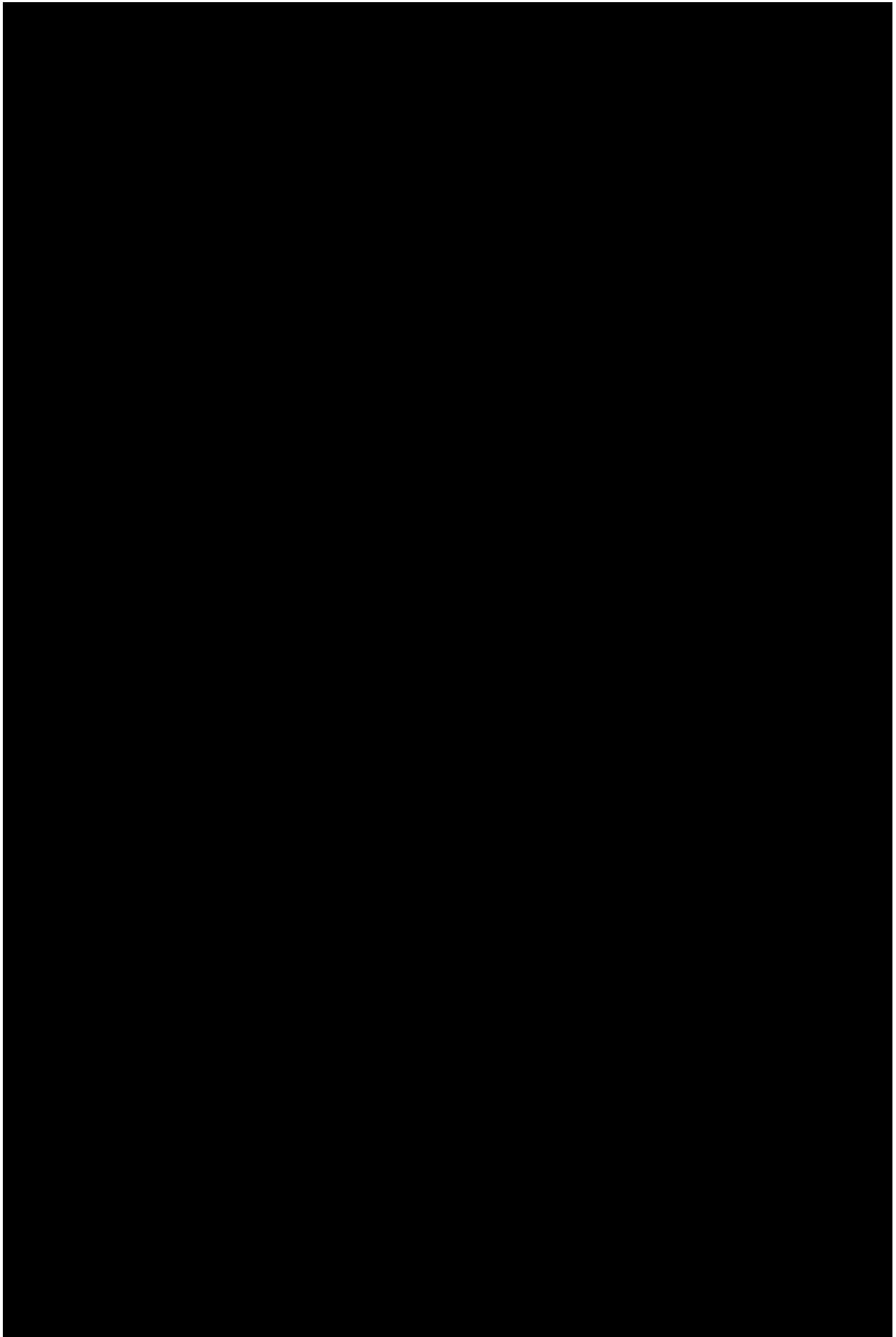


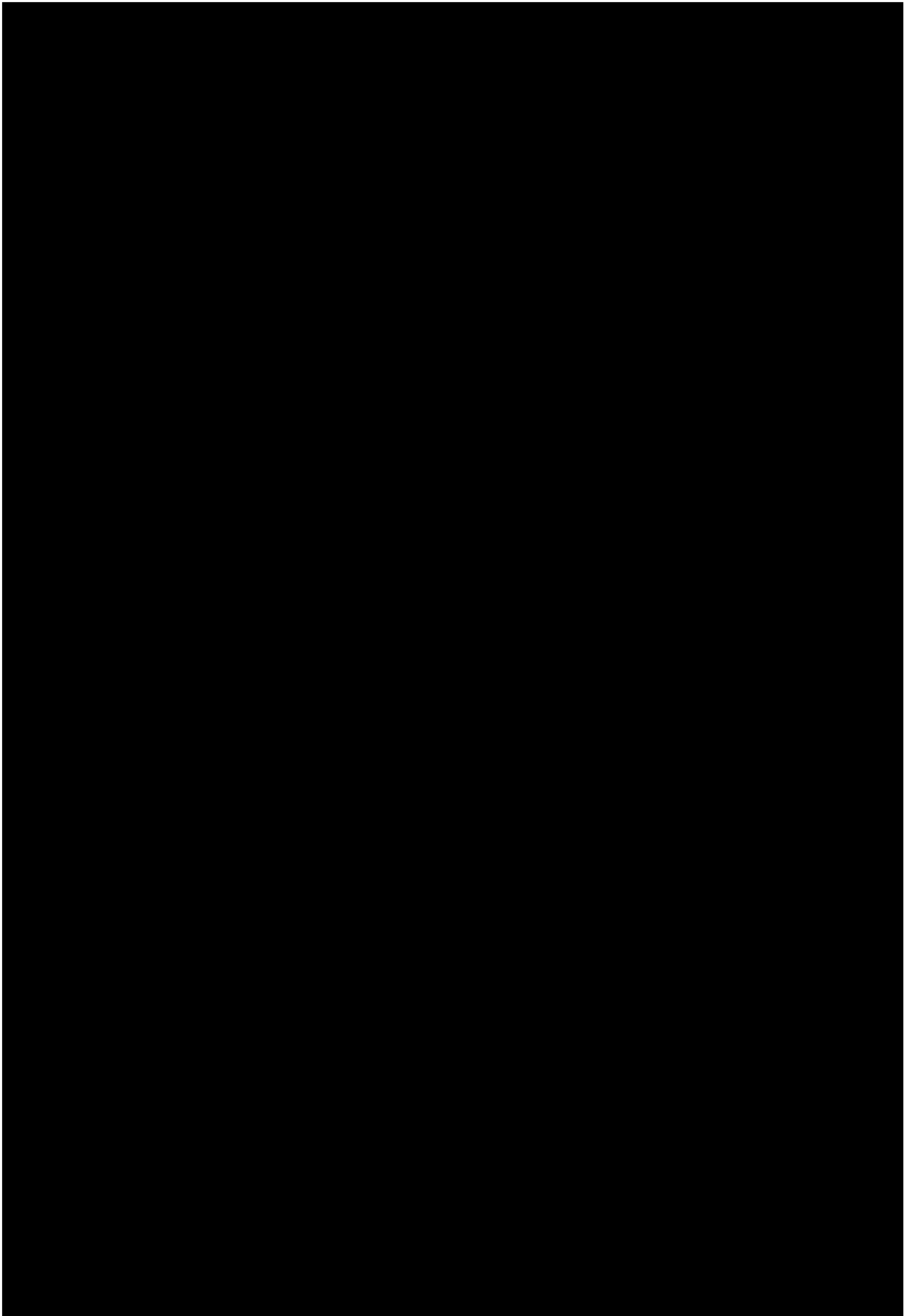


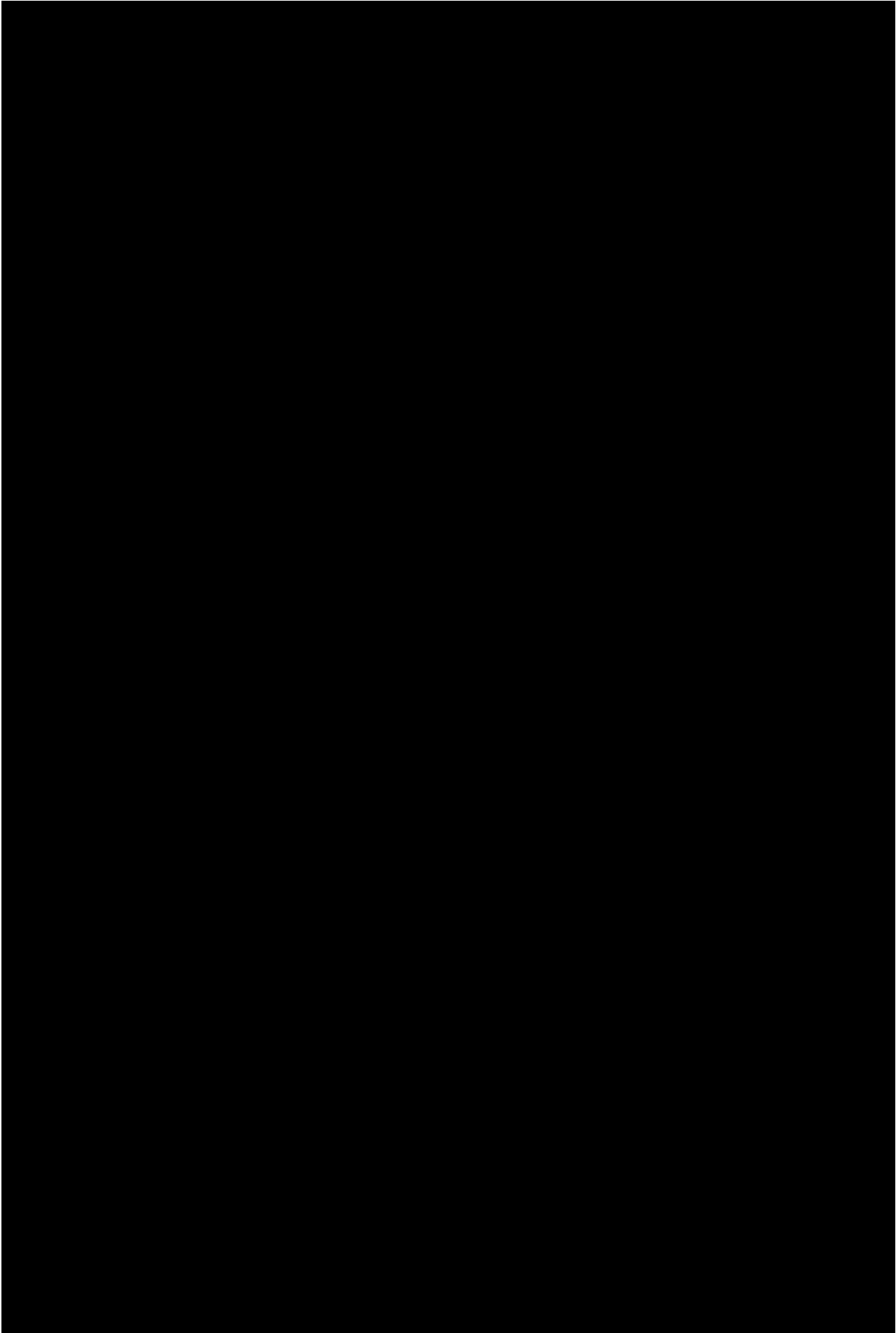


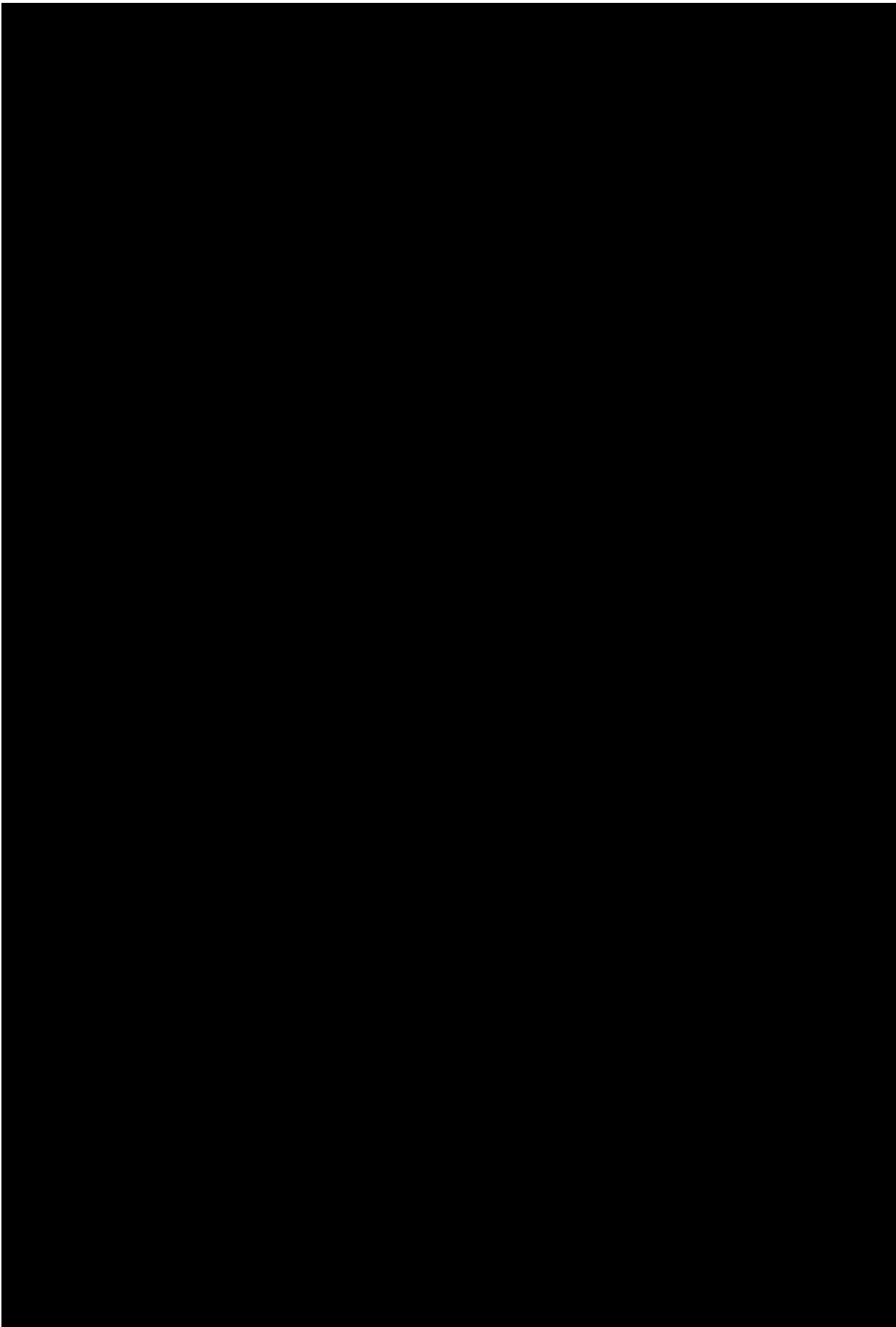


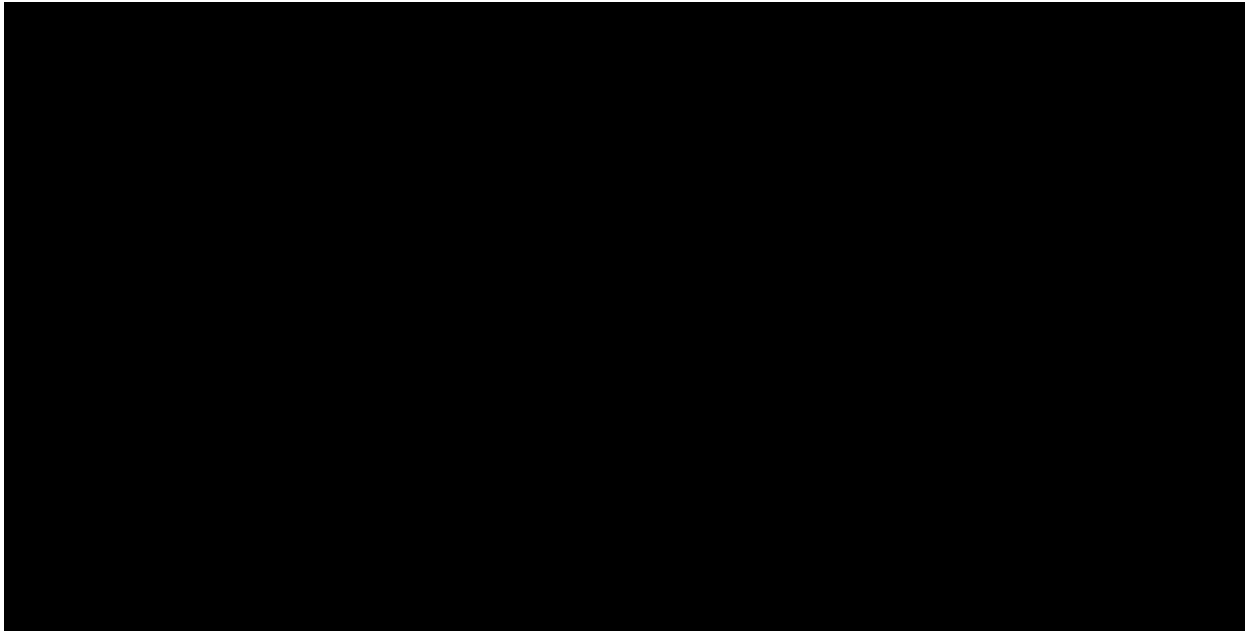






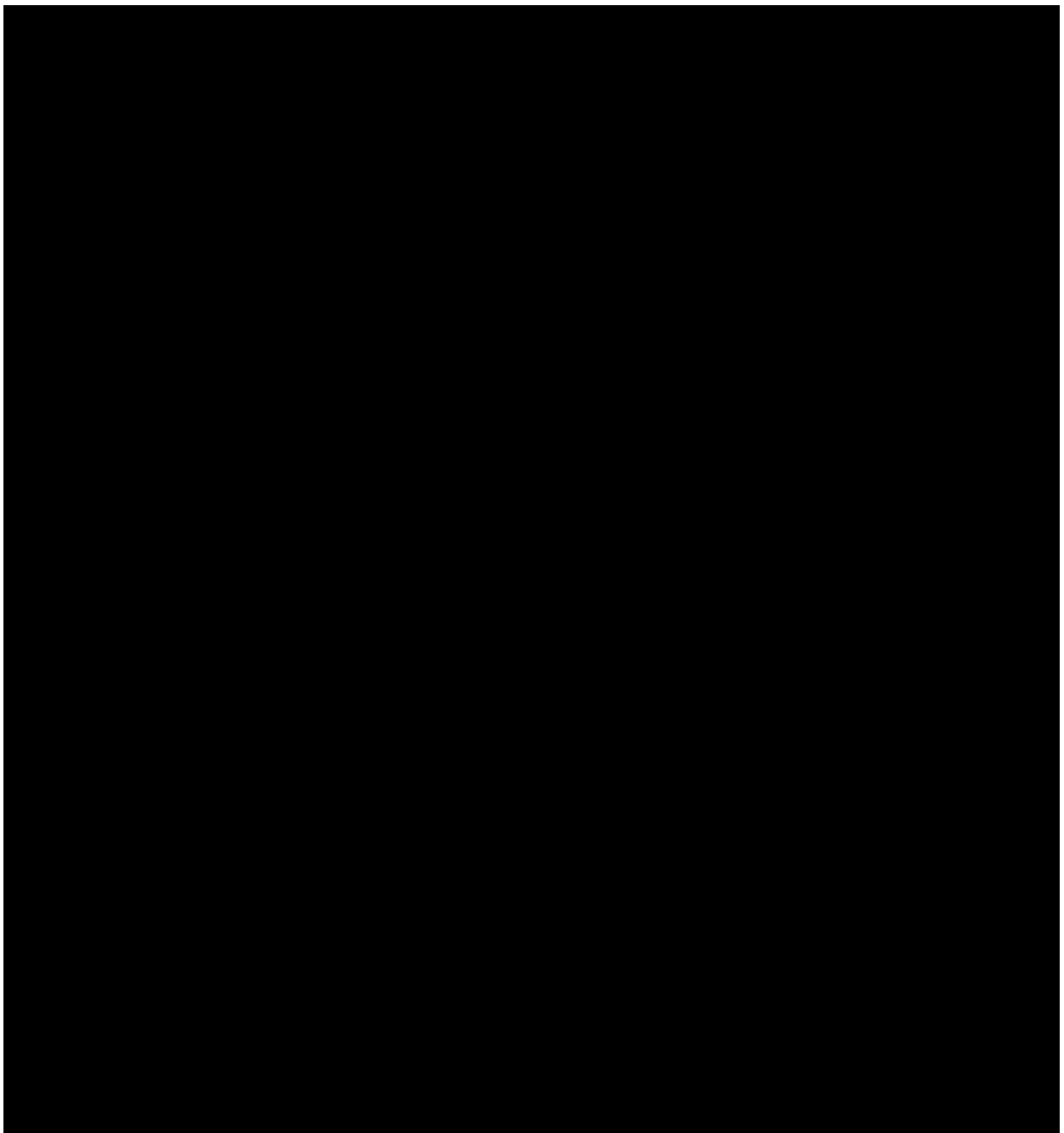


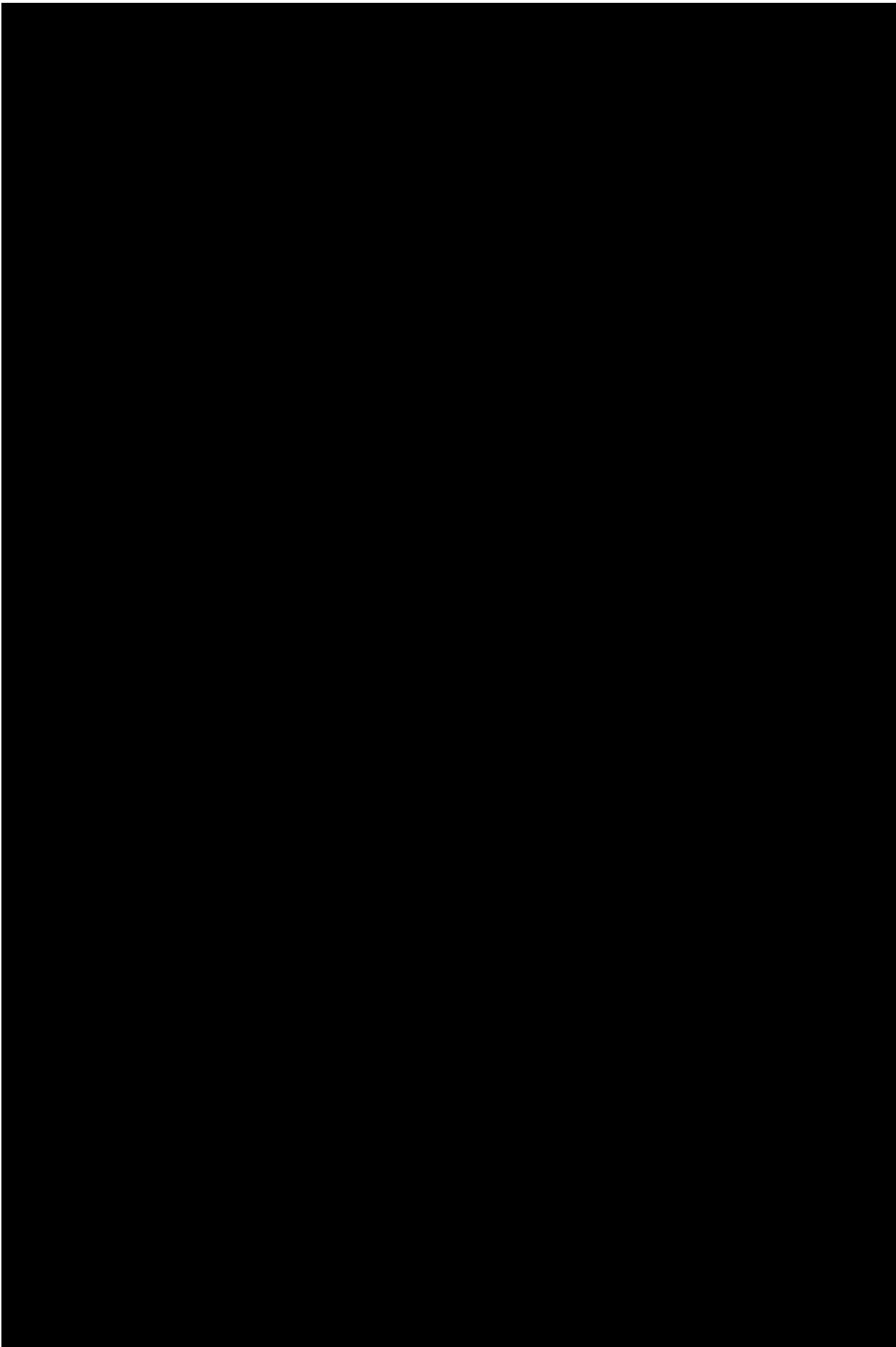


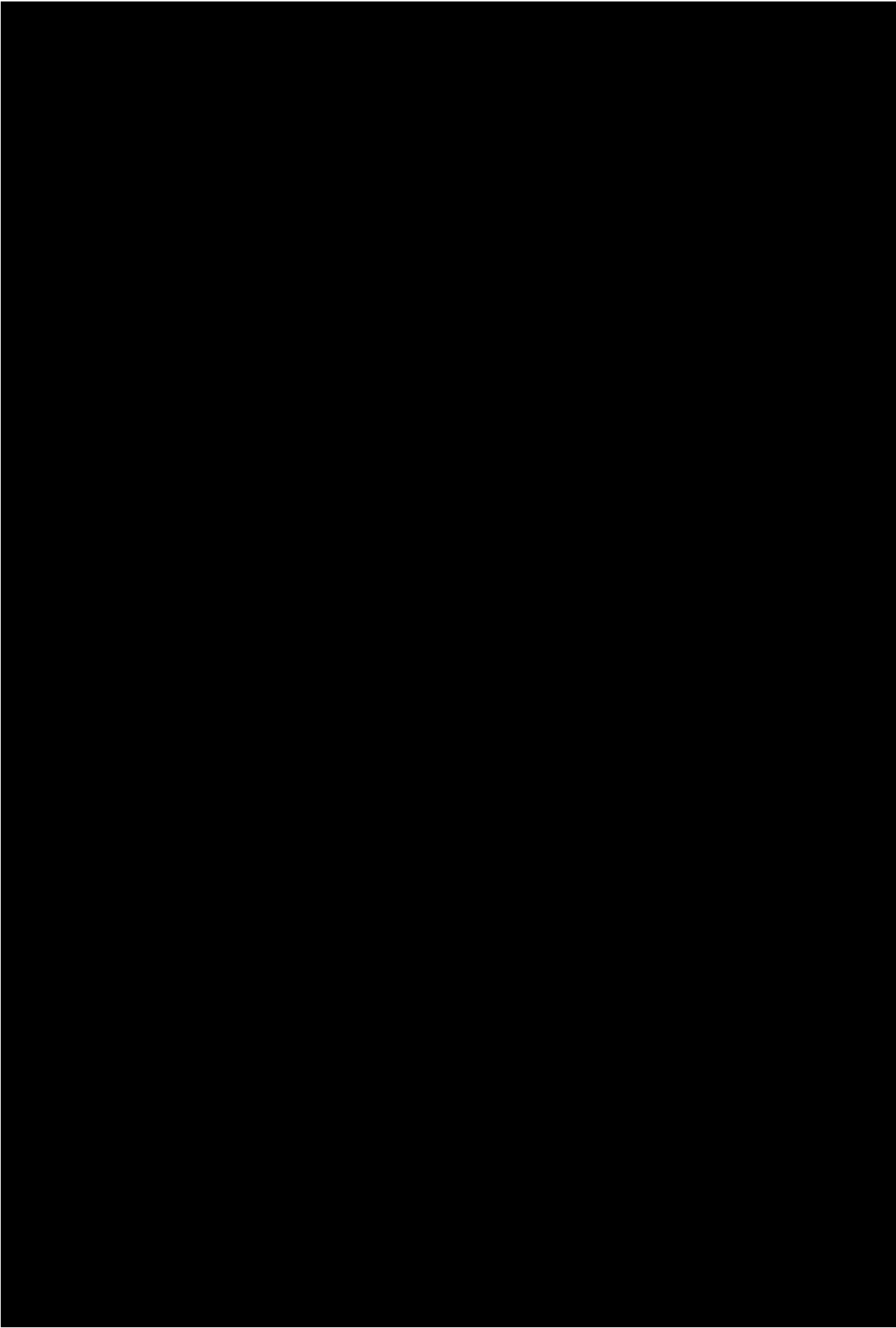


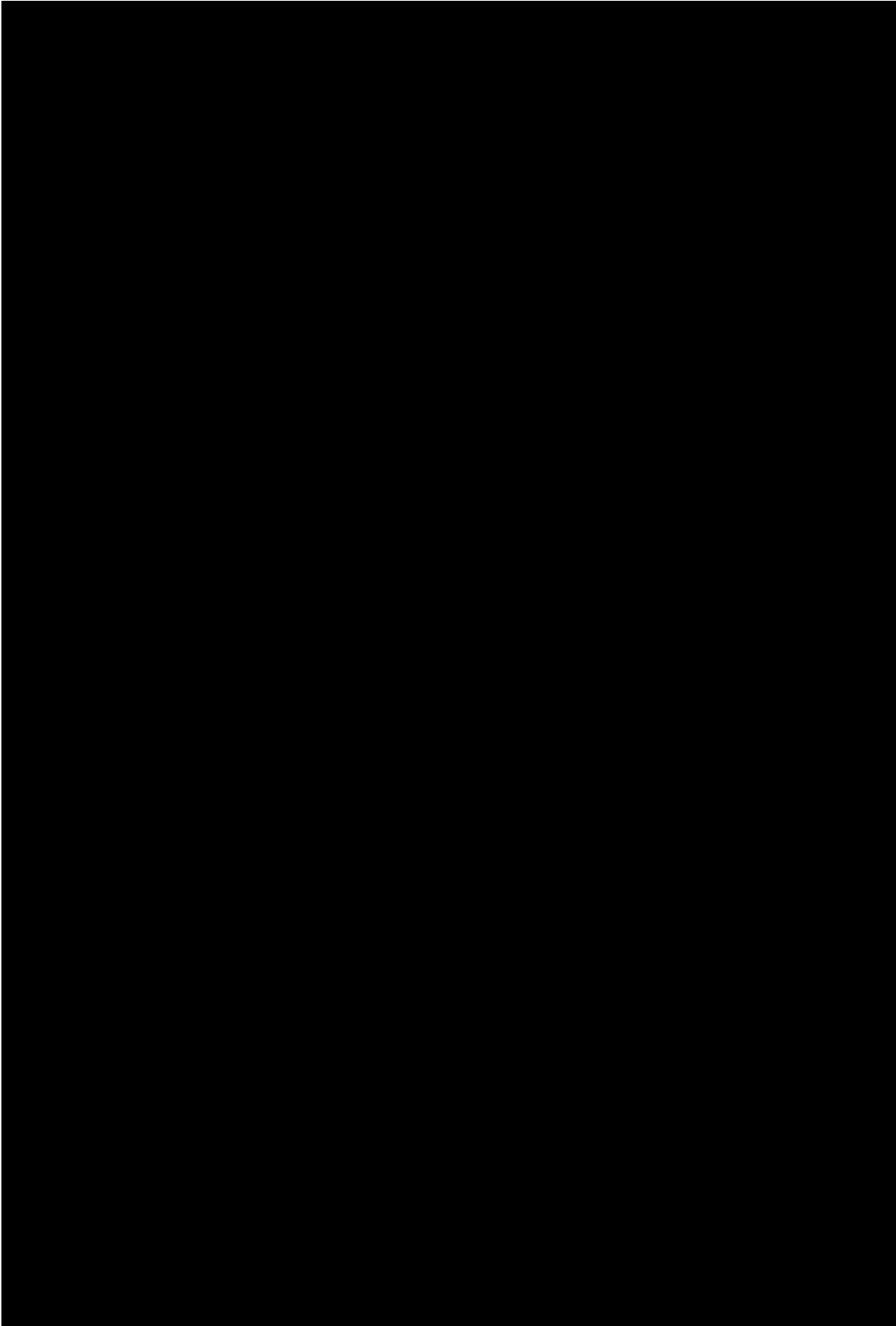
5

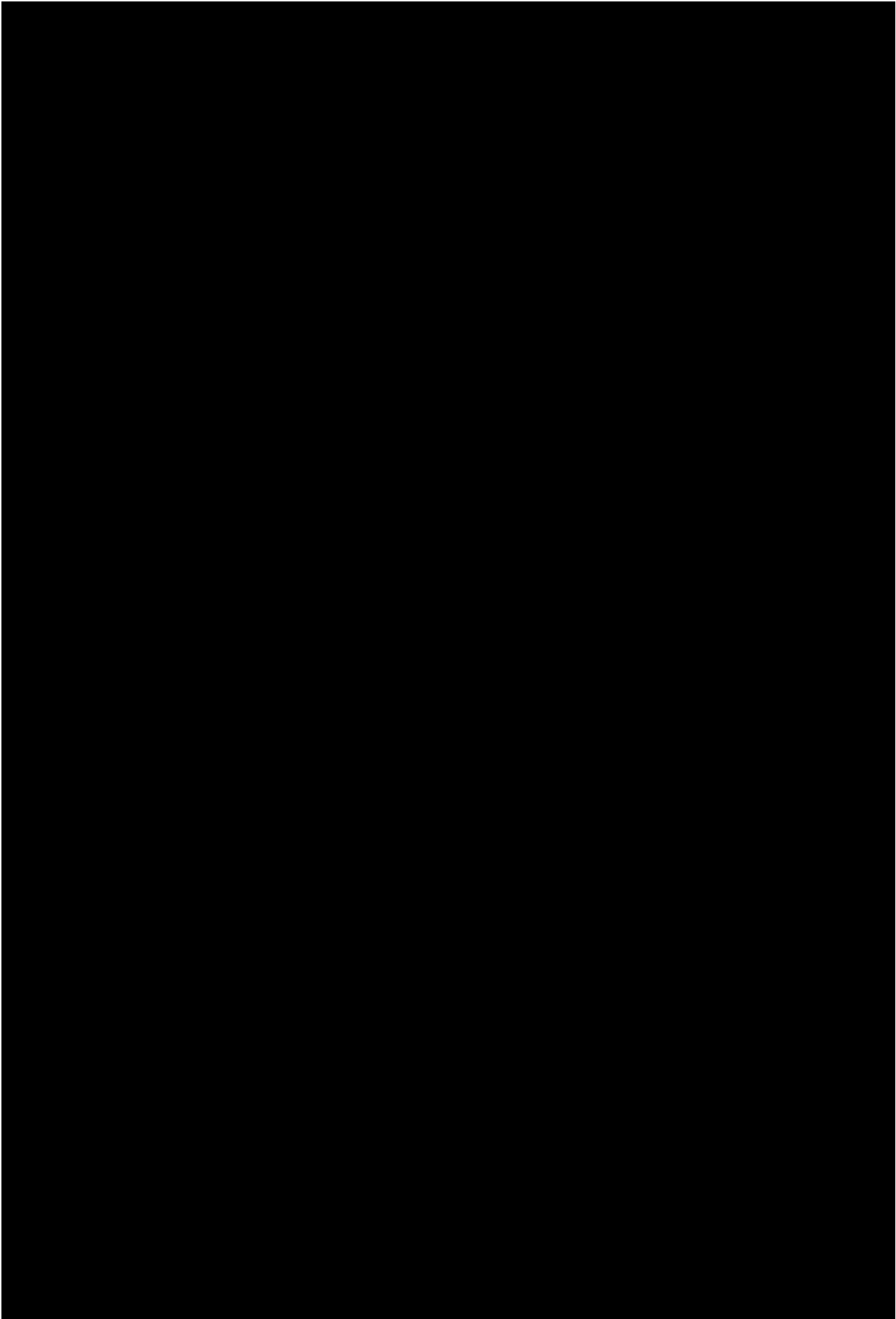
System Implementation

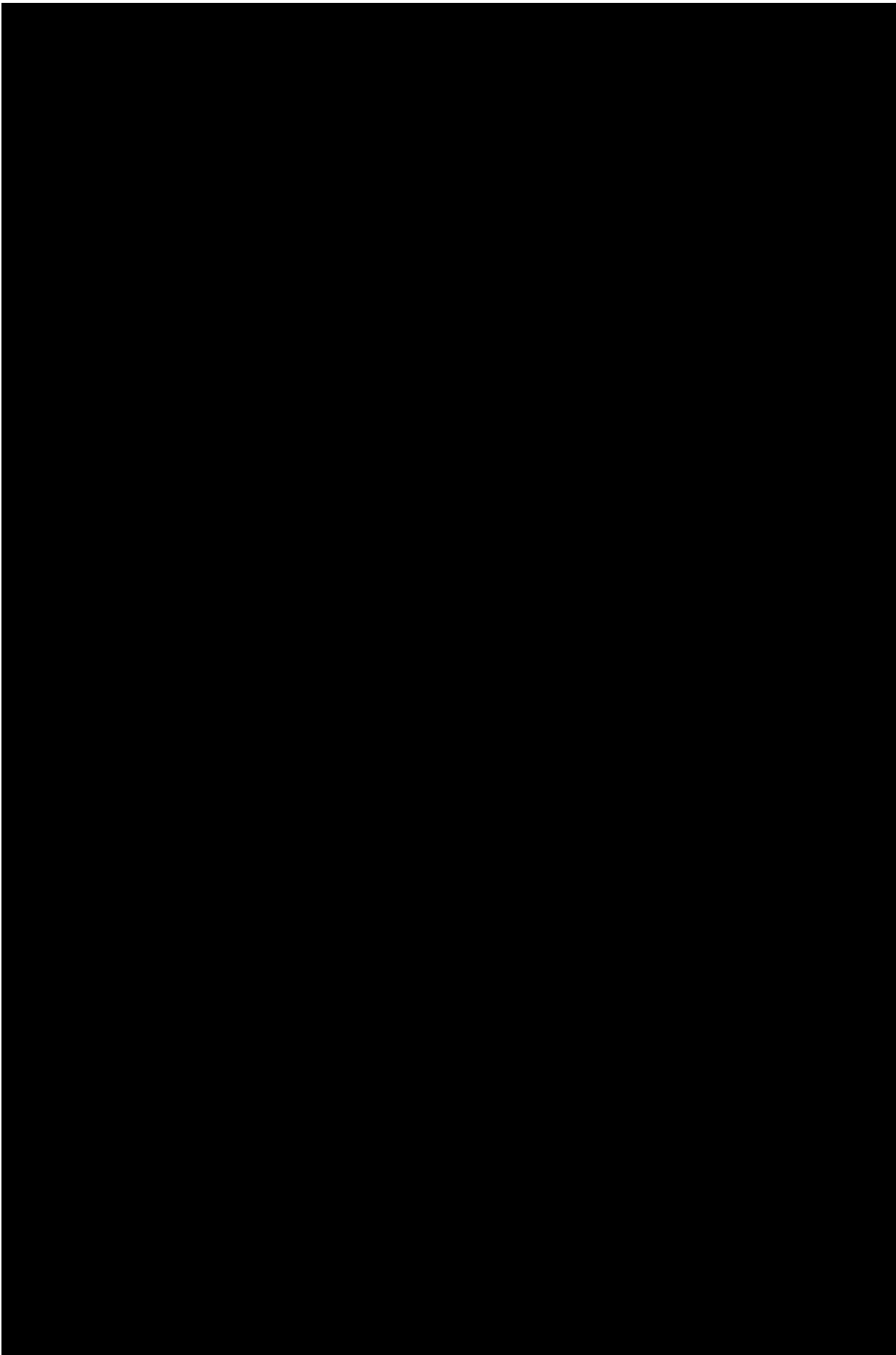


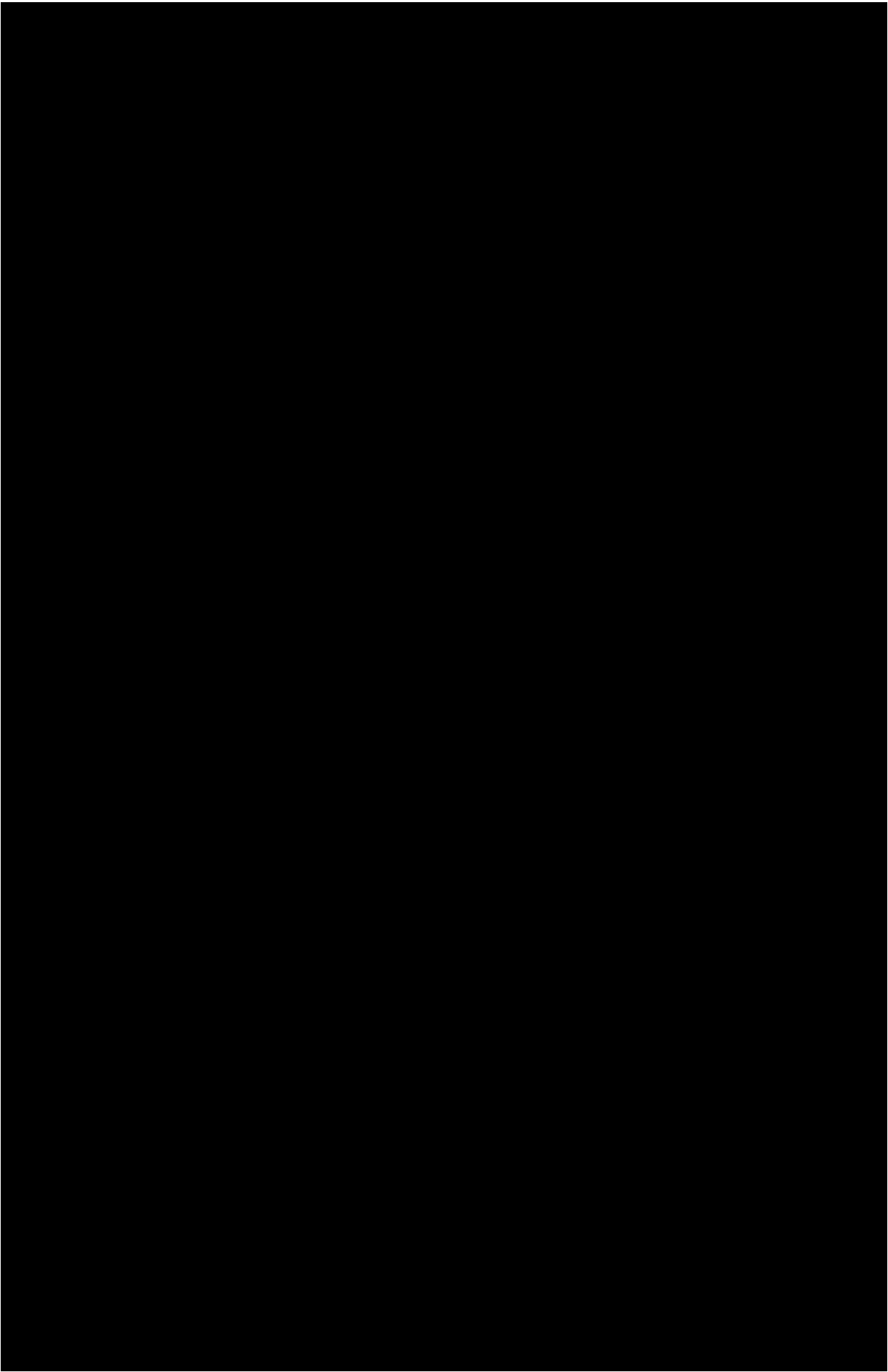


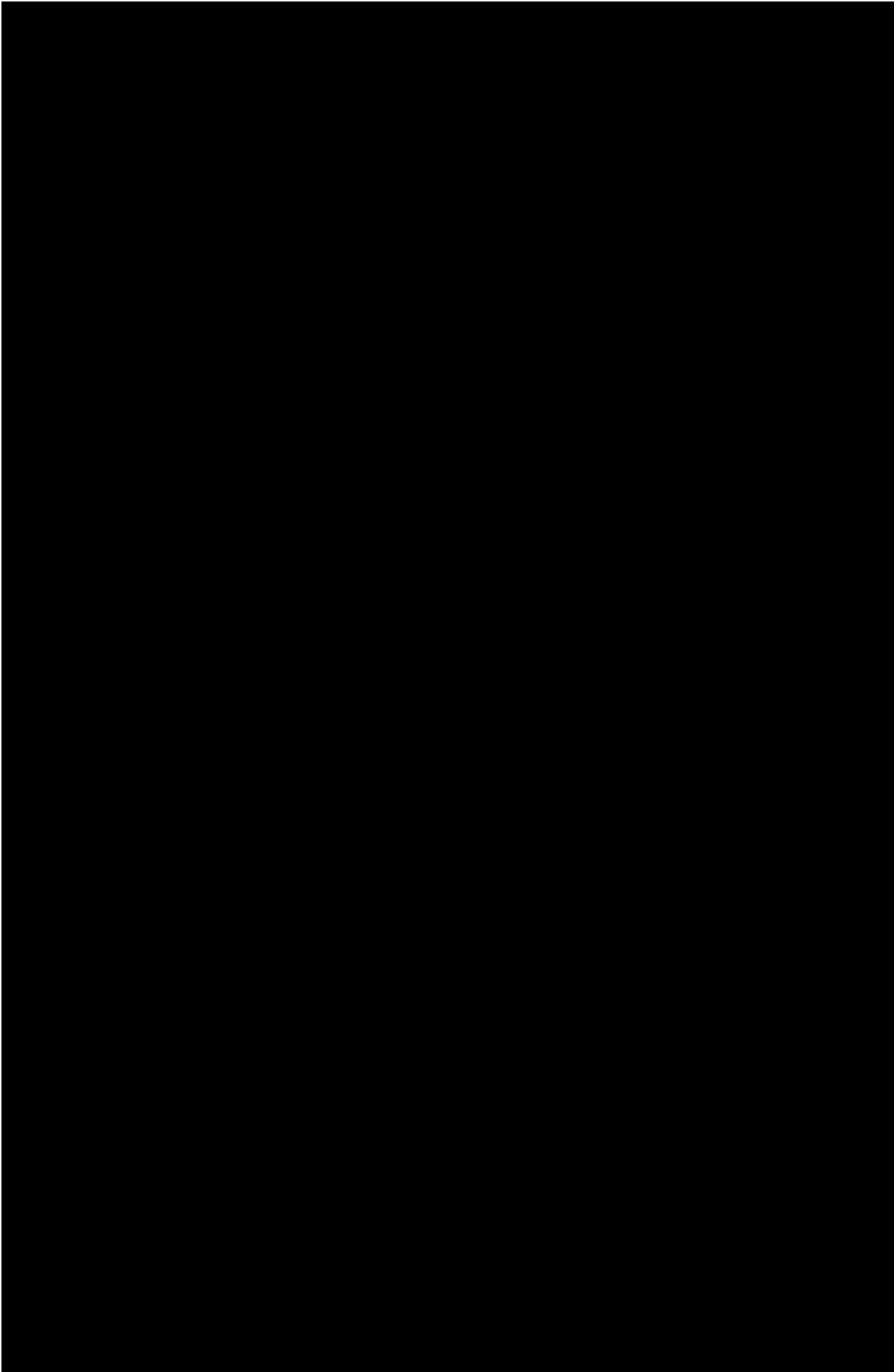


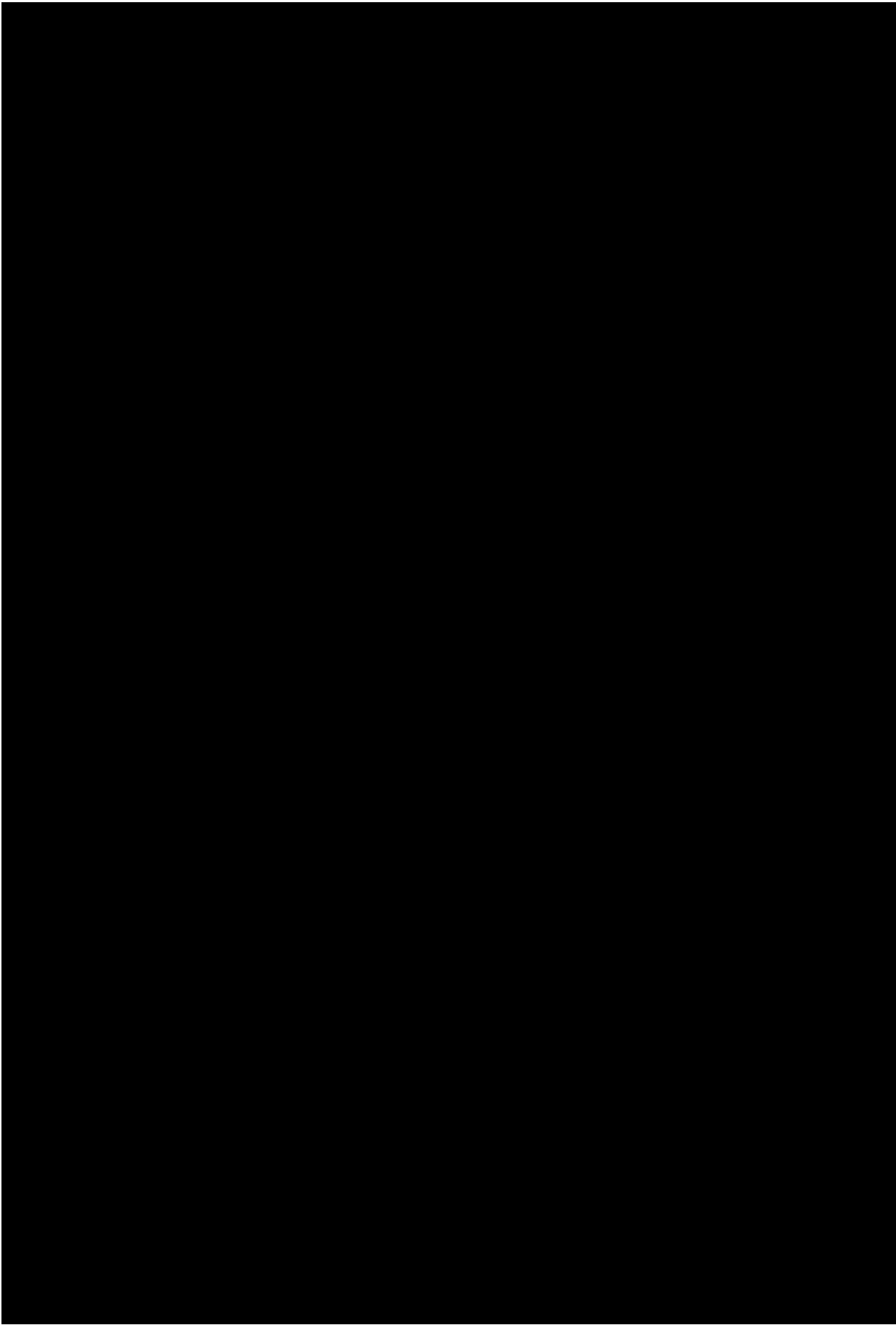


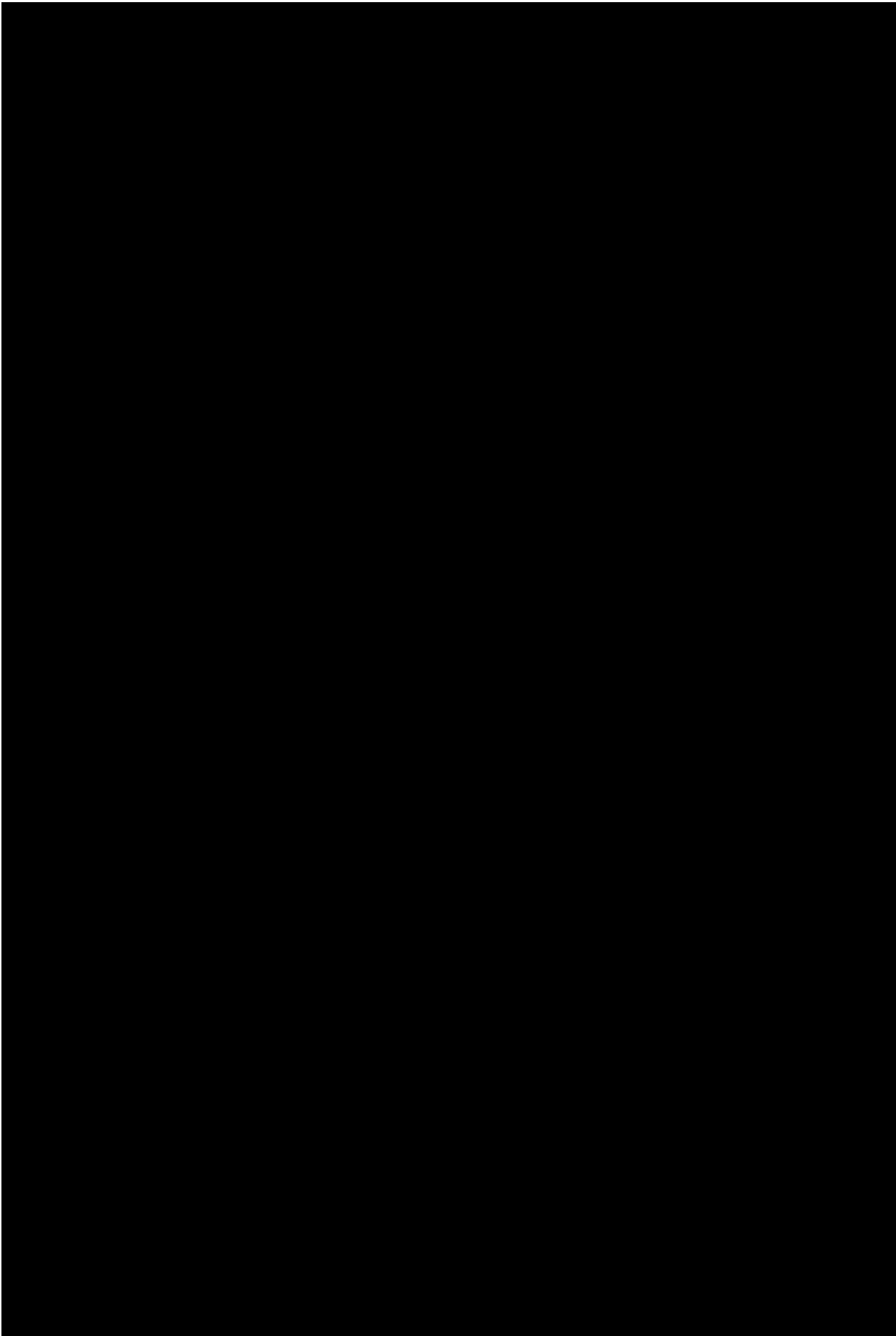


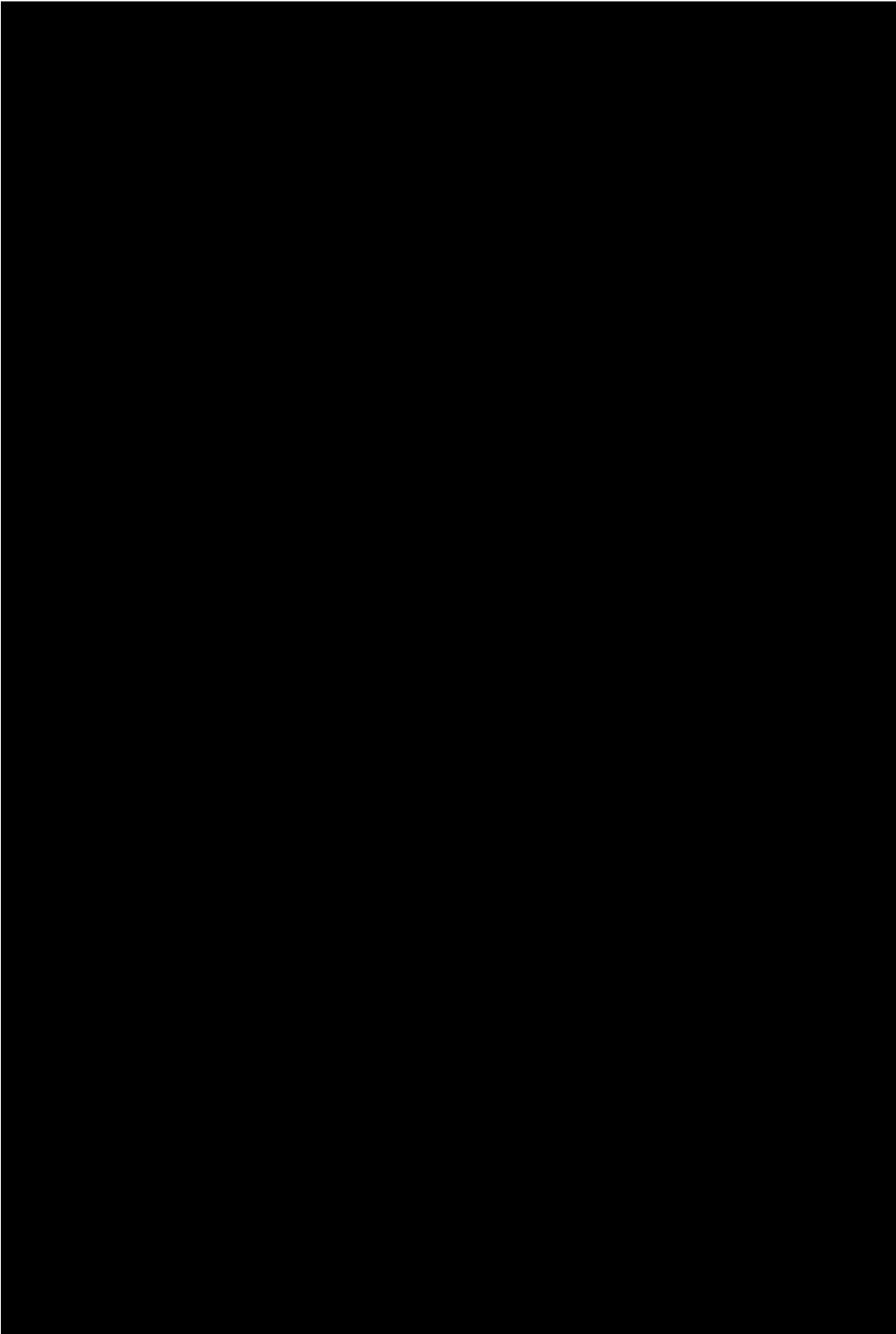


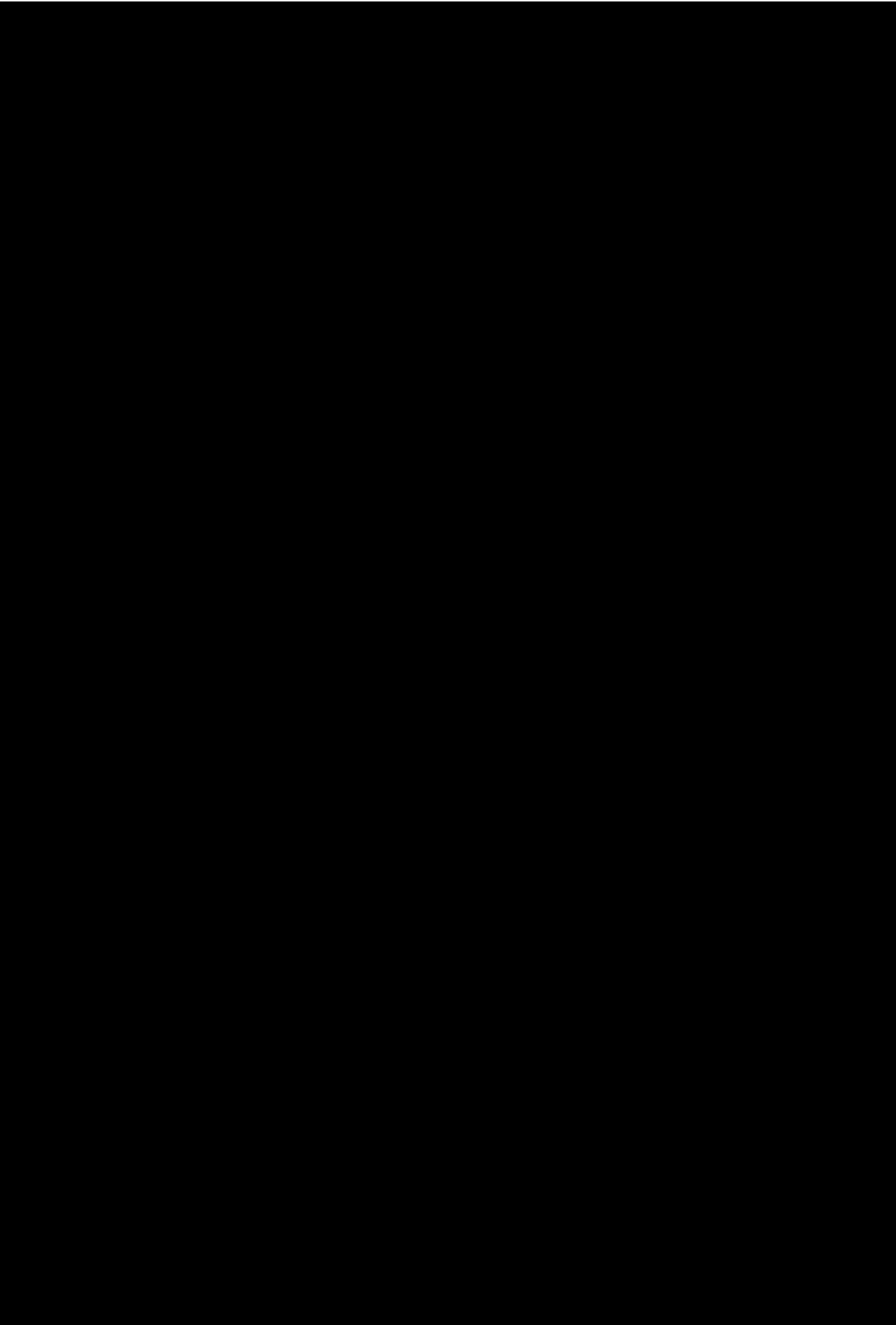


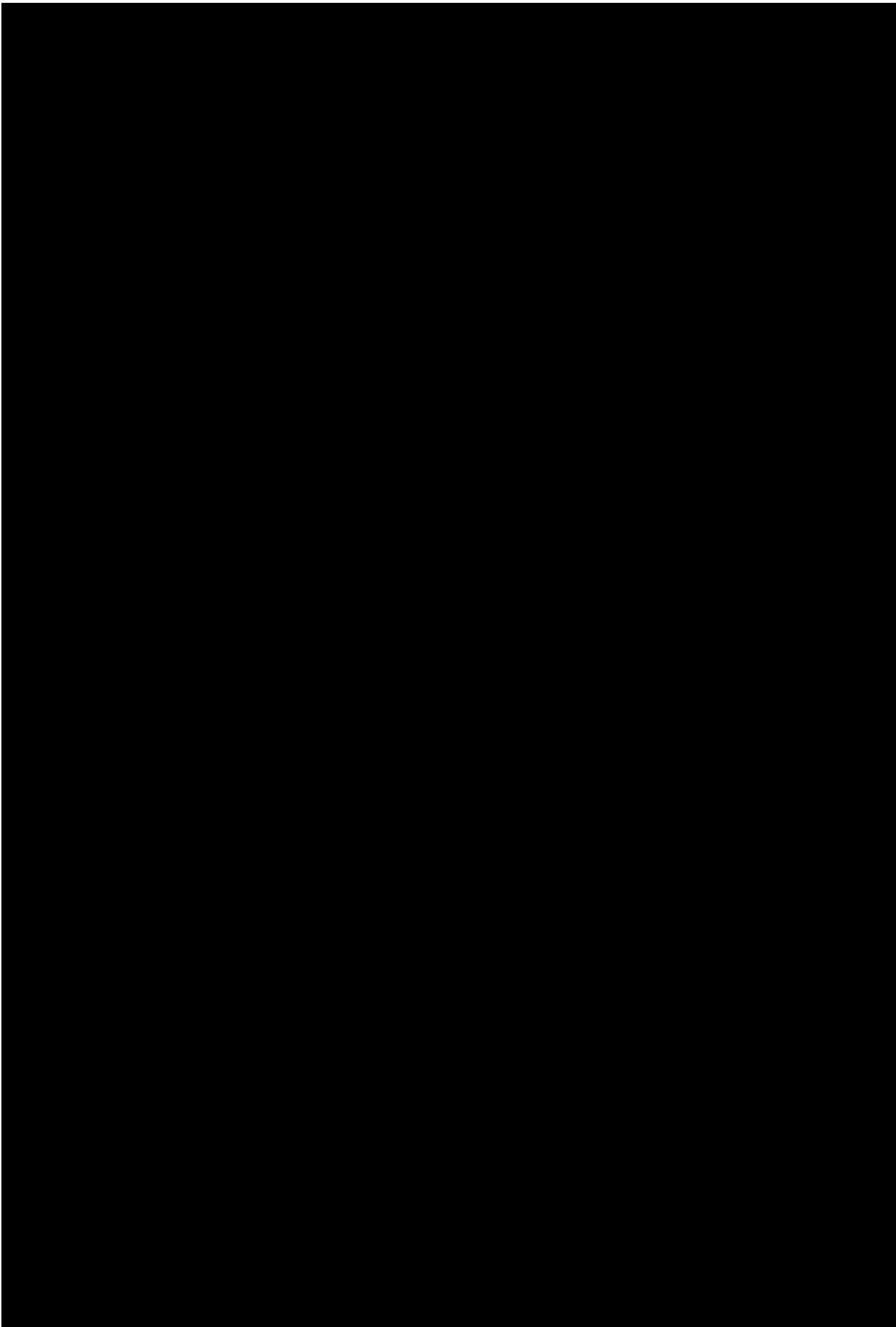


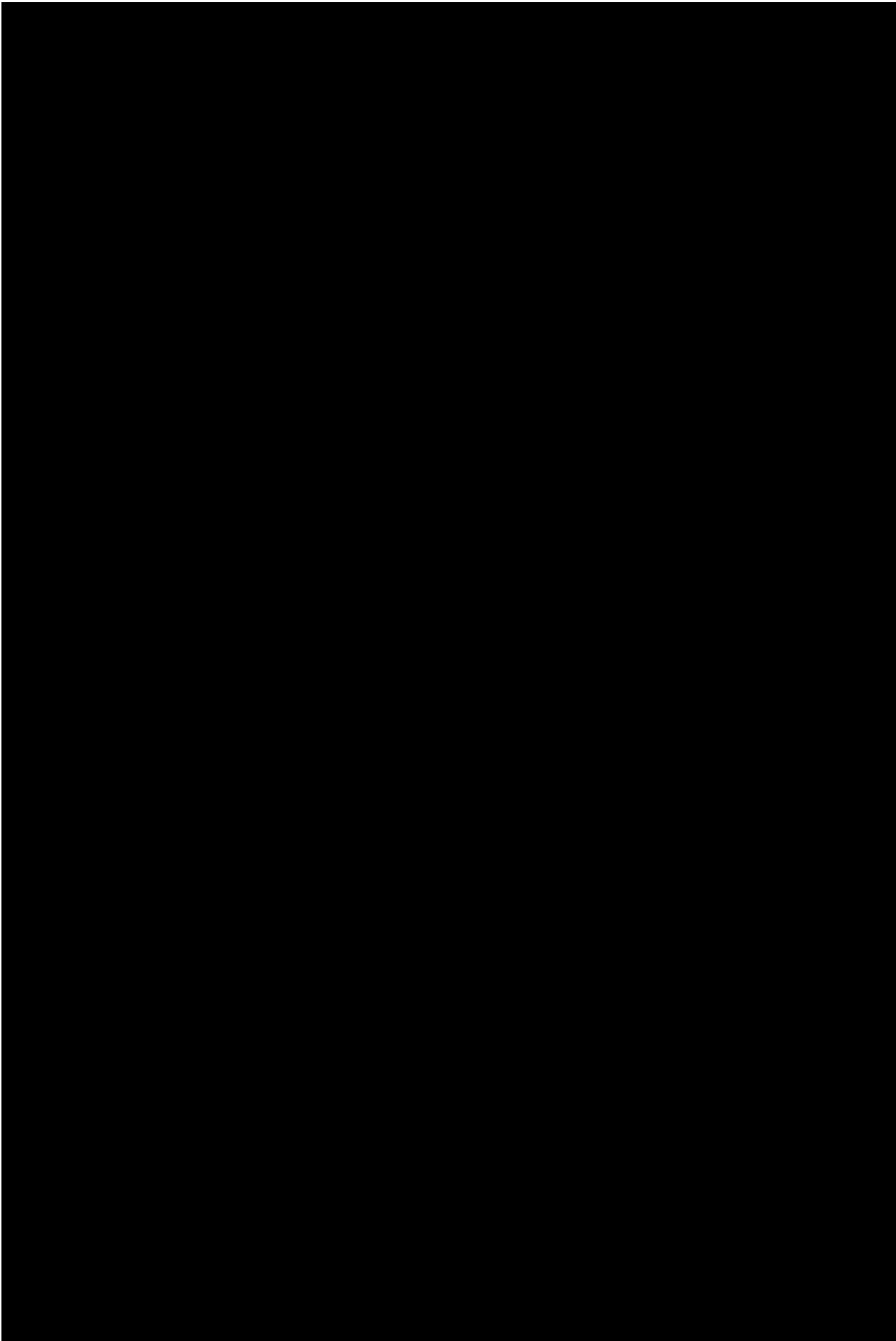


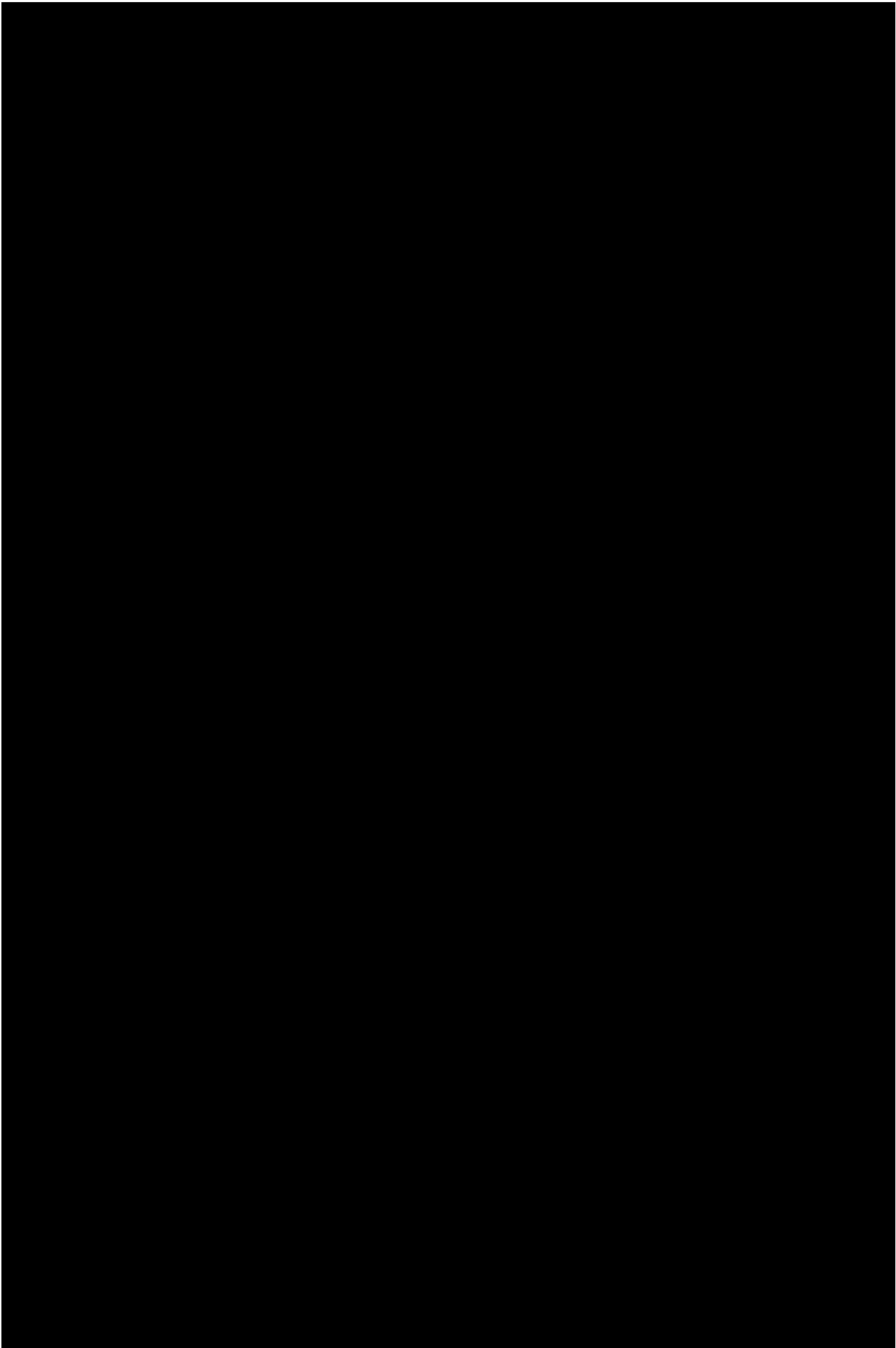


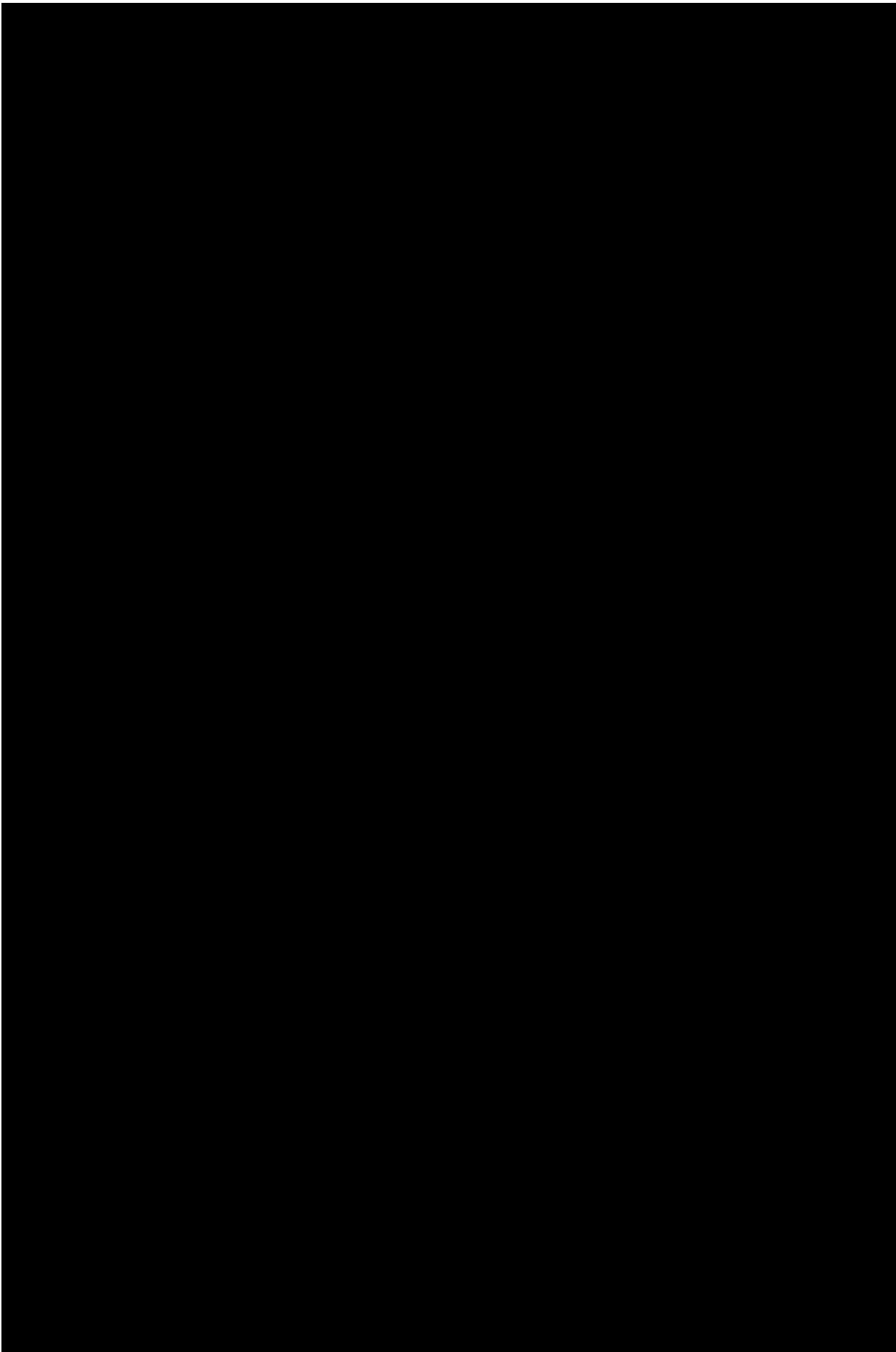


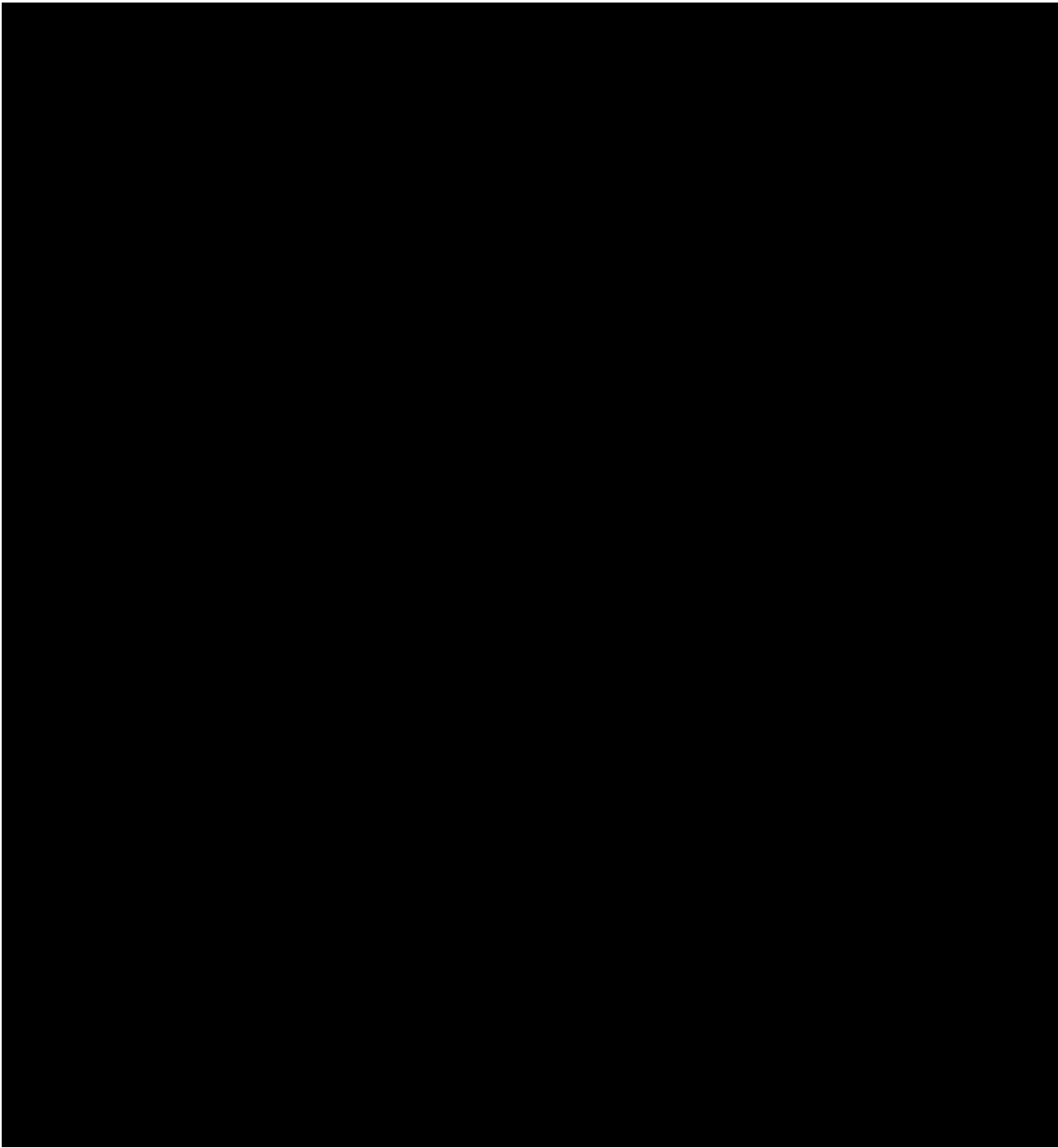


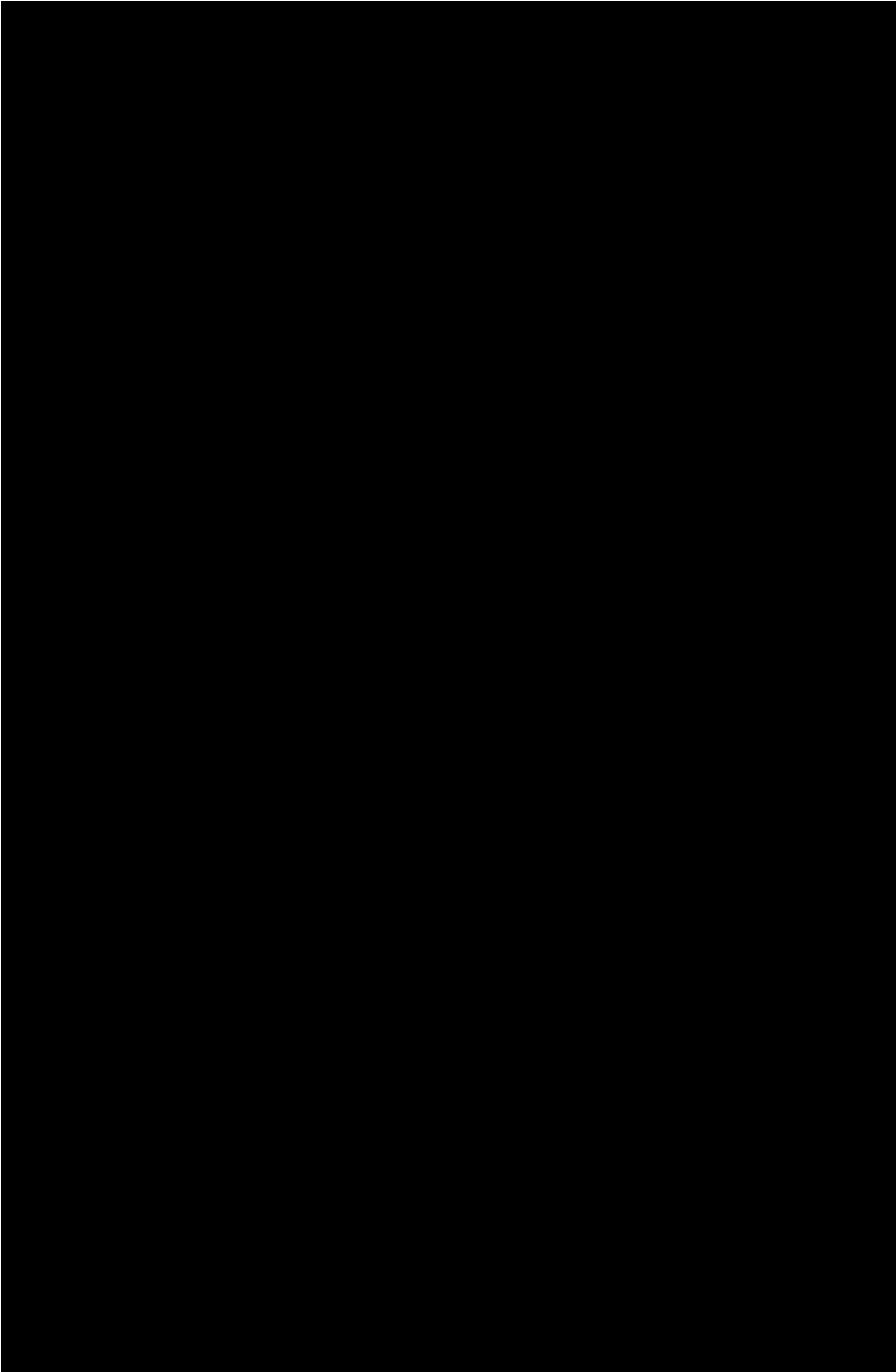


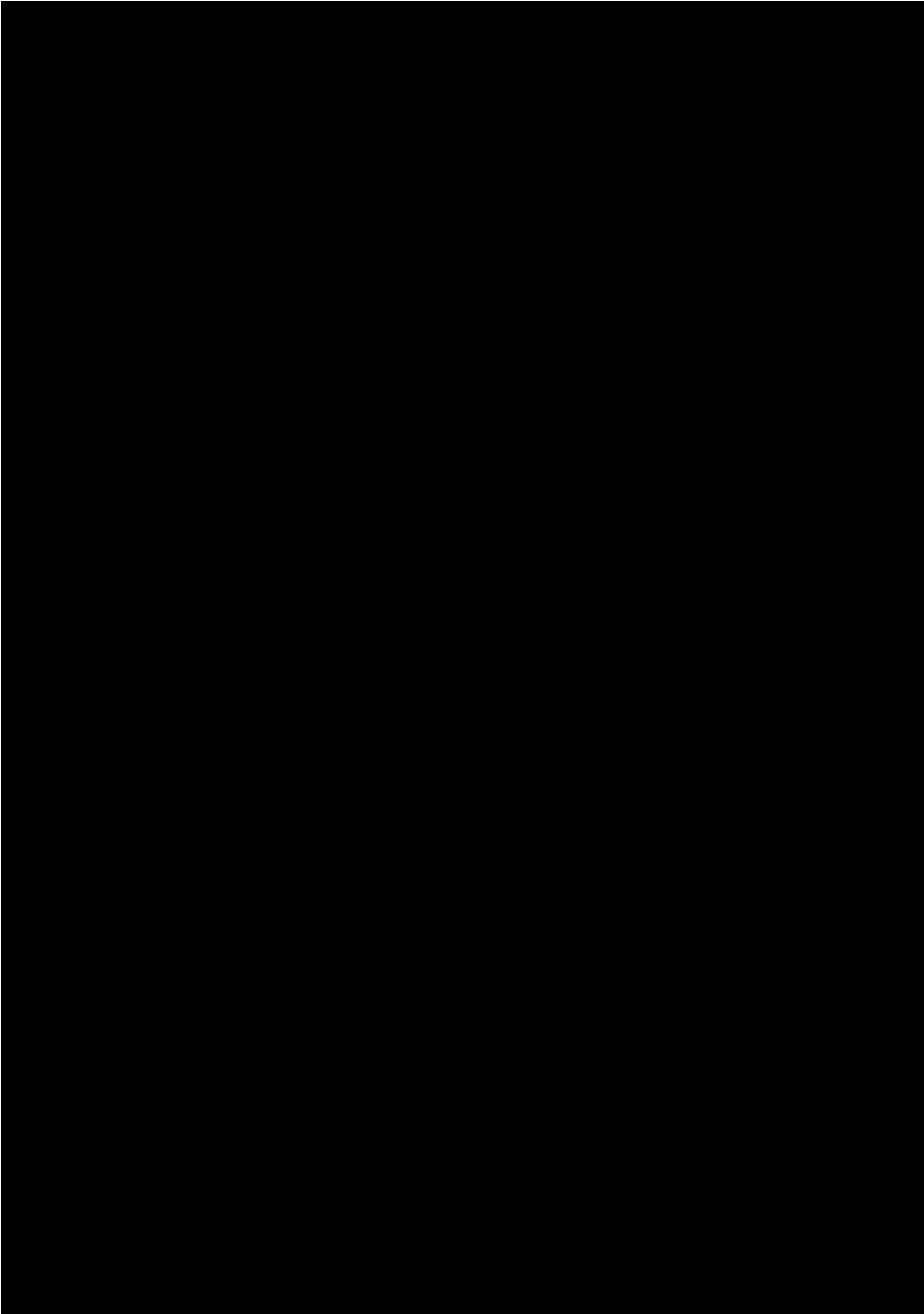


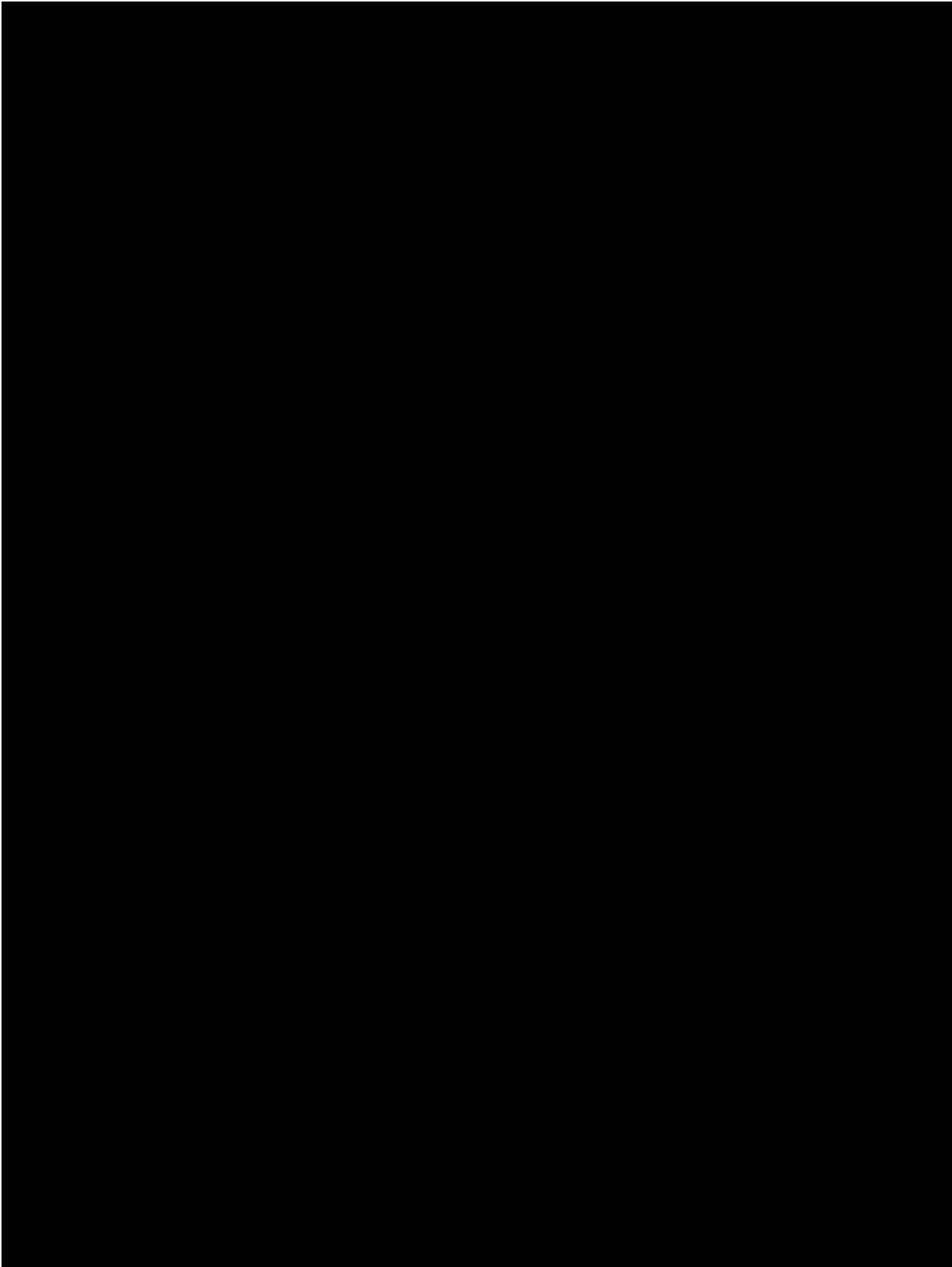






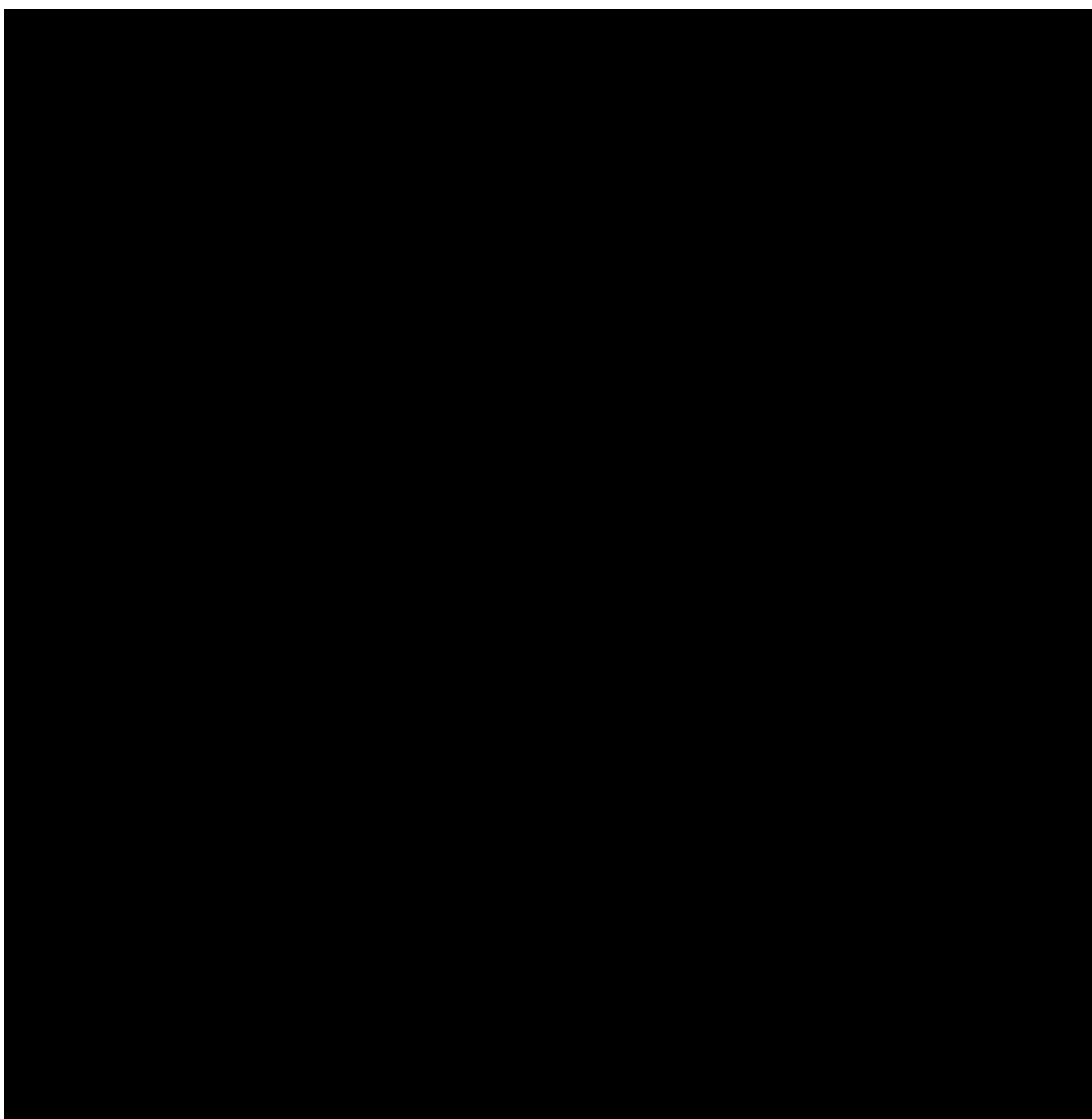


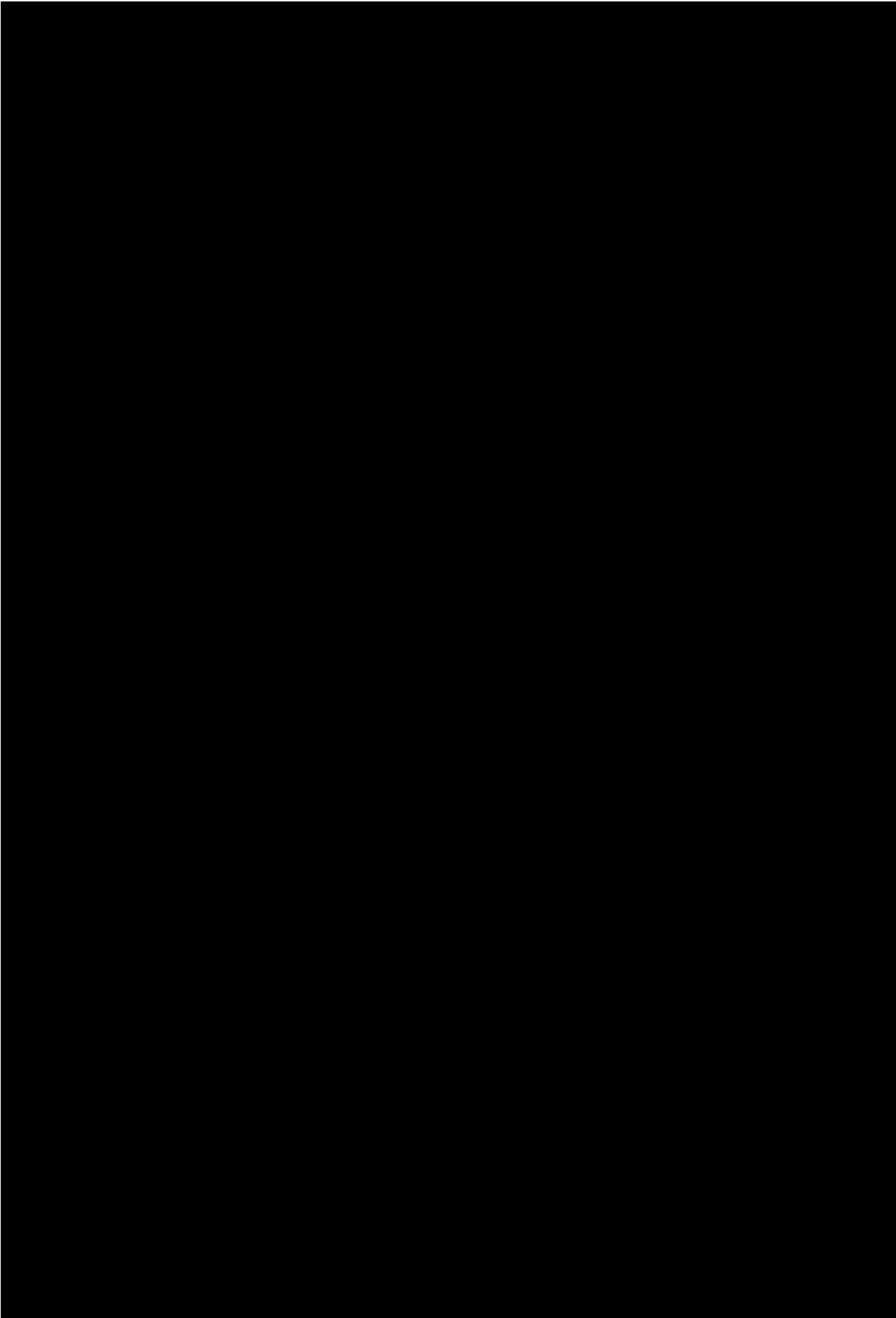


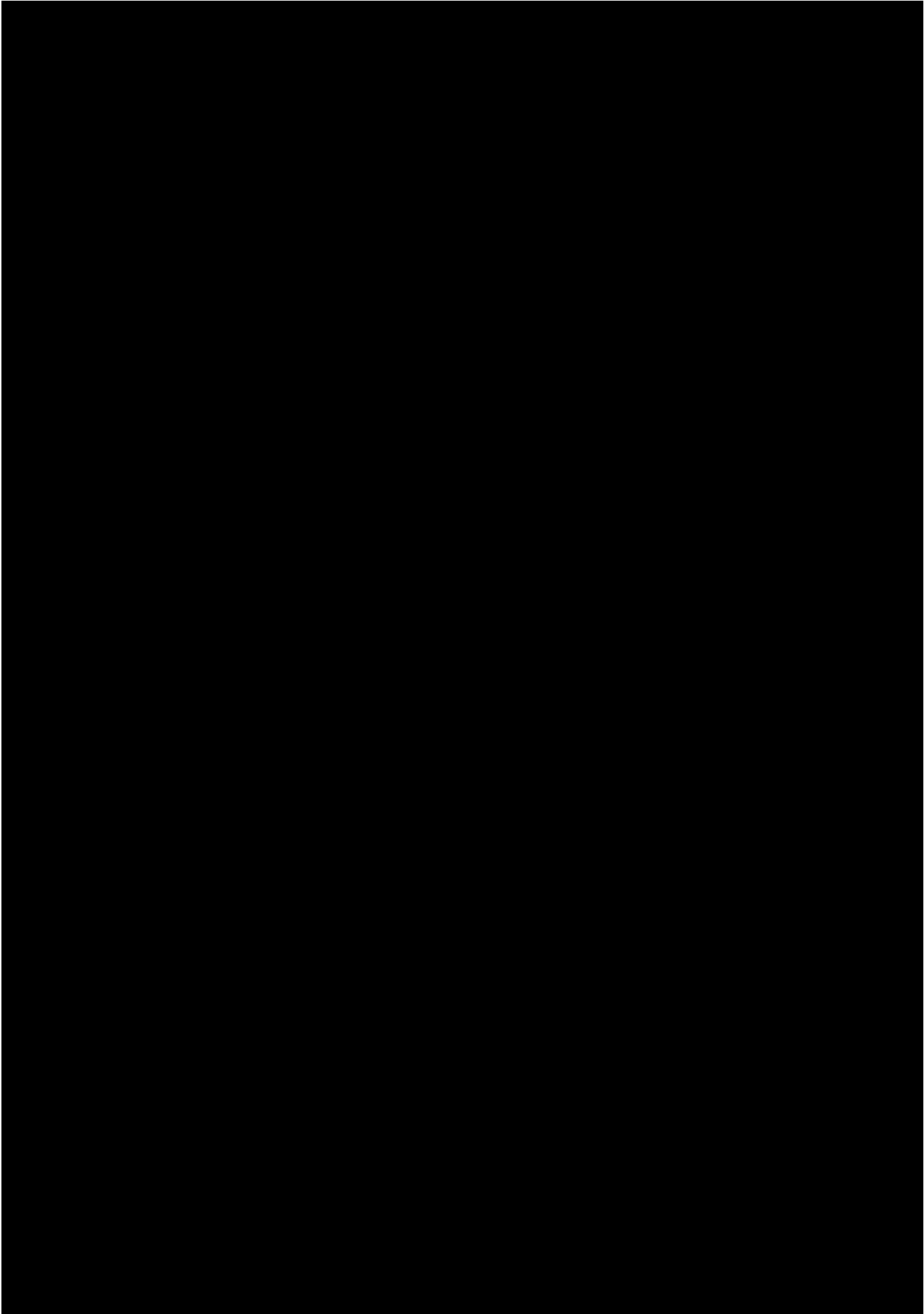


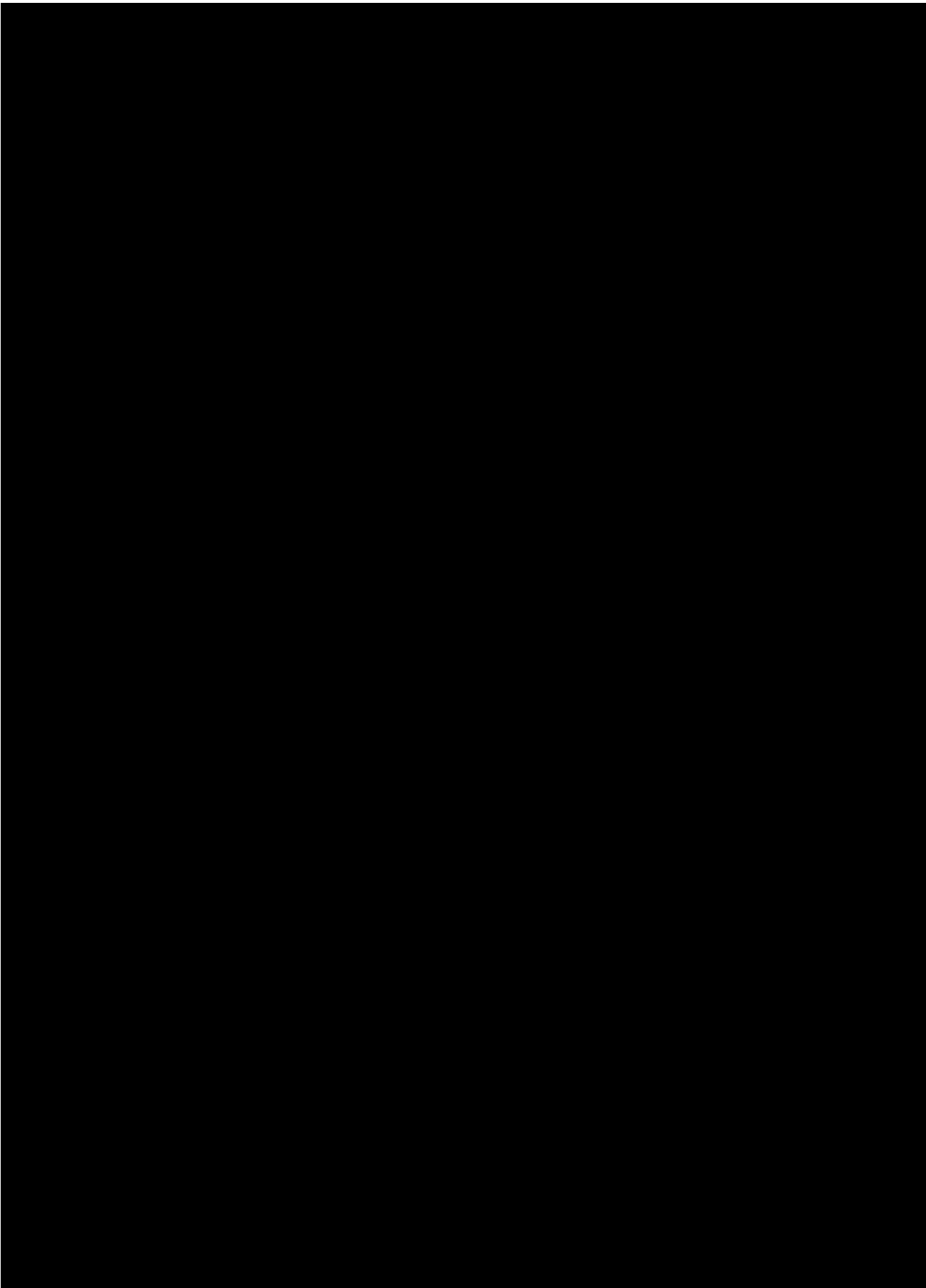
6

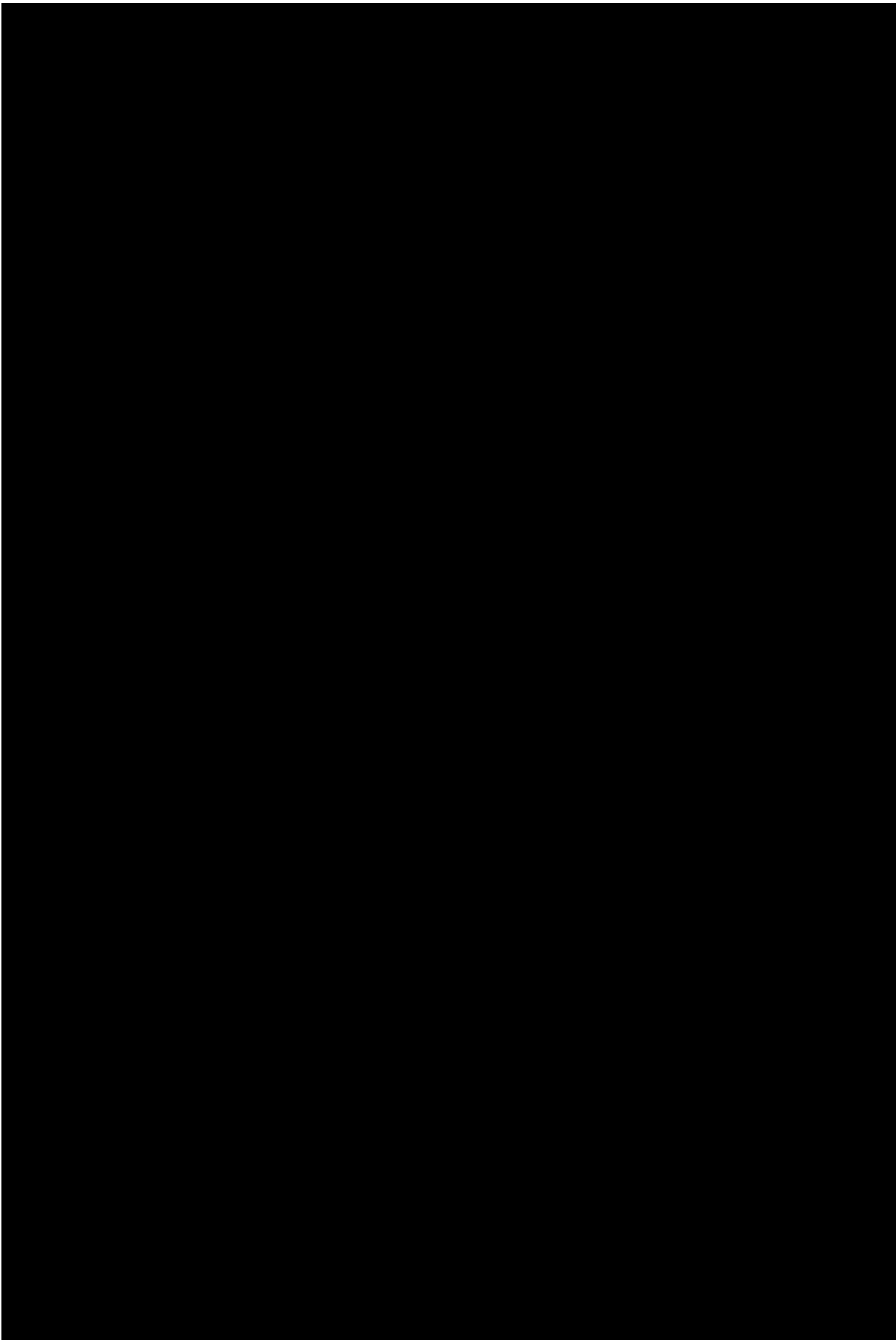
Supplementary System Implementation

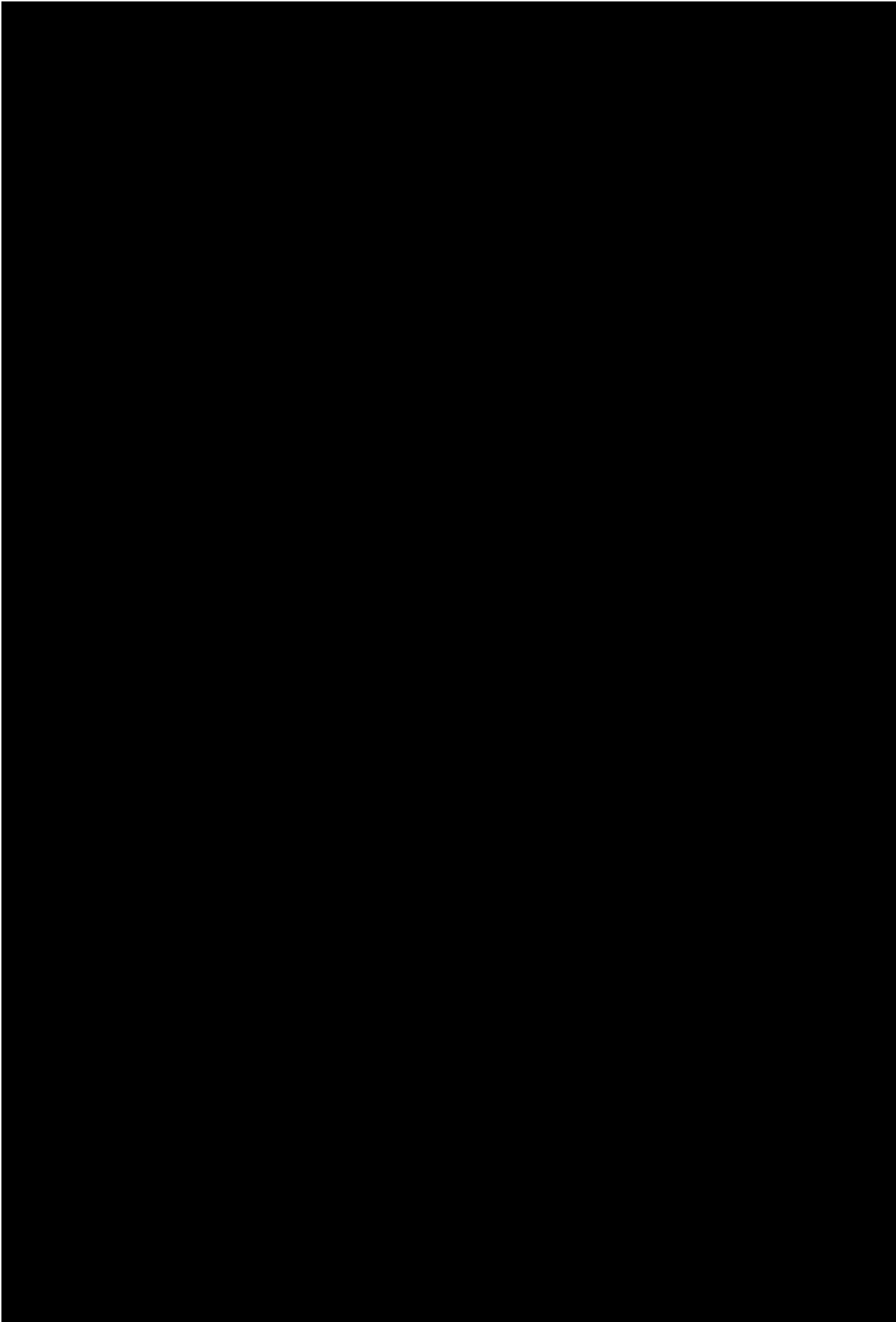


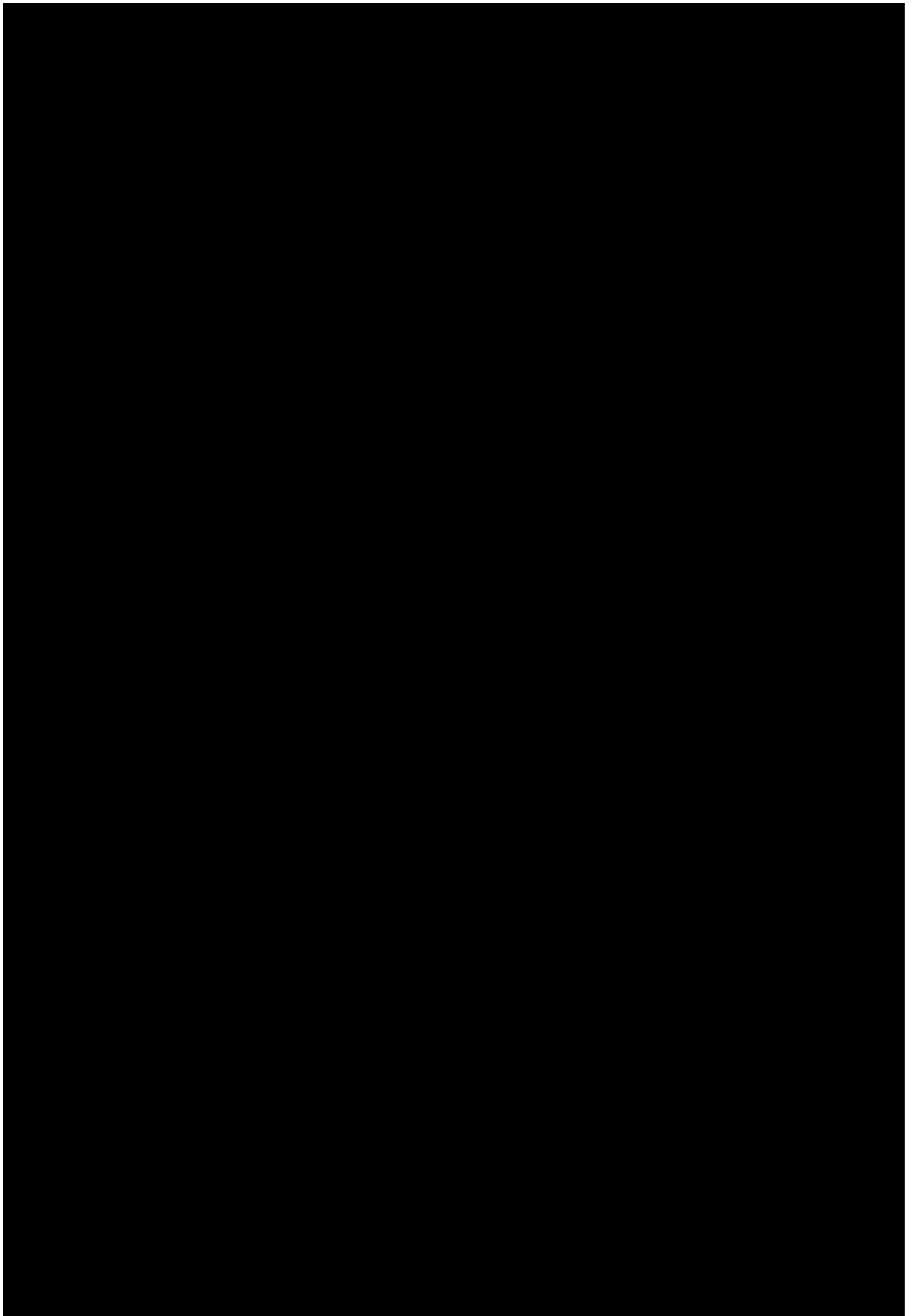




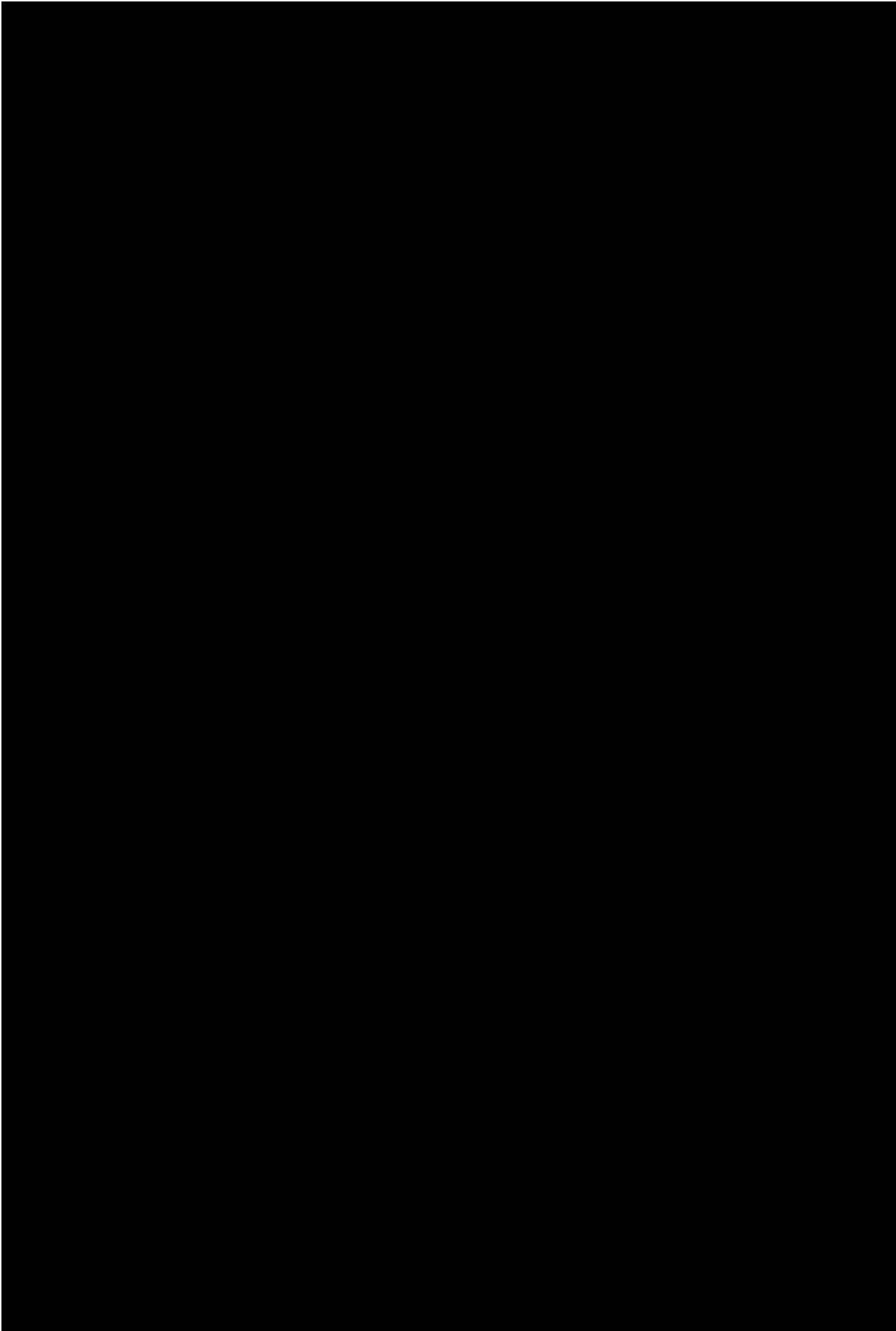


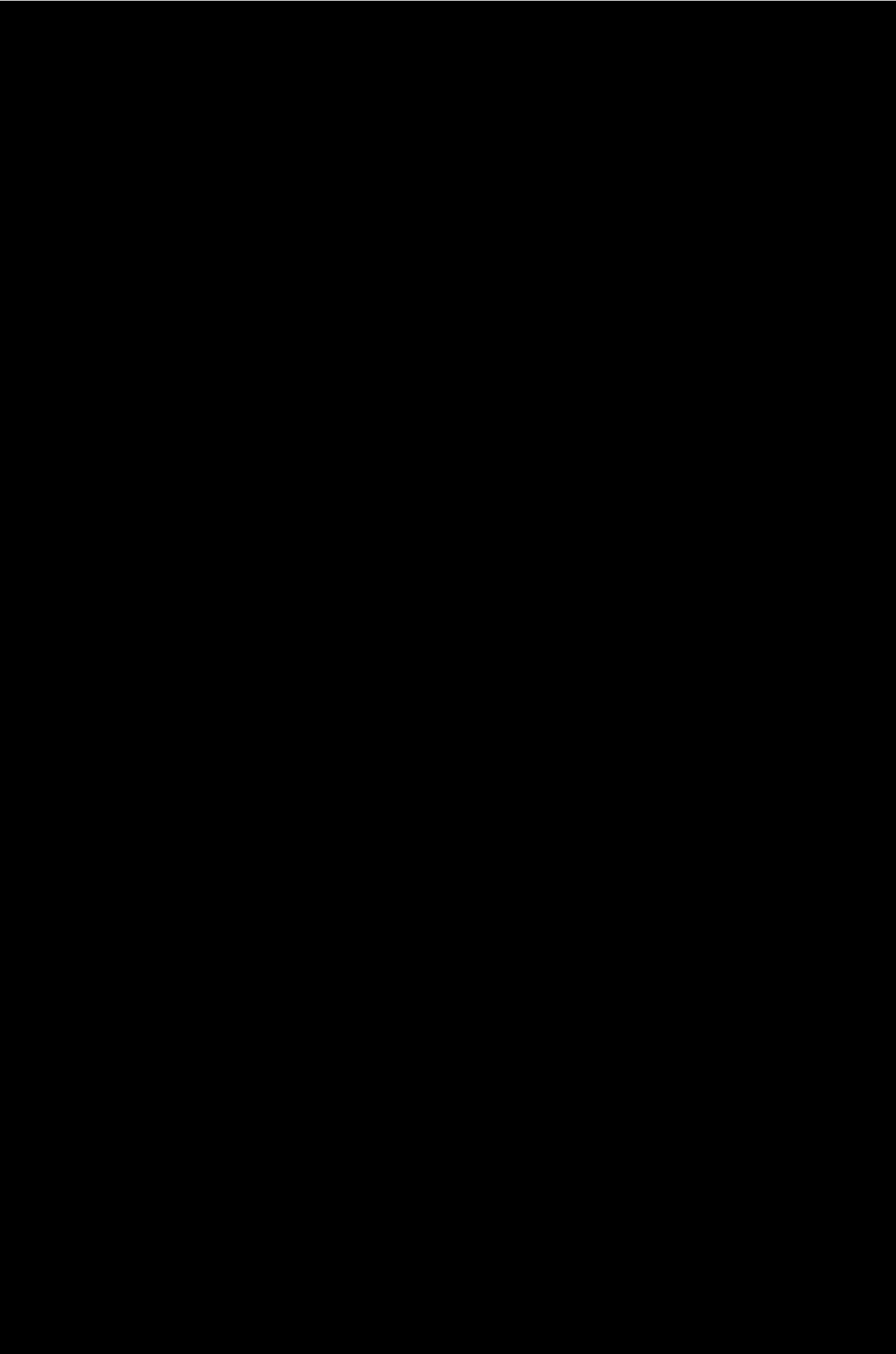


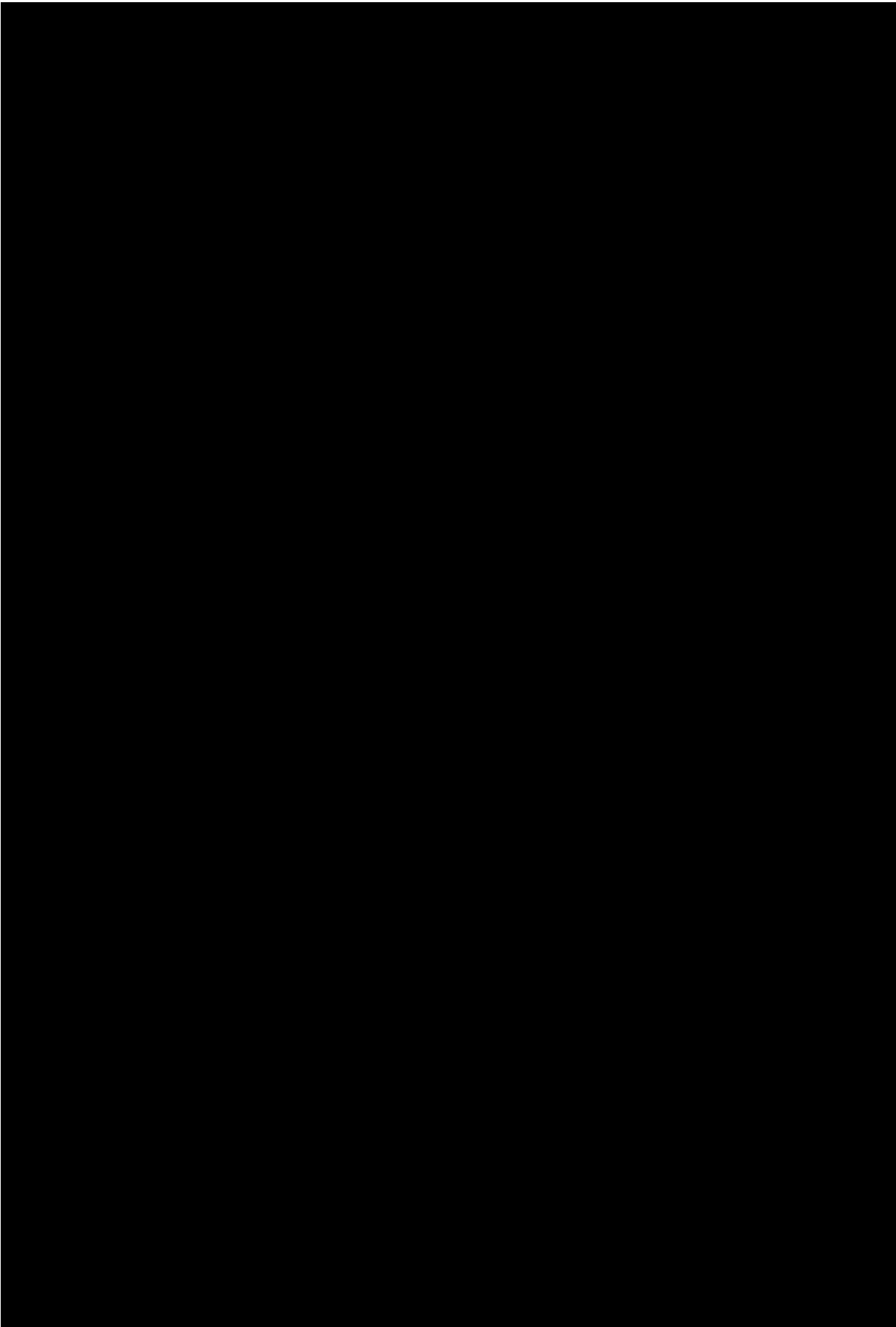


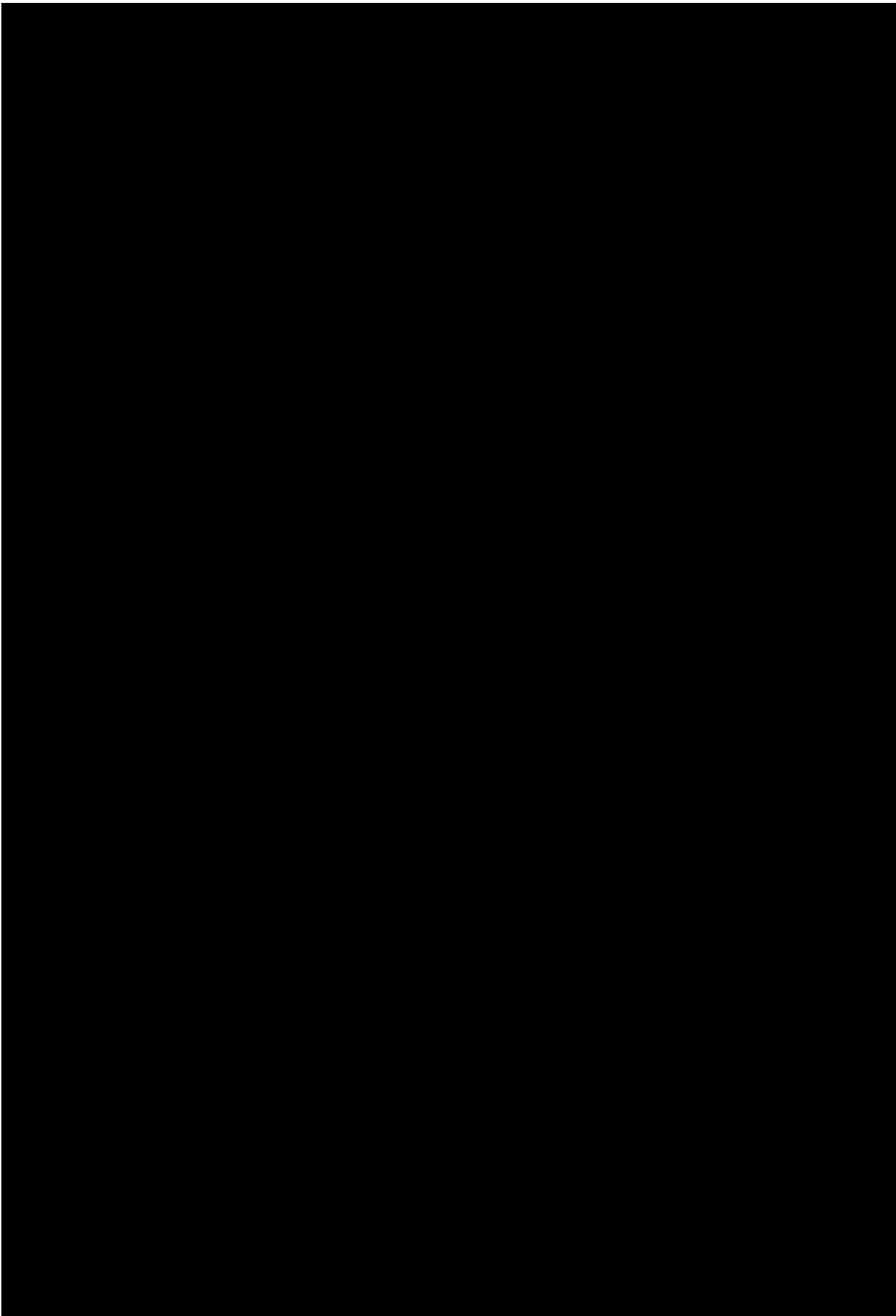


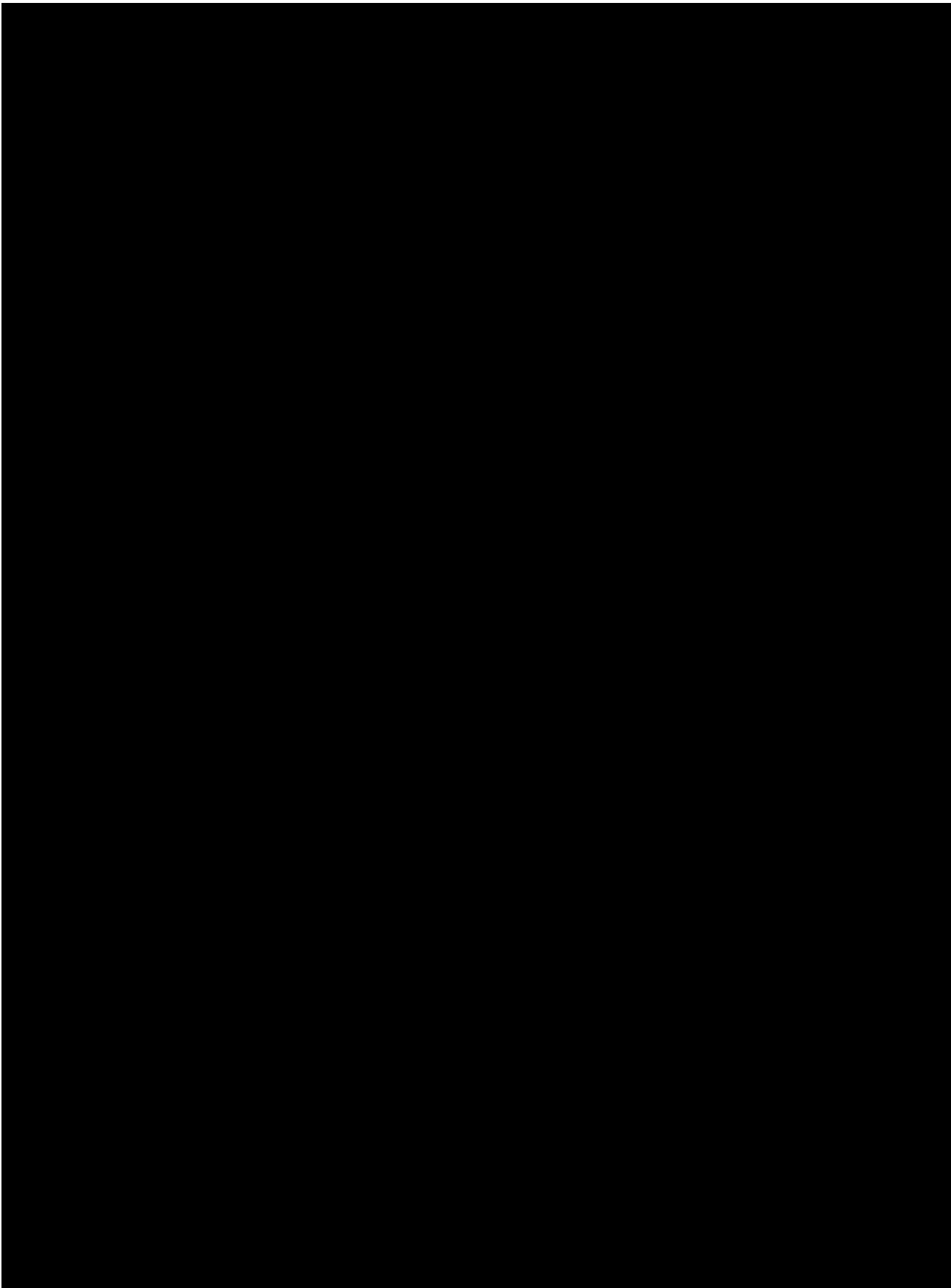
1. *Journal of the American Medical Association*, 2000; 283: 2669-2674.

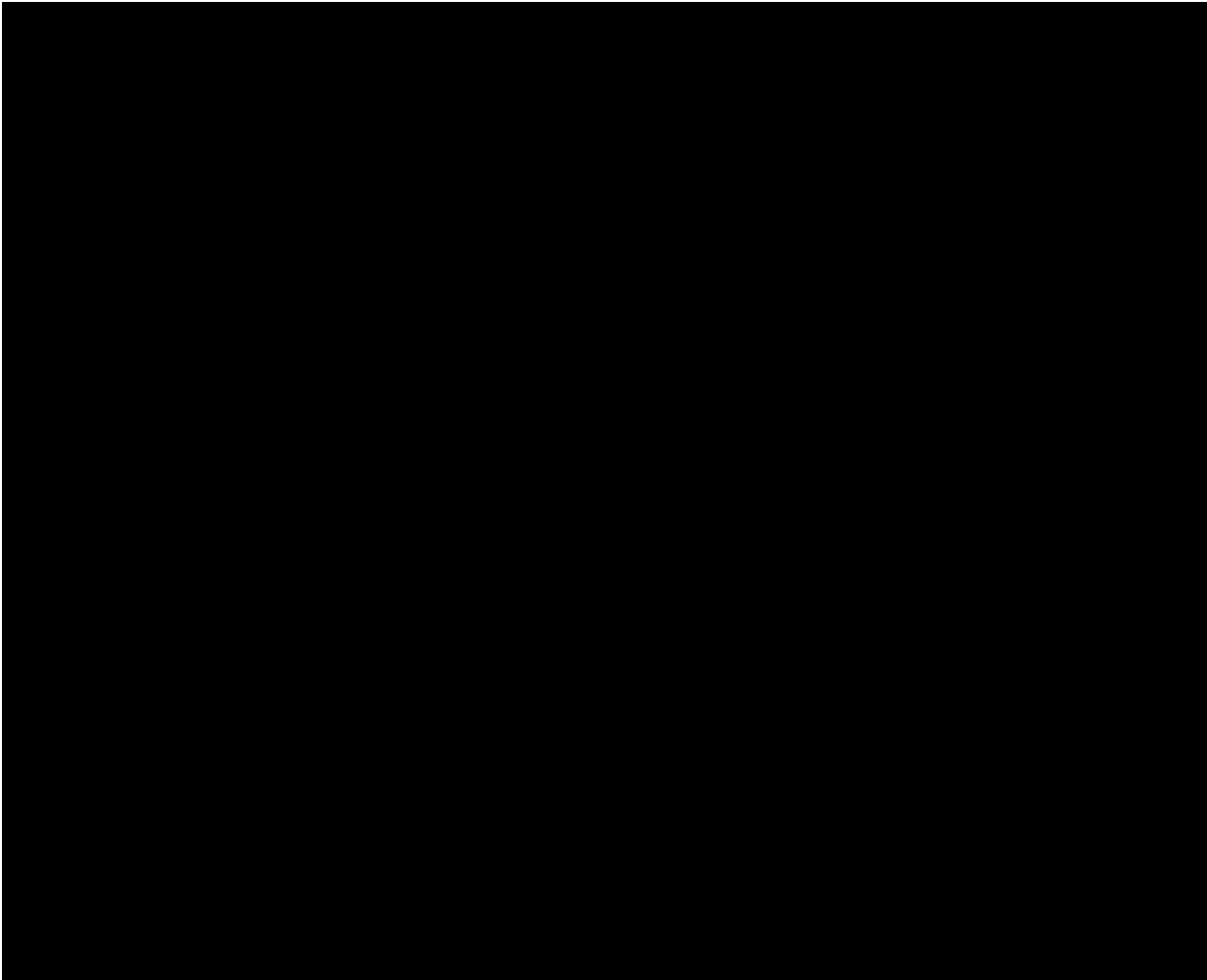












Conclusion

7.1. Conclusion

The conclusions of this thesis are:

- Doctors depend a lot on their experience to diagnose neonatal sepsis because it has non-specific symptoms. The system developed predicts neonatal sepsis automatically without any sensor attached to the neonate.

[REDACTED]

[REDACTED]

while previous researches used 12 hours of neonates clinical records [68] and 44 hours of neonates electronic health record data (heart rate, breathrate, temperature, etc.) [64] as the dataset.

[REDACTED]

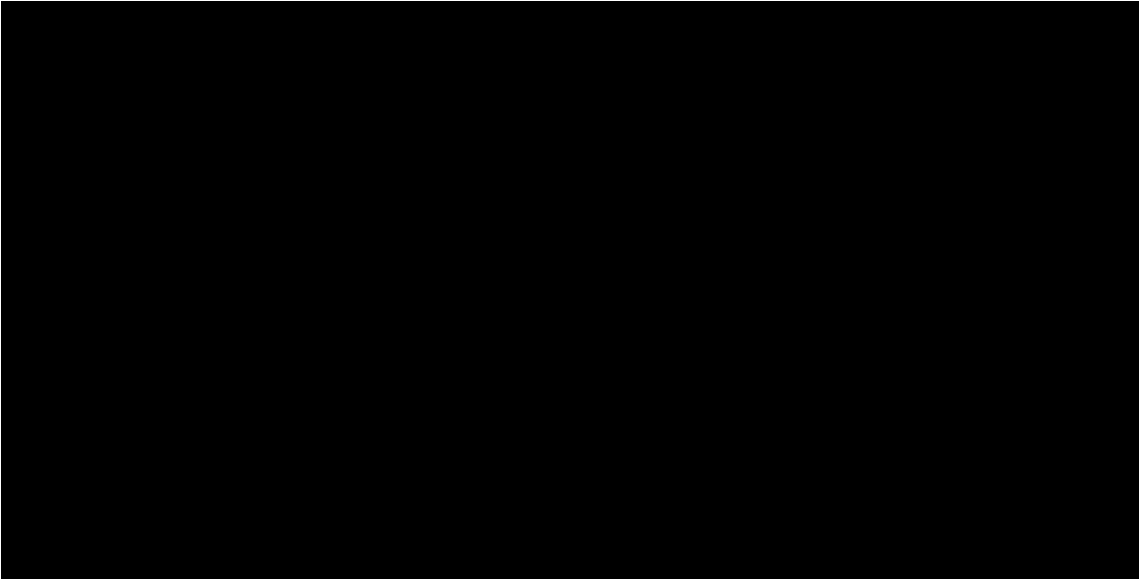
- Based on simulations, the achieved accuracy [REDACTED] could be improved by, in estimate, 5%.

7.2. Future Recommendation

The following points can be taken into account for future recommendations of sepsis prediction research:

[REDACTED]

100



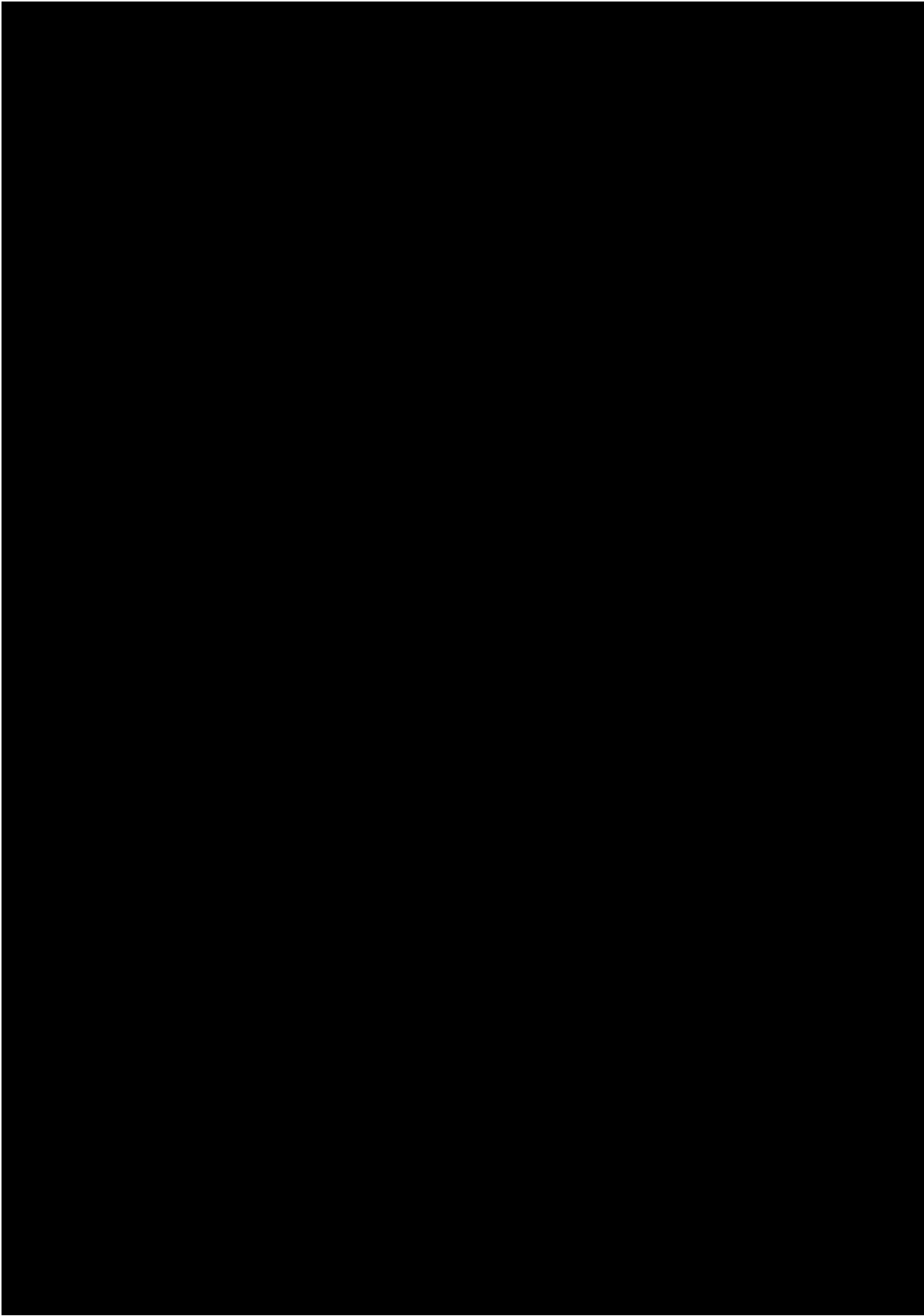
Bibliography

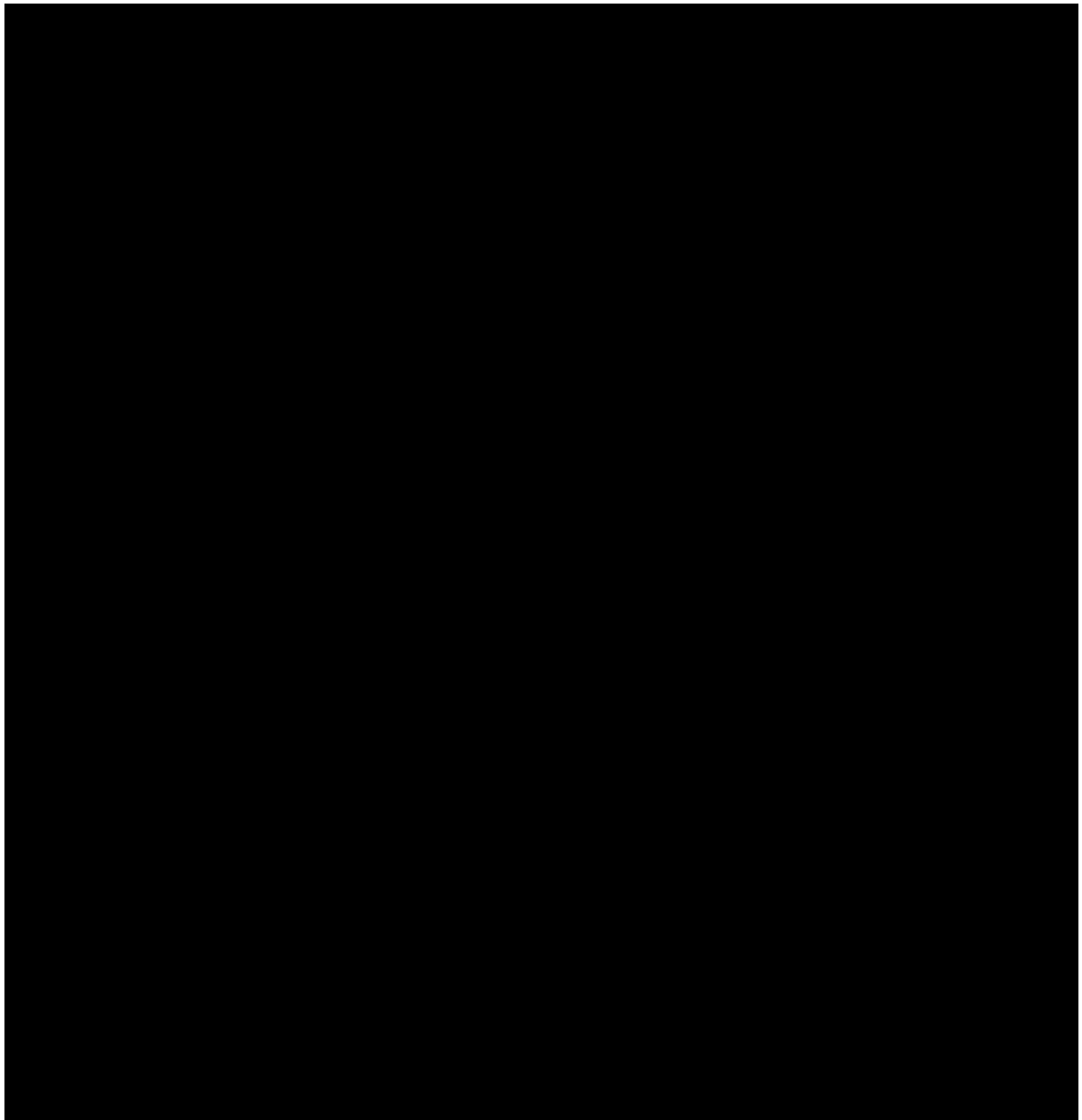
- [1] World Health Organization. Preterm Birth. <https://www.who.int/news-room/fact-sheets/detail/preterm-birth>. 2018
- [2] Liu, L., Oza, S., Hogan, D., Chu, Y., Perin, J., Zhu, J., ... Black, R. E. (2016). Global, regional, and national causes of under-5 mortality in 2000–15: an updated systematic analysis with implications for the Sustainable Development Goals. *The Lancet*, 388(10063), 3027–3035. [https://doi.org/10.1016/s0140-6736\(16\)31593-8](https://doi.org/10.1016/s0140-6736(16)31593-8)
- [3] Fluhr, J. W., Darlenski, R., Taieb, A., Hachem, J.-P., Baudouin, C., Msika, P., ... Berardesca, E. (2010). Functional skin adaptation in infancy - almost complete but not fully competent. *Experimental Dermatology*, 19(6), 483–492. <https://doi.org/10.1111/j.1600-0625.2009.01023.x>
- [4] Anic Jurica, S., Colic, A., Gveric-Ahmetasevic, S., Loncarevic, D., Filipovic-Grcic, B., Stipanovic-Kastelic, J., & Resic, A. (2016). Skin of the very premature newborn – physiology and care. *Paediatrica Croatica*, 60(1), 21–26. <https://doi.org/10.13112/pc.2016.4>
- [5] Rutter, N. (2000). The dermis. *Seminars in Neonatology*, 5(4), 297–302. <https://doi.org/10.1053/siny.2000.0016>
- [6] Baharestani MM. (2007). An overview of neonatal and pediatric wound care knowledge and considerations. *Ostomy/wound Management*. Jun;53(6):34-6, 38, 40, passim.
- [7] Lloyd, R., Goulding, R., Filan, P., & Boylan, G. (2015). Overcoming the practical challenges of electroencephalography for very preterm infants in the neonatal intensive care unit. *Acta Paediatrica*, 104(2), 152–157. <https://doi.org/10.1111/apa.12869>
- [8] Lund, C. H., Nonato, L. B., Kuller, J. M., Franck, L. S., Cullander, C., & Durand, D. K. (1997). Disruption of barrier function in neonatal skin associated with adhesive removal. *The Journal of Pediatrics*, 131(3), 367–372. [https://doi.org/10.1016/s0022-3476\(97\)80060-1](https://doi.org/10.1016/s0022-3476(97)80060-1)
- [9] J. D. Fernandes, M. C. Machado, Z. N. Oliveira, “Children and newborn skin care and prevention”, *An Bras Dermatol*, Vol. 86, No. 1, pp. 102-110, 2011.
- [10] Cleminson, J., & McGuire, W. (1998). Topical emollient for preventing infection in preterm infants (W. McGuire, Ed.). <https://doi.org/10.1002/14651858.cd001150.pub2>
- [11] Darmstadt, G. L., Badrawi, N., Law, P. A., Ahmed, S., Bashir, M., Iskander, I., Said, D. A., Kholy, A. E., Husein, M. H., Alam, A., Winch, P. J., Gipson, R., & Santosham, M. (2004). Topically Applied Sunflower Seed Oil Prevents Invasive Bacterial Infections in Preterm Infants in Egypt. *The Pediatric Infectious Disease Journal*, 23(8), 719–725. <https://doi.org/10.1097/01.inf.0000133047.50836.6f>
- [12] Rutter, N. (1987). Percutaneous Drug Absorption in the Newborn: Hazards and Uses. *Clinics in Perinatology*, 14(4), 911–930. [https://doi.org/10.1016/s0095-5108\(18\)30740-1](https://doi.org/10.1016/s0095-5108(18)30740-1)
- [13] VIVIER, P. M., LEWANDER, W. J., MARTIN, H. E., & LINAKIS, J. G. (1994). Isopropyl alcohol intoxication in a neonate through chronic dermal exposure: A complication of a culturally-based umbilical care practice. *Pediatric Emergency Care*, 10(2), 91–93. <https://doi.org/10.1097/00006565-199404000-00008>
- [14] Jones, B. F. (1998). A reappraisal of the use of infrared thermal image analysis in medicine. *IEEE Transactions on Medical Imaging*, 17(6), 1019–1027. <https://doi.org/10.1109/42.746635>
- [15] Martin, R. J., Miller, M. J., & Carlo, W. A. (1986). Pathogenesis of apnea in preterm infants. *The Journal of Pediatrics*, 109(5), 733–741. [https://doi.org/10.1016/s0022-3476\(86\)80685-0](https://doi.org/10.1016/s0022-3476(86)80685-0)

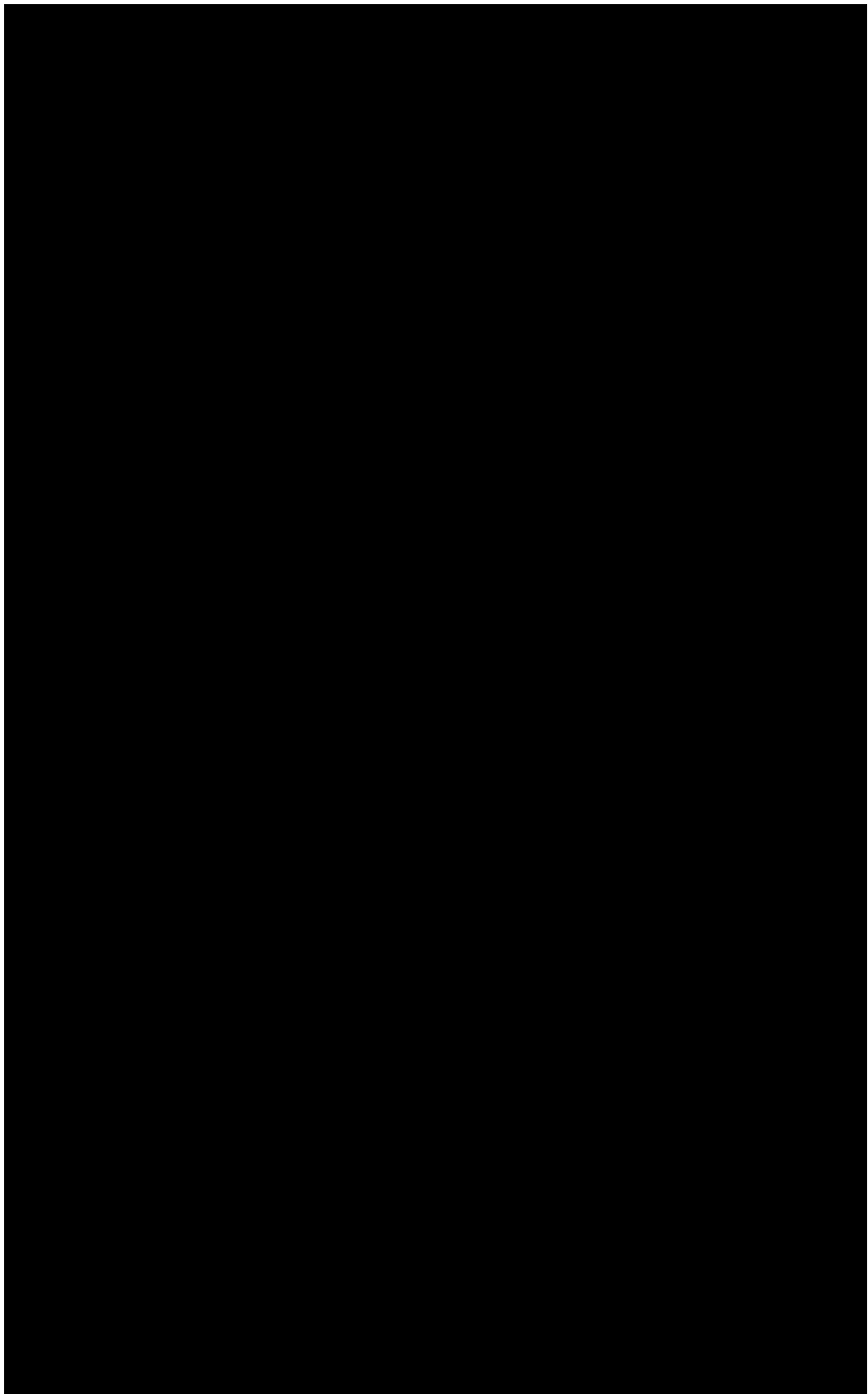
- [16] Soll, R. F. (2008). Heat loss prevention in neonates. *Journal of Perinatology*, 28(S1), S57–S59. <https://doi.org/10.1038/jp.2008.51>
- [17] Brück, K. (1961). Temperature Regulation in the Newborn Infant. *Neonatology*, 3(2–3), 65–119.
- [18] Smith, J., Alcock, G., & Usher, K. (2013). Temperature Measurement in the Preterm and Term Neonate: A Review of the Literature. *Neonatal Network*, 32(1), 16–25. <https://doi.org/10.1891/0730-0832.32.1.16>
- [19] Acolet, D. (2005). Project 27/28: Inquiry Into Quality of Neonatal Care and Its Effect on the Survival of Infants Who Were Born at 27 and 28 Weeks in England, Wales, and Northern Ireland. *PEDIATRICS*, 116(6), 1457–1465. <https://doi.org/10.1542/peds.2004-2691>
- [20] World Health Organization. Thermal Protection of the Newborn https://www.who.int/maternal_child_adolescent/documents/ws42097th/en/1997
- [21] Smith, J. (2014). Methods and Devices of Temperature Measurement in the Neonate: A Narrative Review and Practice Recommendations. *Newborn and Infant Nursing Reviews*, 14(2), 64–71. <https://doi.org/10.1053/j.nainr.2014.03.001>
- [22] Uslu, S., Ozdemir, H., Bulbul, A., Comert, S., Bolat, E., Can, E., & Nuhoglu, A. (2011). A Comparison of Different Methods of Temperature Measurements in Sick Newborns. *Journal of Tropical Pediatrics*, 57(6), 418–423. <https://doi.org/10.1093/tropej/fmq120>
- [23] Rosenthal, H. M., & Leslie, A. (2006). Measuring temperature of NICU patients – A comparison of three devices. *Journal of Neonatal Nursing*, 12(4), 125–129. <https://doi.org/10.1016/j.jnn.2006.05.007>
- [24] El-Radhi, A. S. (2006). Thermometry in paediatric practice. *Archives of Disease in Childhood*, 91(4), 351–356. <https://doi.org/10.1136/ad.2005.088831>
- [25] Mcallister, T. A., Marshall, A., Roud, J. A., Holland, B. M., & Turner, T. L. (1986). OUTBREAK OF SALMONELLA EIMSBUEITEL IN NEWBORN INFANTS SPREAD BY RECTAL THERMOMETERS. *The Lancet*, 327(8492), 1262–1264. [https://doi.org/10.1016/s0140-6736\(86\)91397-8](https://doi.org/10.1016/s0140-6736(86)91397-8)
- [26] Chardon, K., Cardot, V., Léké, A., Delanaud, S., Bach, V., Dewasmes, G., & Telliez, F. (2006). Thermoregulatory Control of Feeding and Sleep in Premature Infants. *Obesity*, 14(9), 1535–1542. <https://doi.org/10.1038/oby.2006.177>
- [27] Antonucci, R., Porcella, A., & Fanos, V. (2009). The infant incubator in the neonatal intensive care unit: unresolved issues and future developments. *Journal of Perinatal Medicine*, 37(6). <https://doi.org/10.1515/jpm.2009.109>
- [28] de Goffau, M. C., Bergman, K. A., de Vries, H. J., Meessen, N. E. L., Degener, J. E., van Dijk, J. M., & Harmsen, H. J. M. (2011). Cold Spots in Neonatal Incubators Are Hot Spots for Microbial Contamination. *Applied and Environmental Microbiology*, 77(24), 8568–8572. <https://doi.org/10.1128/aem.06015-11>
- [29] Lawn, J. E., Cousens, S., & Zupan, J. (2005). 4 million neonatal deaths: When? Where? Why? *The Lancet*, 365(9462), 891–900. [https://doi.org/10.1016/s0140-6736\(05\)71048-5](https://doi.org/10.1016/s0140-6736(05)71048-5)
- [30] Schindler, T., Koller-Smith, L., Lui, K., Bajuk, B., & Bolisetty, S. (2017). Causes of death in very preterm infants cared for in neonatal intensive care units: a population-based retrospective cohort study. *BMC Pediatrics*, 17(1). <https://doi.org/10.1186/s12887-017-0810-3>
- [31] Muhe, L. M., McClure, E. M., Nigussie, A. K., Mekasha, A., Worku, B., Worku, A., ... Goldenberg, R. L. (2019). Major causes of death in preterm infants in selected hospitals in Ethiopia (SIP): a prospective, cross-sectional, observational study. *The Lancet Global Health*, 7(8), e1130–e1138. [https://doi.org/10.1016/s2214-109x\(19\)30220-7](https://doi.org/10.1016/s2214-109x(19)30220-7)
- [32] Signore, A. (2013). About inflammation and infection. *EJNMMI Research*, 3(1), 8. <https://doi.org/10.1186/2191-219x-3-8>
- [33] Tesini, B. L., Overview of Neonatal Infections. <https://www.msmanuals.com/professional/pediatrics/infections-in-neonates/overview-of-neonatal-infections.2018>

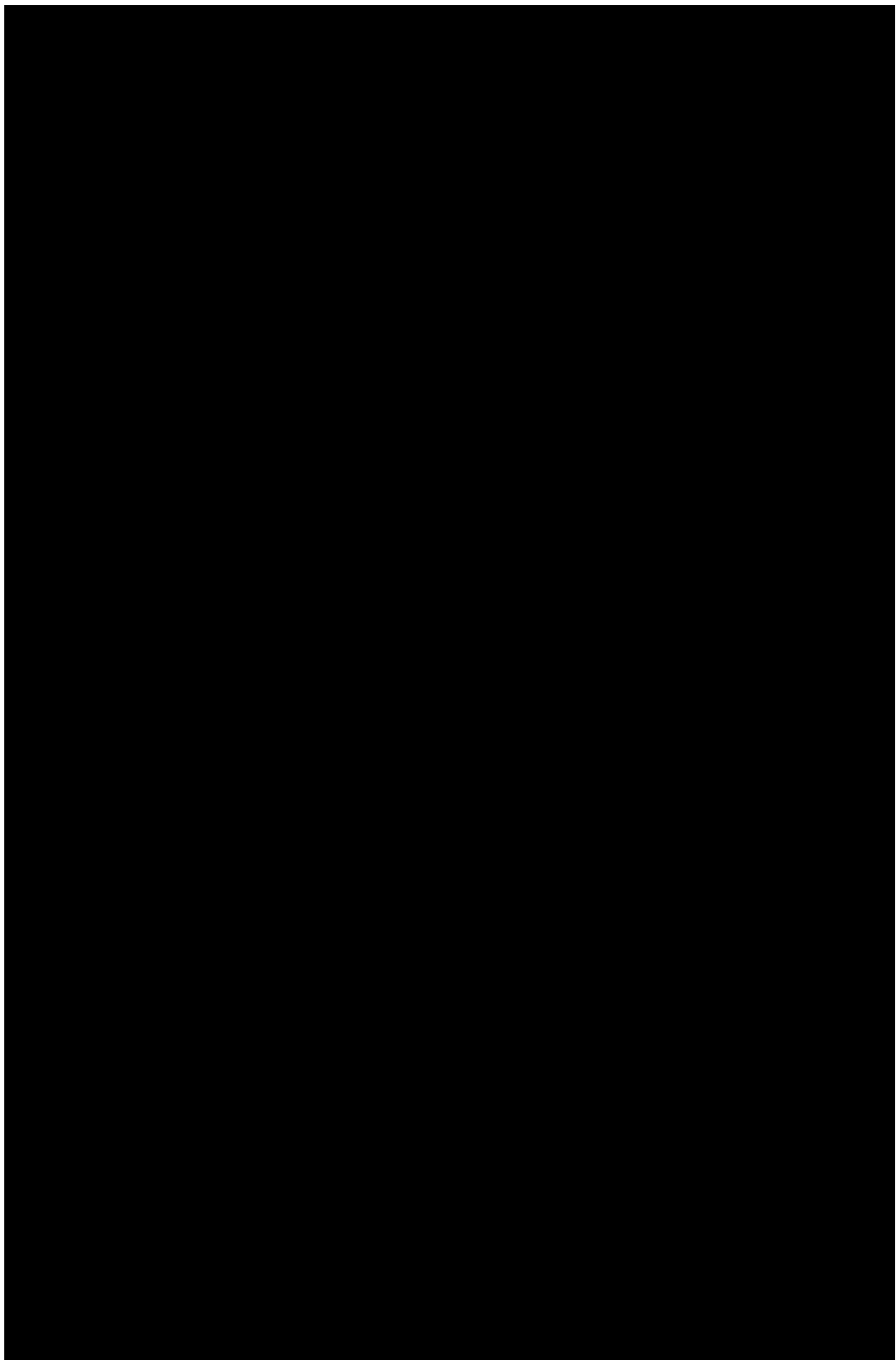
- [34] Hobbie, R. K., & Roth, B. J. (2015). Intermediate Physics for Medicine and Biology. <https://doi.org/10.1007/978-3-319-12682-1>
- [35] Abbas, A. K., Heimann, K., Blazek, V., Orlikowsky, T., & Leonhardt, S. (2012). Neonatal infrared thermography imaging: Analysis of heat flux during different clinical scenarios. *Infrared Physics & Technology*, 55(6), 538–548. <https://doi.org/10.1016/j.infrared.2012.07.001>
- [36] Lytle, J. D., Wilkerson, G. W., & Jaramillo, J. G. (1979). Wideband optical transmission properties of seven thermoplastics. *Applied Optics*, 18(11), 1842. <https://doi.org/10.1364/ao.18.001842>
- [37] Pogge, R. (2008). An Introduction to Solar System Astronomy, <http://www.astronomy.ohio-state.edu/pogge/Ast161/Unit5/atmos.html>
- [38] Mills, A., & Coimbra, Carlos F.M. (2015). Basic heat and mass transfer (Third ed.). San Diego, California: Prentice Hall.
- [39] Togawa, T. (1989). Non-contact skin emissivity: measurement from reflectance using step change in ambient radiation temperature. *Clinical Physics and Physiological Measurement*, 10(1), 39–48. <https://doi.org/10.1088/0143-0815/10/1/004>
- [40] Steketee, J. (1973). Spectral emissivity of skin and pericardium. *Physics in Medicine and Biology*, 18(5), 686–694. <https://doi.org/10.1088/0031-9155/18/5/307>
- [41] Minkina, W. & Dudzik, S. (2009). Infrared thermography : errors and uncertainties. Chichester, U.K: J. Wiley.
- [42] Gunnar Farneback. 2003. Two-frame motion estimation based on polynomial expansion, *Lecture Notes in Computer Science*, (2749), 363-370.
- [43] Bouguet, J. 1999. Pyramidal implementation of the lucas kanade feature tracker.
- [44] MathWorks. OpticalFlowFarneback. Retrieved from <https://nl.mathworks.com/help/vision/ref/opticalflowfarneback.htm>
- [45] Awad, A. I. ve Hassaballah, M. (Ed.). (2016). Image Feature Detectors and Descriptors. *Studies in Computational Intelligence*. Springer International Publishing. doi:10.1007/978-3-319-28854-3
- [46] Karami, E., Prasad, S., & Shehata, M. (2017). Image Matching Using SIFT, SURE, BRIEF and ORB: Performance Comparison for Distorted Images. *ArXiv*, abs/1710.02726.
- [47] Szeliski, R. (2011). Computer Vision. In *Texts in Computer Science*. Springer London. <https://doi.org/10.1007/978-1-84882-935-0>
- [48] Rublee, E., Rabaud, V., Konolige, K., & Bradski, G. (2011, November). ORB: An efficient alternative to SIFT or SURE 2011 International Conference on Computer Vision. 2011 IEEE International Conference on Computer Vision (ICCV). <https://doi.org/10.1109/iccv.2011.6126544>
- [49] Muja, M., & Lowe, D. G. (2014). Scalable Nearest Neighbor Algorithms for High Dimensional Data. *IEEE Transactions on Pattern Analysis and Machine Intelligence*, 36(11), 2227–2240. <https://doi.org/10.1109/tpami.2014.2321376>
- [50] Craig Hunt. 2002. TCP/IP network administration (3rd ed.). O'Reilly & Associates, Inc., USA.
- [51] Camacho-Gonzalez, A., Spearman, P. W., & Stoll, B. J. (2013). Neonatal Infectious Diseases. *Pediatric Clinics of North America*, 60(2), 367–389. <https://doi.org/10.1016/j.pcl.2012.12.003>
- [52] Zea-Vera, A., & Ochoa, T. J. (2015). Challenges in the diagnosis and management of neonatal sepsis. *Journal of Tropical Pediatrics*, 61(1), 1–13. <https://doi.org/10.1093/tropej/fmu079>
- [53] Jawaheer, G., Neal, T. J., & Shaw, N. J. (1997). Blood culture volume and detection of coagulase negative staphylococcal septicaemia in neonates. *Archives of Disease in Childhood - Fetal and Neonatal Edition*, 76(1), F57–F58. <https://doi.org/10.1136/fn.76.1.f57>
- [54] Neal PR, Kleiman MB, Reynolds JK, Allen SD, Lemons JA, Yu PL. (1986). Volume of blood submitted for culture from neonates. *J Clin Microbiol*. 24:353–6.

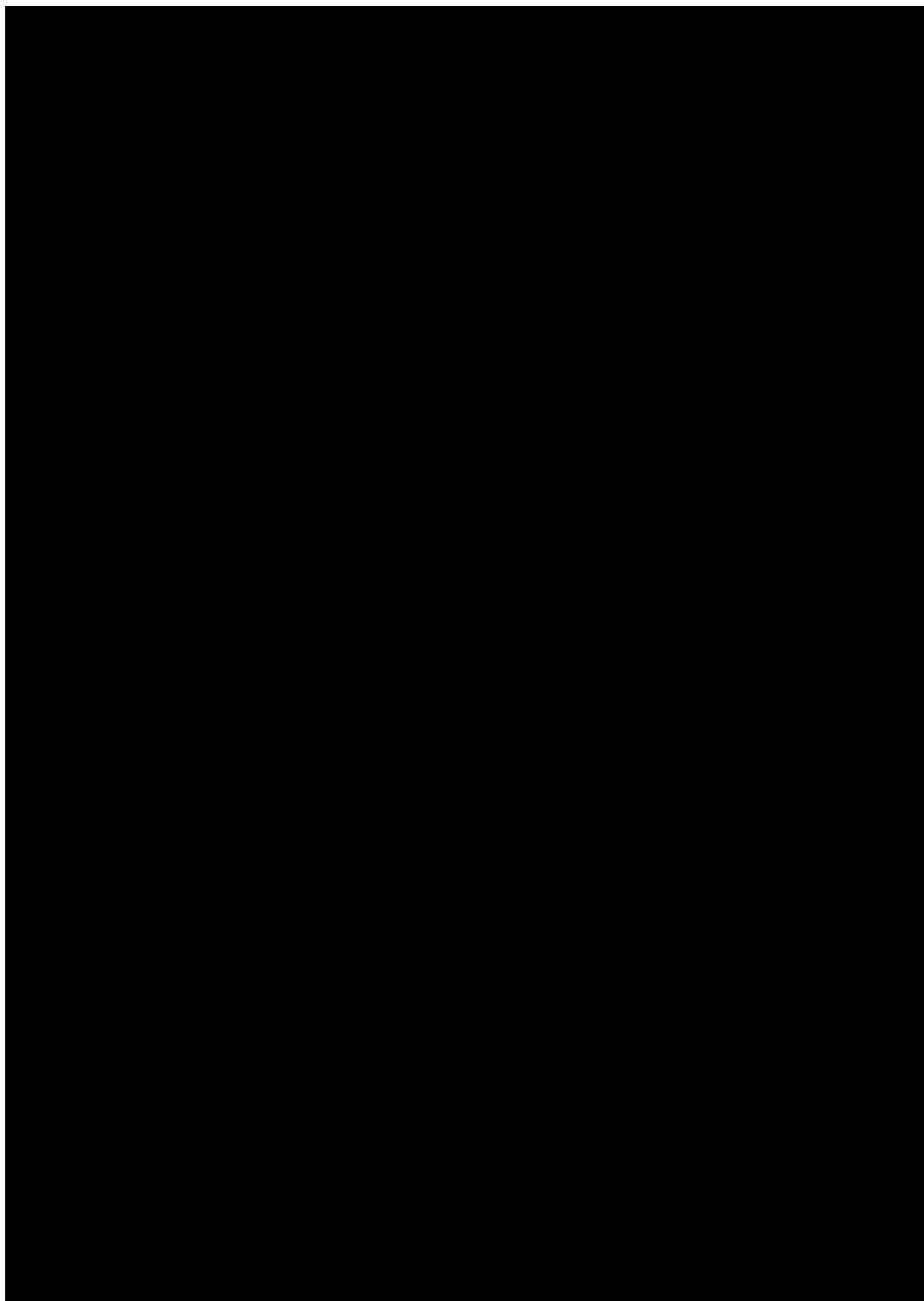
- [55] Simonsen, K. A., Anderson-Berry, A. L., Delair, S. F., & Davies, H. D. (2014). Early-Onset Neonatal Sepsis. *Clinical Microbiology Reviews*, 27(1), 21–47. <https://doi.org/10.1128/cmr.00031-13>
- [56] Leante-Castellanos, J. L., Martínez-Gimeno, A., Cidrás-Pidré, M., Martínez-Munar, G., García-González, A., & Fuentes-Gutiérrez, C. (2017). Central-peripheral Temperature Monitoring as a Marker for Diagnosing Late-onset Neonatal Sepsis. *The Pediatric Infectious Disease Journal*, 36(12), e293–e297. <https://doi.org/10.1097/inf.0000000000001688>
- [57] Messaritakis, J., Anagnostakis, D., Laskari, H., & Katerelos, C. (1990). Rectal-skin temperature difference in septicaemic newborn infants. *Archives of Disease in Childhood*, 65(4 Spec No), 380–382. https://doi.org/10.1136/adc.65.4_spec_no.380
- [58] Leante-Castellanos, J. L., Lloreda-García, J. M., García-González, A., Llopis-Baño, C., Fuentes-Gutiérrez, C., Alonso-Gallego, J. Á., & Martínez-Gimeno, A. (2012). Central-peripheral temperature gradient: an early diagnostic sign of late-onset neonatal sepsis in very low birth weight infants. *Journal of Perinatal Medicine*, 40(5). <https://doi.org/10.1515/jpm-2011-0269>
- [59] Ussat, M., Vogtmann, C., Gebauer, C., Pulzer, F., Thome, U., & Knüpfer, M. (2015). The role of elevated central-peripheral temperature difference in early detection of late-onset sepsis in preterm infants. *Early Human Development*, 91(12), 677–681. <https://doi.org/10.1016/j.earlhumdev.2015.09.007>
- [60] Murki, S., Shankar, R., & Reddy, A. (2006). Rectal Sole Temperature Difference: A Marker of Neonatal Septicemia. *Journal of Neonatology*, 20(1), 45–49. <https://doi.org/10.1177/0973217920060108>
- [61] Bhandari, V. & Narang, A. (1992). Thermoregulatory alterations as a marker for sepsis in normothermic premature neonates. *Indian Pediatrics*, 29(5), 571-5.
- [62] Uddin, S., Khan, A., Hossain, M. E., & Moni, M. A. (2019). Comparing different supervised machine learning algorithms for disease prediction. *BMC Medical Informatics and Decision Making*, 19(1). <https://doi.org/10.1186/s12911-019-1004-8>

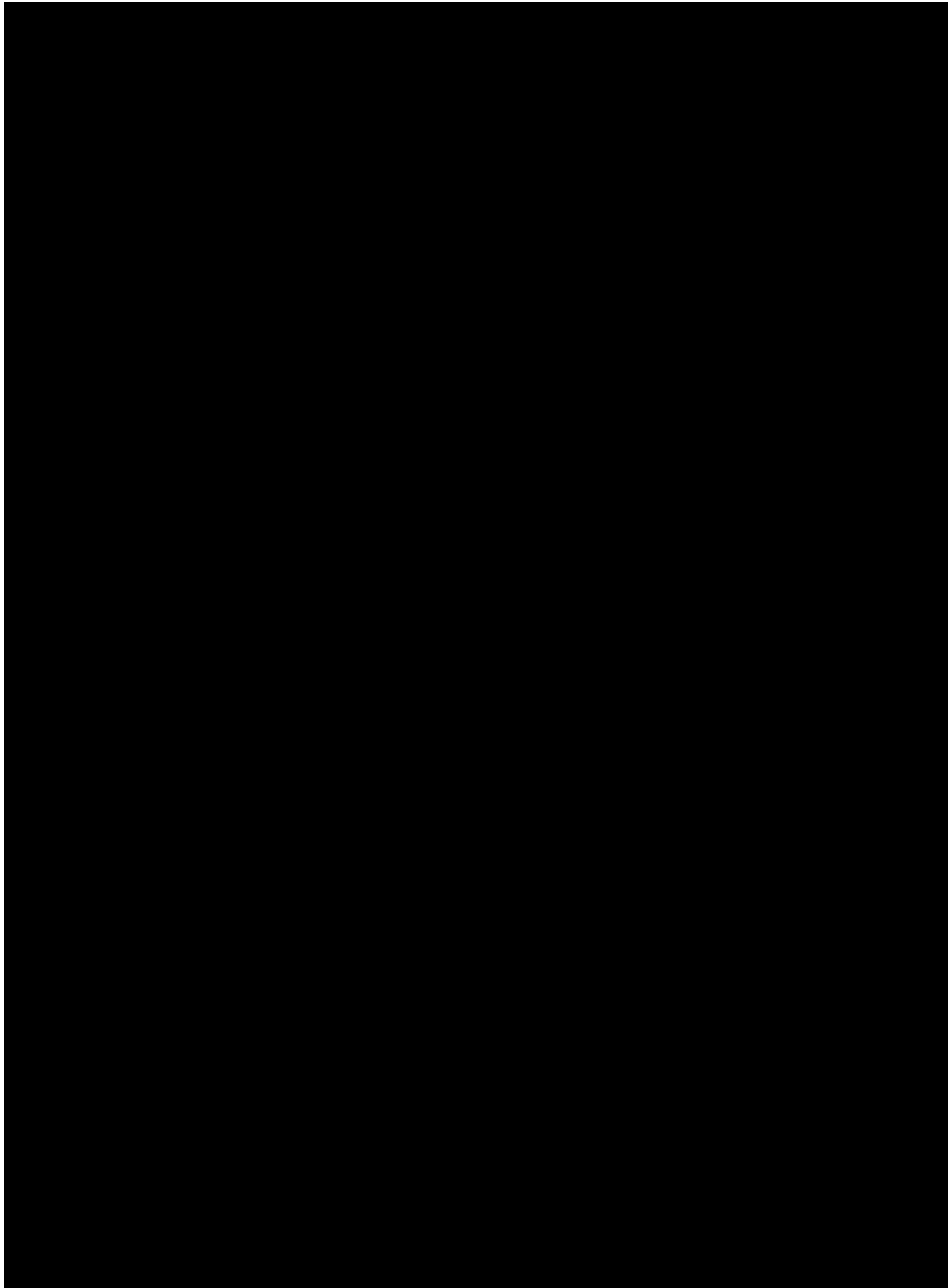












.2. Appendix: FLIR SC305 Datasheet



FLIR SC305

FLIR SC305

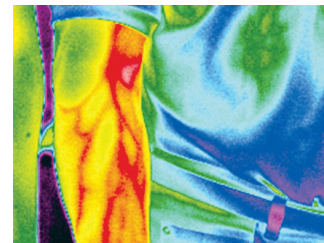
Speed up your design with Infrared

The SC305 is designed from the ground-up to deliver the accurate thermographic imaging and repeatable temperature measurement necessary in demanding science and R&D applications. Each crisp thermal image is built from over 76,000 individual picture elements that are sampled by the camera's on-board electronics and firmware. SC305 features include:

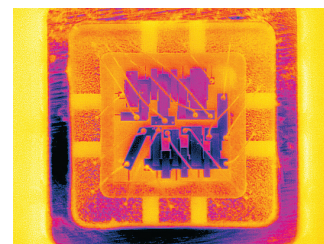


Key features and Benefits:

- **Uncooled Microbolometer Detector** – Maintenance-free and provides excellent long wave imaging performance
- **Optics and Focus** – standard built-in 25° lens with optional 6°, 15°, 45°, and 90° lenses available to achieve other fields of view; manual and auto focus standard
- **Microscopy and Close-up Measurement** – Optional 100 μm , 50 μm , and 25 μm microscope optics and microscope stand are available for small target imaging and measurement
- **Precise Timing and Control** – Optically-isolated digital I/O connections eliminate communication latencies with digital in and out for shutter disable and program control along with a V-sync connector for triggering and synchronization
- **Plug-and-Play Compatibility** – Ideal system integration solution with universal plug and play and GigE Vision Control protocols. The camera can be fully configured from the PC, allowing command, control, and collection of full frame data from the camera in real time.
- **Versatility** – Compact, rugged, and lightweight with straightforward 3-sided mounting feature that permits quick installation and easy movement for new application requirements
- **Fast Data Transfer** – Equipped with an RJ-45 gigabit Ethernet connection that supplies a 16-bit 320 x 240 images at rates as high as 60 Hz along with linear temperature data; GenICam and GigE Vision Compliant
- **Tailored to Your Application** – FLIR Systems offers a complete line of accessories including optics, enclosures, data systems, and software tools to suit the most demanding applications.



320 x 240 pixels IR resolution and thermal sensitivity of 50mK provides optimized image details and temperature difference information.



Infrared measurement allows you to see a thermal problem and measure temperature over surfaces accurately.

Typical applications:

The FLIR SC305 camera is an excellent choice for those who want to work in R&D but do not need the highest frame rates or a resolution higher than 320 x 240 pixels. For those who need to use the camera in R&D, it is highly recommended to use the FLIR ResearchIR software.

FLIR SC305 Technical Specifications

| Imaging and optical data | |
|--|--|
| Field of view (FOV) | 25° x 18.8° |
| Minimum focus distance | 0.4 m (1.31ft.) |
| Focal Length | 18 mm (0.7 in.) |
| Spatial resolution | 1.36 mrad |
| Lens identification | Automatic |
| F-number | 1.3 |
| Thermal sensitivity / NETD | <0.05°C @ +30°C (+86°F) / 50 mK |
| Image frequency | 9 Hz |
| Focus | Automatic or manual (built in motor) |
| Detector data | |
| Detector type | Focal Plane Array (FPA), uncooled microbolometer |
| Spectral range | 7.5 - 13 µm |
| IR resolution | 320 x 240 pixels |
| Detector pitch | 25 µm |
| Detector time constant | Typical 12ms |
| Measurement | |
| Object temperature range | -20°C to +120°C 0 to +350°C |
| Accuracy | ±2°C or ±2% of reading |
| Measurement Analysis | |
| Atmosphere transmission correction | Automatic, based on inputs for distance, atmospheric temperature and relative humidity |
| Optics transmission correction | Automatic, based on signals from internal sensors |
| Emissivity correction | Variable from 0.01 to 1.0 |
| Reflected apparent temperature correction | Automatic, based on input of reflected temperature |
| External optics / windows correction | Automatic, based on input of optics / window transmission and temperature |
| Measurement corrections | Global object parameters |
| Ethernet | |
| Ethernet | Control and image |
| Ethernet, type | Gigabit Ethernet |
| Ethernet, standard | IEEE 802.3 |
| Ethernet, connector type | RJ-45 |
| Ethernet, communication | TCP/IP socket-based FLIR proprietary and GenICam protocol |
| Ethernet, image streaming | 16-bit 320 x 240 pixels @ 9 Hz - Signal linear - Temperature linear - Radiometric GigE Vision and GenICam compatible |
| Ethernet, protocols | TCP, UDP, SNMP, RTP, HTTP, ICMP, IGMP, ftp, SMTP, SMB (CIFS), DHCP, MDNS (Bonjour), uPnP |
| Digital input / output | |
| Digital input, purpose | Image tag (start, stop, general), Image flow ctrl. (Stream on/off), Input ext. device (programmatically read) |
| Digital input | 2 opto-isolated, 10-30 VDC |
| Digital output, purpose | Output to ext. device (programmatically set) |
| Digital output | 2 opto-isolated, 10-30 VDC, max 100 mA |
| Digital I/O, isolation voltage | 500 VRMS |
| Digital I/O, supply voltage | 12/24 VDC, max 200 mA |
| Digital I/O, connector type | 6-pole jackable screw terminal |
| Power system | |
| External power operation | 12/24 VDC, 24 W absolute max |
| External power, connector type | 2-pole jackable screw terminal |
| Voltage | Allowed range 10-30 VDC |
| Environmental data | |
| Operating temperature range | -15°C to +50°C |
| Storage temperature range | -40°C to +70°C |
| Humidity (operating and storage) | IEC 60068-2-30/24 h 95% relative humidity +25°C to +40°C |
| EMC | • EN 61000-6-2:2001 (Immunity) • EN 61000-6-3:2001 (Emission) • FCC 47 CFR Part 15 Class B (Emission) |
| Encapsulation | IP 40 (IEC 60529) |
| Bump | 25 g (IEC 60028-2-29) |
| Vibration | 2 g (IEC 60068-2-6) |
| Physical data | |
| Weight | 0.7 kg |
| Camera size (L x W x H) | 170 x 70 x 70 mm |
| Tripod mounting | UNC1/4"-20 (on three sides) |
| Base mounting | 2 x M4 thread mounting holes (on three sides) |
| Housing material | Aluminium |
| Scope of delivery | |
| Hard transport case or cardboard box | |
| Infrared camera with lens | |
| Calibration certificate | |
| Ethernet™ cable | |
| Mains cable | |
| Power cable, pig-tailed | |
| Power supply | |
| Printed Getting Started Guide | |
| Printed Important Information Guide | |
| User documentation CD-ROM | |
| Utility CD-ROM | |
| Warranty extension card or Registration card | |
| Optional accessories | |
| IR lens f = 30 mm, 15° incl. case | |
| IR lens f = 10 mm, 45° incl. case | |
| Close-up 4x (100 µm) incl. case | |
| Close-up 2x (50 µm) incl. case | |
| Lens 76 mm (6") with case and mounting support for A/SC3XX | |
| Lens 4 mm (90°) with case and mounting support for A/SC3XX | |
| Close-up 1x (25 µm) incl. case and mounting support for A/SC3XX | |
| High temp. option +1200°C/+2192°F for FLIR T/B2XX to T/B4XX and A/SC3XX Series | |
| Power supply for A/SC3XX and A/SC6XX | |
| Power cord EU | |
| Power cord US | |
| Power cord UK | |
| Ethernet cable CAT-6, 2m/6.6 ft. | |
| Power cable, pig-tailed | |
| Hard transport case for A/SC3XX and A/SC6XX series | |
| Delivery Box for A/SC3XX | |
| Recommended softwares for documentation and analysis: | |
| - ThermoVision (TM) Systems Developers Kit | |
| - FLIR ResearchIR | |
| - FLIR QuickPlot | |

Specifications and prices subject to change without notice. Copyright © 2010 FLIR Systems. All right reserved including the right of reproduction in whole or in part in any form.

Asia Pacific Headquarter
Hong Kong
 FLIR Systems Co Ltd.
 Room 1613 – 16, Tower 2
 Grand Central Plaza
 138 Shatin Rural Committee
 Road, N.T., Hong Kong
 Tel: +852 2792 8955
 Fax: +852 2792 8952
 Email: flir@flir.com.hk

China Head Office - Shanghai
 FLIR Systems (Shanghai) Co., Ltd
 Tel: +86 21 5169 7636
 Fax: +86 21 5466 0289
 e-mail: info@flir.cn

Japan Office - Tokyo
 FLIR Systems Japan K.K.
 Tel: +81 3 6277 5681
 Fax: +81 3 6277 5682
 e-mail: info@flir.jp

Korea Office - Seoul
 FLIR Systems Korea Co., Ltd
 Tel: +82 2 565 2714
 Fax: +82 2 565 2718
 e-mail: sales@flirkorea.com

Taiwan Representative Office
 Tel: +886 2 27579662
 Fax: +886 2 27576723
 e-Mail: flir@flir.com.hk

India Representative Office
 Tel: +91 11 4606 7100
 Fax: +91 11 4606 7110
 e-mail: flir@flir.com.hk


www.flir.com/thg

100929 SC305 datasheet_EN

